

Pharmacometric modeling of fluoropyrimidines

Dissertation

zur

Erlangung des Doktorgrades (Dr. rer. nat.)

der

Mathematisch-Naturwissenschaftlichen Fakultät

der

Rheinischen Friedrich-Wilhelms-Universität Bonn

vorgelegt von

EDUARD SCHMULENSON

aus

Riga, Lettland

Bonn 2022

Angefertigt mit Genehmigung der Mathematisch-Naturwissenschaftlichen Fakultät der
Rheinischen Friedrich-Wilhelms-Universität Bonn.

Erstgutachter: Prof. Dr. Ulrich Jaehde

Zweitgutachter: Prof. Dr. Dr. Markus Jörger

Tag der Promotion: 22.02.2023

Erscheinungsjahr: 2023

Danksagung

An dieser Stelle möchte ich allen Menschen, die auf unterschiedlichste Weise zum Gelingen dieser Arbeit beigetragen haben, meinen Dank aussprechen.

Mein aufrichtiger Dank gilt meinem Doktorvater Prof. Dr. Ulrich Jaehde für das in mich gesetzte Vertrauen sowie für die mir überlassenen, hochinteressanten Projekte. Seine Begeisterung für die Wissenschaft und insbesondere für die Pharmakometrie inspirieren mich täglich aufs Neue. Seine stete Unterstützung und die bereichernden Diskussionen weiß ich sehr zu schätzen. Ich habe aus dieser Zeit viel lernen und mitnehmen können.

Ganz herzlich danke ich Prof. Dr. Dr. Markus Jörger für die ausgezeichnete Zusammenarbeit im Rahmen der RECAP-Studie, des 5FU-TDM-Reviews sowie für die Übernahme des Koreferats. Durch seine großartige Unterstützung und hilfreiche Kritik hat er maßgeblich zum Gelingen beider Projekte beigetragen.

Ich bedanke mich sehr bei Prof. Dr. Gerd Bendas und Prof. Dr. Jan Hasenauer für die Bereitschaft zur Teilnahme an der Prüfungskommission.

Mein besonderer Dank gilt allen Koautorinnen und Koautoren, ohne die ein Erscheinen der Publikationen im Rahmen dieser Arbeit nicht möglich gewesen wäre. Ich bedanke mich herzlich für den steten, interessanten fachlichen Austausch.

Ich danke Prof. Dr. Gerd Mikus für die überaus wertvollen Diskussionen. Seine konstruktive Kritik hat einen großen Beitrag zur Veröffentlichung der Publikationen geleistet.

Auch der SAKK danke ich herzlich für die Möglichkeit der Mitarbeit an der RECAP-Studie. Insbesondere Daniela Bärtschi bin ich für die hervorragende Zusammenarbeit sehr dankbar.

Ich bin allen Patientinnen und Patienten zutiefst dankbar, die sich trotz ihrer belastenden Situationen zur Teilnahme an den Studien bereit erklärt haben.

Ich danke allen Mitgliedern des Arbeitskreises Klinische Pharmazie herzlichst für die großartige Zusammenarbeit, gegenseitige Hilfe und das schöne Miteinander. Ich werde die Zeit immer in guter Erinnerung behalten. Insbesondere möchte ich Patricia Egidi, Dr. Imke Ortland, Maximilian Günther, Anna Böhmer, Olga Teplytska und Nigina Zimmermann für die schöne Zeit danken. Auch Iris Ullrich bin ich sehr dankbar für die stets tolle Hilfe.

Des Weiteren danke ich meiner Masterstudentin Nigina Zimmermann, die durch ihre großartige Arbeit am 5FU-SMI-Projekt maßgeblich zum Gelingen dieser Arbeit beigetragen hat.

Ebenfalls bedanke ich mich bei der Bonn International Graduate School of Drug Sciences für die finanzielle Unterstützung während der Promotion.

Ich bin Anna Böhmer und Olga Teplytska sehr dankbar für das akribische Korrekturlesen dieser Arbeit.

Zu guter Letzt danke ich meinen Freunden und meiner Familie. Besonderer Dank gebührt meinen Eltern, Oma Bluma und meiner Frau Astrid. Ich bin zutiefst dankbar für euren Rückhalt, euer Verständnis und euren Glauben an mich!

Für meine Familie

List of publications

This cumulative thesis is based on the following publications:

1. Schmulenson E, Zimmermann N, Mikus G, Joerger M, Jaehde U. Current status and future outlooks on therapeutic drug monitoring of fluorouracil. *Expert Opin Drug Metab Toxicol* 2021; 17: 1407 – 1422. DOI: 10.1080/17425255.2021.2029403
2. Schmulenson E, Bovet C, Theurillat R, Decosterd LA, Largiadèr CR, Prost J-C, Csajka C, Bärtschi D, Guckenberger M, von Moos R, Bastian S*, Joerger M*, Jaehde U*. Population pharmacokinetic analyses of regorafenib and capecitabine in patients with locally advanced rectal cancer (SAKK 41/16 RECAP). *Br J Clin Pharmacol* 2022; 88: 5336 – 5347. DOI: 10.1111/bcp.15461
3. Schmulenson E*, Zimmermann N*, Müller L, Kapsa S, Sihinevich I, Jaehde U. Influence of the skeletal muscle index on pharmacokinetics and toxicity of fluorouracil. *Cancer Med* 2023; 12: 2580 – 2589. DOI: 10.1002/cam4.5118
4. Schmulenson E, Krolop L, Simons S, Ringsdorf S, Ko YD, Jaehde U. Evaluation of patient-reported severity of hand-foot syndrome under capecitabine using a Markov modeling approach. *Cancer Chemother Pharmacol* 2020; 86: 435 – 444. DOI: 10.1007/s00280-020-04128-7

* contributed equally

Table of content

List of abbreviations.....	VIII
1. Introduction	1
1.1 Dose individualization and pharmacometric modeling in oncology.....	1
1.1.1 Dose individualization in oncology	1
1.1.2 Dose individualization according to body composition of cancer patients	2
1.1.3 Principles of population pharmacometric modeling	4
1.1.4 Pharmacometric modeling approaches in oncology	5
1.2 Investigated drugs.....	9
1.2.1 Fluorouracil	9
1.2.2 Capecitabine	11
1.2.3 Regorafenib.....	13
2. Aim and objectives.....	15
3. Current status and future outlooks on therapeutic drug monitoring of fluorouracil.....	17
4. Population pharmacokinetic analyses of regorafenib and capecitabine in patients with locally advanced rectal cancer (SAKK 41/16 RECAP)	21
5. Influence of the skeletal muscle index on pharmacokinetics and toxicity of fluorouracil	25
6. Evaluation of patient-reported severity of hand–foot syndrome under capecitabine using a Markov modeling approach.....	29
7. Conclusions	33
8. Summary	37
9. References	39
Further information on assistance received and resources used.....	57
Appendix	59

List of abbreviations

5FU	Fluorouracil
ABC	ATP-binding cassette
ADL	Activities of daily living
AUC	Area under the concentration-time curve
BCRP	Breast cancer resistance protein
BSA	Body surface area
CI	Confidence interval
CT	Computed tomography
CTCAE	Common Terminology Criteria for Adverse Events
CYP	Cytochrome P450
DFCR	5'-deoxy-5-fluorocytidine
DFUR	5'-deoxy-5-fluorouridine
DHF	5, 6-dihydro-5-fluorouracil
DPD	Dihydropyrimidine dehydrogenase
DPYD	Dihydropyrimidine dehydrogenase coding gene
EHR	Electronic health record
EMA	European Medicines Agency
FdUMP	Fluorodeoxyuridine monophosphate
FdUTP	Fluorodeoxyuridine triphosphate
FUTP	Fluorouridine triphosphate
HFS	Hand-foot syndrome
HPLC	High-performance liquid chromatography
IATDMCT	International Association of Therapeutic Drug Monitoring and Clinical Toxicology
IIV	Inter-individual variability
L3	Third lumbar vertebra
LBM	Lean body mass
LC-MS/MS	Liquid chromatography-tandem mass spectroscopy
mCTMM	Minimal continuous-time Markov model
MET	Mean equilibration time
NLME	Non-linear mixed effects
NPV	Negative predictive value
OFV	Objective function value

PBMC	Peripheral mononuclear blood cells
pcVPC	Prediction-corrected visual predictive check
PK	Pharmacokinetics
PO	Proportional odds
PPV	Positive predictive value
PRO	Patient-reported outcome
PRO-CTCAE	Patient-reported outcomes version of the Common Terminology Criteria for Adverse Events
RAS	Rat sarcoma
RSE	Relative standard error
SmPC	Summary of product characteristics
SNP	Single nucleotide polymorphism
sVEGFR	Soluble vascular endothelial growth factor receptor
TDM	Therapeutic drug monitoring
VPC	Visual predictive check

1. Introduction

1.1 Dose individualization and pharmacometric modeling in oncology

1.1.1 Dose individualization in oncology

Precision medicine which is defined as a tailored approach to preventing, diagnosing and treating diseases in individual patients is an advancing area, especially in the field of oncology [1, 2]. So far, precision medicine is mainly focused on genotyping and pharmacogenetic approaches which allow for cancer diagnosis and proper drug selection for individual patients. For various anticancer drugs, such screening approaches are mandatorily performed. For example, patients with colorectal cancer are often treated with the chemotherapeutic agent cetuximab. In order to ensure optimal efficacy, patients are screened for mutations of the rat sarcoma (*RAS*) gene before cetuximab administration. If *RAS* mutations are present, cetuximab should not be administered due to an unfavorable benefit-to-risk ratio [3]. Other prominent anticancer drugs which require pre-therapeutic genotyping are the monoclonal antibody trastuzumab (screening for overexpression of human epidermal growth factor receptor 2), or the fluoropyrimidines fluorouracil (5FU) and its oral prodrug capecitabine. The two latter drugs will be discussed in further detail in chapters 1.2.1 and 1.2.2, respectively.

However, besides drug selection, the optimal drug dosage is crucial as well to ensure a safe and efficacious therapy. Given the potential large inter-individual differences in pharmacokinetic and pharmacodynamic response to anticancer drugs a tailored drug dosage is of high importance as part of precision medicine [4, 5]. It is therefore reasonable to target a pharmacokinetic parameter which is linked to the pharmacodynamics of a drug or to directly use a pharmacodynamic parameter for dose individualization, if feasible. In particular, pharmacokinetic dose individualization of anticancer drugs is becoming more present in clinical practice and is described in further detail in the following section.

Pharmacokinetic dose individualization in oncology

In order to perform a pharmacokinetic dose individualization, several requirements have to be met. An established relationship between dose and the pharmacokinetic parameter of interest is crucial as well as a relationship between the pharmacokinetics and pharmacodynamics of a drug. Patients can be dosed according to e.g. their body surface area (BSA), renal function, age or sex if these characteristics are related to the pharmacokinetics of the drug. In oncology, drug dosing is commonly performed based on the patient's BSA. BSA is mainly calculated by the formula of Du Bois and Du Bois which was developed based on data from only nine subjects [6]. BSA usage was implemented into animal studies in order to perform allometric scaling and was adopted to determine the individual dose of the majority of anticancer drugs since the 1950s [7]. However, for most anticancer drugs, a

relationship between BSA and pharmacokinetic parameters could not be established and there is manifold evidence that this dosing approach lacks scientific basis [7–9]. In fact, dosing of patients according to their BSA results in a wide range of inter-individual variability (IIV) of pharmacokinetic parameters in patients. Baker et al. demonstrated that only five of the investigated 33 anticancer drugs showed a reduction in IIV after BSA-based dosing. In these five drugs, BSA was able to explain 15 to 35% of the IIV [10]. Consequently, this may potentially lead to reduced efficacy or the occurrence of preventable toxicity in a high proportion of patients given the narrow therapeutic range of most anticancer drugs [7, 9].

To overcome the disadvantages of BSA-based dosing, measuring drug concentrations, e.g. in serum or plasma within the framework of a therapeutic drug monitoring (TDM) is a promising approach for pharmacokinetic dose individualization. TDM allows for dose adaptations based on a calculated pharmacokinetic target parameter which reflects drug exposure such as the area under the concentration-time curve (AUC). Furthermore, a feedback mechanism is the cornerstone of every TDM since the quantified target parameter is continuously evaluated and thus, dose adjustments can be performed prior to the next drug administration. In order to keep patient burden as low as possible, only very few samples are needed for quantification of individual pharmacokinetic target parameters. This is possible by using the Bayes method. Here, typical pharmacokinetic parameters, e.g. drug clearance or volume of distribution (including patient-specific influence factors such as age, sex or renal function) of a population and their distributions are used as *a priori* information, combined with measured individual drug concentrations in order to calculate individual pharmacokinetic parameters. This combination allows for a transition from the population-based *a priori* probability to the individualized *a posteriori* probability. The calculation of individual pharmacokinetic parameters requires an existing population pharmacokinetic model which should be based on a patient population that is similar to the individual patient. Such a model contains information on pharmacokinetic variability and influence factors, the so-called covariates [11]. After estimating individual parameters, simulations of the future concentration-time course are performed in order to assess the current and alternative dose regimens *in silico* [12].

A detailed insight into TDM of anticancer drugs and its scientific evidence, using the example of 5FU, is presented in chapter 3. This comprehensive literature review particularly addressed the possibilities of implementing routine TDM as an indispensable part of precision medicine.

1.1.2 Dose individualization according to body composition of cancer patients

For cancer patients, nutrition is one of the cornerstones to achieve a successful anticancer treatment as proper nutrition is strongly associated with higher quality of life [13, 14] or overall survival [15]. The

main nutritional problem in cancer patients is the progressive loss of skeletal muscle mass and muscle strength (also called sarcopenia) which occurs regardless of cancer stage [16, 17]. The prevalence of low muscle mass in cancer patients was reported to be over 50% which substantially exceeds the prevalence in healthy individuals of the same median age (about 15%) [18]. Reduced muscle mass is an independent predictor for lower quality of life, tumor progression and reduced overall survival [19–23]. Notably, sarcopenia is not necessarily associated with loss of body weight as only about 10% of cancer patients are underweight [19] and the prevalence of patients with “sarcopenic obesity” was reported to vary between 9 and 25% [24]. Therefore, it is insufficient to only assess body weight or body mass index of cancer patients in order to properly diagnose a sarcopenic condition. Measuring the patient’s body composition by computed tomography (CT) or magnetic resonance imaging are considered to be the gold standards to assess not only muscle quantity but also its quality, i.e. microscopic and macroscopic aspects describing muscle architecture and composition [16]. Muscle quality has been found to be an important aspect of sarcopenia as well [16].

The knowledge of body composition is not only important for overall cancer prognosis but also for anticancer therapy. As physicochemical properties of drugs are key determinants for distribution into different body tissues (e.g. fat or muscle), alterations in body composition therefore potentially impact the pharmacokinetics of a drug [25]. In fact, there are several reports suggesting a relationship between body composition and anticancer drug pharmacokinetics. Gusella et al. identified significant relationships between the volume of distribution of the hydrophilic drug 5FU and total body water as well as volume of distribution and fat-free mass. They were better predictors for the pharmacokinetics of the drug than BSA which is traditionally used to individualize a 5FU dose [26]. Sarcopenic patients under therapy with sorafenib were reported to exhibit significantly higher AUC than non-sarcopenic patients [27]. Similar results were observed in patients treated with vandetanib as a low skeletal muscle index was associated with higher plasma concentrations [28]. Lean body mass (total body weight excluding body fat mass) was a significant predictor for epirubicin clearance as well since it explained about 18% of the IIV [29]. Consequently, the altered drug pharmacokinetics may lead to increased dose-limiting drug toxicity [21, 27, 28, 30, 31].

As BSA-based dosing (see chapter 1.1.1) is not able to account for the changes in body composition, the need for other dose individualization strategies for anticancer drugs is of high interest [32]. In order to gain a better understanding of the influence of body composition on pharmacokinetics and toxicity of anticancer drugs the project presented in chapter 5 was conducted. It aimed to provide insights into the influence of the skeletal muscle index (SMI) on the pharmacokinetics and toxicity of 5FU. As SMI can be calculated from routinely performed CT scans it is a rather easily accessible

measure of body composition, making it a potentially valuable marker for a deeper understanding of body composition influence on this hydrophilic drug.

1.1.3 Principles of population pharmacometric modeling

Pharmacometrics is an interdisciplinary research field, combining aspects of mathematics and pharmacy. The aim of this discipline is to develop mathematical and statistical models to quantify information about drug, patient or patient populations, and disease. These models are used to identify covariates as sources of pharmacokinetic or pharmacodynamic variability as well as to explore new scenarios via simulations, e.g. by assessing new dose regimens [33]. In general, a population pharmacometric model consists of three main elements. First, a structural model has to be developed which describes the time course of a dependent variable, such as drug concentration or a drug effect parameter on a population level. Such structural models are mainly characterized by a compartmental structure which is described by mathematical equations. These equations aim to link pharmacometric parameters such as drug clearance or volume of distribution to an independent variable (time, drug dose) in order to describe the observed dependent variable, e.g. drug concentration. After establishing the structural model, it is extended by a statistical model. It quantifies all types of variability, namely IIV, intra-individual (or inter-occasion) variability and the residual unexplained variability (due to e.g. measurement or documentation errors). This allows the estimation of individual pharmacometric parameters. The third component of pharmacometric models is the covariate model which aims to identify predictors of the variability quantified in the statistical model. The selection of such covariates is a crucial process in model development as physiological plausibility as well as statistical significance of the identified covariate effect should be ensured [33, 34].

Most commonly, nonlinear mixed effects (NLME) modeling approaches are applied in pharmacometrics. The term “mixed effects” consists of “fixed effects”, referring to population values of structural model parameters (e.g. drug clearance or volume of distribution in a population pharmacokinetic model) without the inclusion of variability. “Random effects” comprise all of the above-mentioned forms of variability [33]. Using NLME models, it is possible to simultaneously analyze patients within a population and to obtain population pharmacokinetic/pharmacodynamic parameters as well as their variability. Parameter estimation in NLME models is achieved by maximizing the likelihood of predicting the observation given the model. Most population modeling software packages use this maximum likelihood estimation method to minimize an objective function value (OFV) which is expressed as minus twice the natural logarithm of the likelihood. It is a single number which provides a summary of how well the model fits the observed data compared to another nested model. Most commonly, the maximum likelihood is approximated by gradient-based methods

such as the first-order conditional estimation or second-order Laplacian algorithms [34]. Furthermore, the NLME approach allows the analysis of datasets with only sparse individual sampling which is mainly the case in clinical settings [35]. All of the developed pharmacometric models in this thesis (chapters 4 – 6) were developed using NLME modeling approaches with maximum likelihood estimation.

1.1.4 Pharmacometric modeling approaches in oncology

Development and management of anticancer drug therapies can be substantially supported by pharmacometric modeling approaches. As described above, conventional population pharmacokinetic models can be used to inform a TDM and thus, continuously optimize individual dosing in cancer patients. Drug-drug interactions in oncology can be investigated via population pharmacokinetics as well, either by simply including co-medication as a binary covariate (i.e. intake/no intake of co-medication) [36] or by exploring the impact of the pharmacokinetics of the perpetrator on the victim drug [37]. This particular topic was explored in the publication presented in chapter 4. Here, potential drug-drug interactions of two oral anticancer drugs in patients with rectal cancer were investigated by applying population pharmacokinetic modeling approaches. Namely, capecitabine (chapter 1.2.2) and regorafenib (chapter 1.2.3), which were combinedly administered for the first time in a clinical trial, were analyzed in this project.

In addition, there are various modeling approaches comprising a wide variety of pharmacodynamic and clinical endpoints in oncology. Promising approaches are described in the following sections.

Biomarker analysis

Generally, biomarkers are defined as characteristics which can be “objectively measured and evaluated as [...] indicator[s] of normal biological processes, pathogenic processes, or pharmacologic responses to a therapeutic intervention” [38]. Their applications include the use for diagnostics, disease prognosis, and as surrogate for clinical endpoints. Surrogate endpoints are invaluable for drug development as they may allow to conclude on a long-term clinical endpoint such as survival [38]. Pharmacogenetic biomarkers are of high interest as supporting tools in anticancer therapy, and partly already in clinical use, as described in chapter 1.1.1. Pharmacometric modeling approaches can assist in quantifying the impact of such biomarkers on the pharmacokinetics or pharmacodynamics of a drug and thus, proper dose adjustments can be proposed. Sáez-Belló et al. identified that single nucleotide polymorphisms (SNP) of the ATP-binding cassette transporter gene, which codes for active drug transporters such as P-glycoprotein, increased clearances of 5FU and its precursor 5'-deoxy-5-fluorouridine by 184% and 182%, respectively [39]. A population pharmacokinetic model of the anticancer drug mitotane which is the only approved treatment for adrenocortical carcinoma revealed

that a SNP of the metabolizing enzyme cytochrome P450 (CYP) 2C19 as well as polymorphisms of the genes coding for two different organic anion transporter polypeptides were predictors of mitotane clearance [40]. Another example is tamoxifen which is widely used in treating breast cancer. The exposure of its active metabolite endoxifen exhibits a wide variability, hence a substantial proportion of patients does not attain the target trough concentration of > 5.97 ng/mL. Ultimately, this leads to a decreased efficacy. This variability is partly attributed to polymorphisms of the metabolizing enzyme CYP2D6 [41]. In a recent population pharmacokinetic study by Puzkiel et al. plasma concentrations of tamoxifen and its six metabolites, including endoxifen and intermediate metabolites were analyzed along with 63 SNP in 928 breast cancer patients. It was shown that CYP2D6 phenotypes (poor, intermediate, normal, ultrarapid metabolizers) as well as SNP of other CYP enzymes (CYP3A4, CYP2C19) were predictive for the formation of intermediate metabolites and endoxifen from tamoxifen. Based on this analysis, different dose regimens were proposed according to the identified genotypes and phenotypes by performing simulation analyses [42].

Other promising pharmacometric models contain biomarkers which are often surrogate markers for pharmacodynamic response. Especially, biomarkers for tyrosine kinase inhibitors (TKI) have extensively been investigated. These are soluble forms of vascular endothelial growth factor receptors (sVEGFR) which are responsible for tumor angiogenesis and are targeted by various TKI such as axitinib and sunitinib. A pharmacometric modeling framework by Schindler et al. successfully identified relationships between axitinib pharmacokinetics, sVEGFR subtype 3 (sVEGFR-3), tumor size and overall survival [43]. Diekstra et al. and Hansson et al. proposed different modeling frameworks which linked sunitinib pharmacokinetics with sVEGFR and progression-free and overall survival, respectively [44, 45]. Another example where a pharmacometric model was used to identify a biomarker as a predictor for pharmacodynamic response in cancer patients is the relationship between atezolizumab, the biomarker interleukin-18 and tumor size [46].

Toxicity analysis

In the recent years, pharmacometric modeling frameworks aiming to combine pharmacokinetics, pharmacodynamics and clinical outcome of a drug have been increasingly developed. By using such models whole clinical trials can be simulated which allows further guidance for planning future studies. This “model-informed drug development” approach can be used in every phase of pre-clinical or clinical drug development and is therefore of particular interest for pharmaceutical industry [47].

Some of the presented models in section “Biomarker analysis” are good examples for such integrated modeling frameworks [43–46]. Whereas these modeling approaches focused on different efficacy parameters (progression-free survival, overall survival, tumor size), it is at least equally important to

investigate the toxicity of anticancer drugs as a clinical outcome. The management of toxic effects of anticancer treatment is crucial in order to enable a successful therapy as these adverse events can lead to interruptions or discontinuations of therapy as well as possibly causing permanent damage or death. Therefore, it is important for clinicians to assess the severity of these adverse events in order to initiate appropriate measures. For continuous toxicity data, such as leukocyte concentration as a marker for myelosuppression, routine laboratory measurements are sufficient for assessment. However, in the case of subjective, categorical data, the Common Terminology Criteria for Adverse Events (CTCAE) are widely used in the field of oncology [48]. Here, toxicity is graded on a scale consisting of six categories (Tab. 1) by clinicians. Taking diarrhea as an example for a common symptom in anticancer therapy, grade 0 corresponds to the absence of diarrhea, grade 1 to an increase of up to four stools per day, grade 2 to an increase of four to six stools per day with limited instrumental activity of daily living (ADL), grade 3 to an increase of over seven stools per day with limited self-care ADL, grade 4 to life-threatening consequences requiring urgent actions and grade 5 corresponds to death due to the adverse event [48]. In the recent years, however, various studies suggested that this clinician-based assessment substantially underestimates adverse event severity reported by cancer patients [49–53]. In fact, a systematic review consisting of 28 studies additionally concluded that agreements between CTCAE and patient-reported adverse event grading were “moderate at best” [54]. Therefore, the focus is shifting towards the patient’s perspective and a patient-reported outcome (PRO) version of the CTCAE (PRO-CTCAE) has been developed by the National Cancer Institute [55]. The applicability of PRO-CTCAE in anticancer therapy management is increasingly explored, with promising results regarding the improvement of quality-of-life measures [56].

Tab. 1 Adverse event grades according to CTCAE v5.0 [48]

Grade	Description
0	No symptoms
1	Mild; asymptomatic or mild symptoms; clinical or diagnostic observations only
2	Moderate; minimal, local or noninvasive intervention indicated
3	Severe or medically significant but not immediately life-threatening
4	Life-threatening consequences; urgent intervention indicated
5	Death related to adverse event

Similar to the presented biomarker models, toxicity data can be equally used in pharmacometrics as such models can help to quantify the relationship between pharmacokinetics/pharmacodynamics and

drug toxicity. A prominent example for a pharmacometric toxicity model is the model by Friberg et al. in which chemotherapy-induced myelosuppression is quantified with a semi-mechanistic model of the leukocyte concentration-time course, regardless of the drug used [57]. However, this type of model can only be applied to continuous data. For categorical data which are not objectively quantifiable, such as (PRO-)CTCAE grades, logistic modeling approaches are more appropriate. Sheiner published the first proportional odds (PO) model, i.e. a logistic model for ordered categorical data, in the field of pharmacometrics in 1994, modeling the time course of pain relief scores under therapy with bromfenac [58]. In PO models, the observed categorical dependent variable is treated as independent from the next observation in an individual. However, depending on the frequency of collection, these observations may become autocorrelated, i.e. dependent of each other. In order to account for autocorrelations, Markov elements can be incorporated into PO models. This approach was first applied in the study by Karlsson et al. where sleep stages in insomnia patients were analyzed [59]. Such discrete-time Markov models assume that the influence of the present observation on the next one is independent of the time interval between them. Especially for observational trials in routine care, choosing this modeling approach may not be feasible as time intervals between consecutive observations are expected to vary over the time course of the study. Continuous-time Markov models account for these varying time intervals as with increasing time, the influence of the present observations on the next one decreases. Introduced by Bergstrand et al. in 2009 [60], it has been widely adopted since then [61–65]. A comparison between the structures of PO models and these two major Markov modeling approaches is depicted in Fig. 1.

In the recent years, the application of pharmacometric Markov models has been extensively studied and multiple adjustments and extensions were successfully implemented. These include a minimal-continuous time Markov model which is of particular interest in sparse-data situations (see also chapter 6) [66], hidden Markov models where a hidden state is modeled representing e.g. an underlying disease state [67], as well as modeling frameworks combining Markov models with parametric survival models which allow for simultaneous analysis of multiple levels of information (e.g. severity, frequency and duration of adverse events) [68, 69]. Whereas the cited models cover a wide variety of clinical endpoints, PROs have been a minor focus of these studies with only few studies covering this type of data [68–70]. So far, no pharmacometric Markov models of PROs were developed for cancer patients. This fact was a major motivation to design the project presented in chapter 6 of this thesis. As PRO grading gains more traction in the management of anticancer therapy, it is of particular interest to develop pharmacometric models which can potentially support clinical decision-making. The suitability of using such a model for simulation analyses was analyzed in chapter 6. Grades

of palmar-plantar erythrodysesthesia (hand-foot syndrome, HFS) as a common adverse event under therapy with capecitabine (chapter 1.2.2) was the investigated clinical outcome.

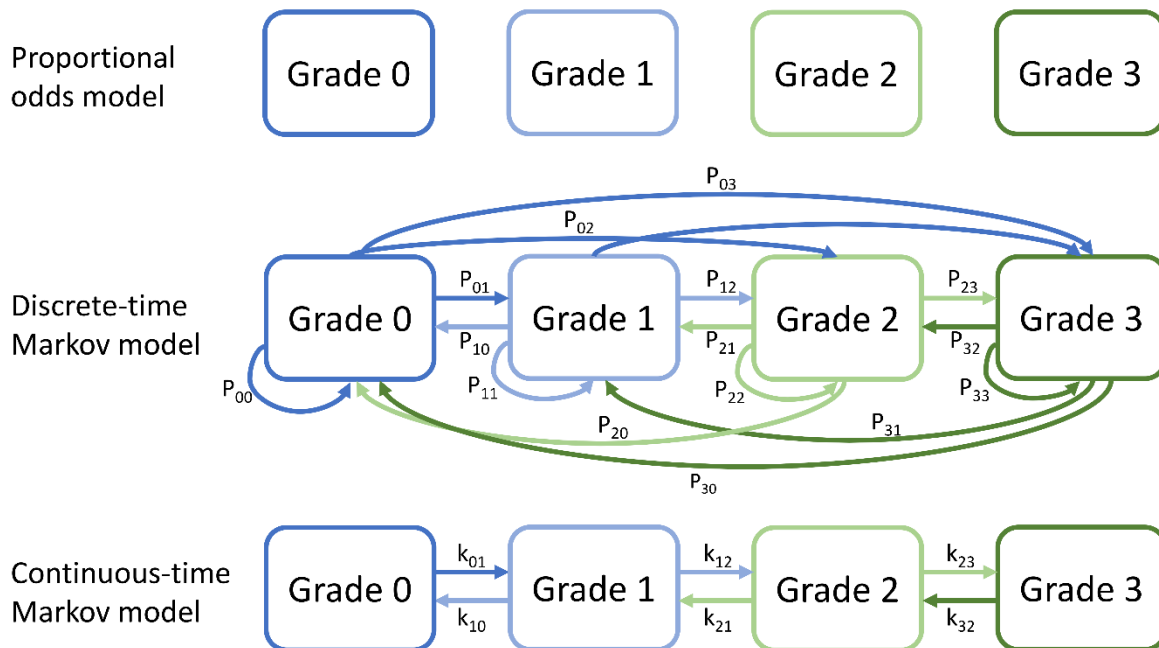


Fig. 1 Structures of a proportional odds model (top), a discrete-time Markov model (middle) and a continuous-time Markov model (bottom), exemplified for adverse event grades consisting of four grades (0 to 3). In a proportional odds model, observations are assumed to be independent from each other. In a discrete-time Markov model, transition probabilities between grades can be estimated which introduce the Markov property. These transition probabilities are assumed to be independent from the time between two subsequent observations. In a continuous-time Markov model, the transition between two grades is defined by differential equations where the influence of the preceding grade declines with increasing time. Constants governing the rate between two grades are therefore estimated [66, 70]. $P_{x,y}$: transition probability between grades x and y; $k_{x,y}$: transition rate constant between grades x and y.

1.2 Investigated drugs

1.2.1 Fluorouracil

Fluorouracil (5FU, Fig. 2) has been developed in the 1950s by Heidelberger et al. following the observation that rat hepatoma incorporated the pyrimidine base uracil into RNA to a much greater extent than normal tissues. Hence, these findings suggested that targeting uracil metabolism with antimetabolites was a suitable approach for anticancer therapy [71, 72]. 5FU is an analogue of endogenous uracil with a fluorine atom at position 5 of the pyrimidine ring (instead of hydrogen).

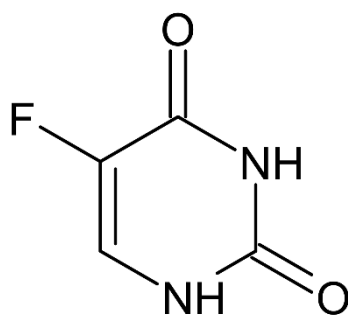


Fig. 2 Chemical structure of fluorouracil [73]

Despite its availability for many decades 5FU is still one of the cornerstones for treating colorectal cancer [74, 75], head and neck cancer [76], gastric cancer [77] and pancreatic cancer [78]. It is the most frequently used anticancer drug for colorectal cancer [74, 75]. Whereas 5FU monotherapy and bolus injections were widely applied in the past [79], today's evidence has shifted toward continuous infusions and combination therapies with other cytostatic agents (oxaliplatin, cisplatin, irinotecan) and monoclonal antibodies (panitumumab, cetuximab, bevacizumab) due to a more favorable response and safety profile [80–86]. Additionally, the combination of 5FU and folinate showed an increased response rate along with a prolonged overall survival [87]. Folate is therefore a substantial part of 5FU-based regimens [82].

Pharmacokinetics and pharmacogenetics

Pharmacokinetics of 5FU is highly variable due to the dependence on route of administration (bolus or continuous infusion) and dose. 5FU is a hydrophilic drug so that there is particular interest in investigating its pharmacokinetics dependent on different body compositions. As described in chapter 1.1.2, there are reports that different measures of body composition are indeed associated with 5FU pharmacokinetics and toxicity [26, 30, 31]. 5FU is a prodrug which is intracellularly converted to its active metabolites fluorodeoxyuridine monophosphate (FdUMP), fluorodeoxyuridine triphosphate (FdUTP) and fluorouridine triphosphate (FUTP). However, the conversion to active metabolites comprises only a small fraction of 5FU metabolism. The vast majority of a 5FU dose, about 80%, is metabolized to the pharmacologically inactive compound 5,6-dihydro-5-fluorouracil (DHF) by the enzyme dihydropyrimidine dehydrogenase (DPD) which is the rate-limiting step of 5FU metabolism [72]. DHF is eventually converted to fluoro- β -alanine which is renally eliminated [88]. Nonlinear elimination was observed because of saturable hepatic metabolism by DPD [89, 90]. In addition, age [91], sex [92], BSA [93] and body weight [94] have been reported to contribute to explaining variability in 5FU clearance. However, the genotype of the DPD encoding gene, *DPYD*, potentially has the biggest influence on 5FU pharmacokinetics. There are four well-studied genotypes, namely *DPYD**2A,

*DPYD**13, c.2846A>T (rs67376798) and c.1129-5923C>G (rs75017182, c.1236G>A/HapB3) which are associated with severe 5FU toxicity [95].

Pharmacodynamics and exposure-response relationship

The three metabolites FdUMP, FdUTP and FUTP are responsible for the pharmacological activity after 5FU administration. Whereas FUTP and FdUTP directly damage RNA and DNA, respectively, by incorporation, FdUMP is a potent inhibitor of the enzyme thymidylate synthase which is the most important enzyme for *de novo* synthesis of pyrimidines [72]. Relevant biomarkers include, as described in the section above, *DPYD* genotypes. Phenotyping DPD activity is applied as well by quantifying endogenous uracil concentration as it is also metabolized by DPD or by estimating the endogenous dihydrouracil to uracil ratio (UH₂/U) which serves as a surrogate for the ratio of DHF to 5FU [82, 96]. Advantages and disadvantages of these approaches are comprehensively discussed in chapter 3.

Due to its narrow therapeutic index and high pharmacokinetic variability, 5FU is a suitable drug for conducting TDM in order to achieve the desired target exposure. Numerous studies showed that an AUC target between 20 and 30 mg×h/L was strongly associated with improved therapy response and safety [97–102]. A detailed insight into 5FU pharmacokinetics, pharmacogenetics, exposure-response relationships and its suitability for TDM is provided in chapter 3.

Toxicity

The main dose-limiting adverse events are myelosuppression and gastrointestinal disorders (diarrhea, nausea, emesis) [103]. In addition, mucositis and hand-foot syndrome (HFS) are associated with 5FU treatment as well [104]. However, 5FU toxicity is highly dependent on the route of administration. Whereas myelosuppression is associated with bolus administration, diarrhea, mucositis and HFS occur more frequently during continuous infusion [105].

1.2.2 Capecitabine

Various difficulties are associated with clinical use of 5FU including the potential risk of infection or thromboembolism as well as increased treatment costs, mainly due to intravenous administration [104]. Therefore, there was a clinical need for a more convenient and tolerable fluoropyrimidine treatment resulting in the development of the oral prodrug of 5FU, capecitabine (Fig. 3). It is approved for the treatment of colorectal and gastric cancer as well as breast cancer [106]. Capecitabine is administered as a monotherapeutic agent but similar to 5FU, various combination regimens exist, including co-administration of oxaliplatin, irinotecan or docetaxel [107–109]. Like 5FU, capecitabine is usually dosed according to the patient's BSA [106]. The BSA-normalized starting dose is further

dependent on either capecitabine mono- or combination therapy or if capecitabine is either continuously administered or with a rest period of seven days [106]. A recent retrospective study in 1126 patients with a fixed dose and in 1193 patients with a BSA-based dose of capecitabine showed, however, that fixed-dose capecitabine had a similar toxicity profile and progression-free survival [110].

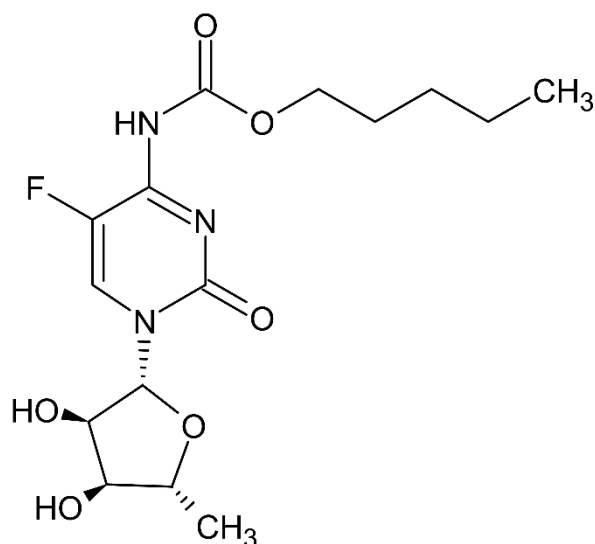


Fig. 3 Chemical structure of capecitabine [73]

Pharmacokinetics

After oral intake, capecitabine is reported to be fully and rapidly absorbed (between 0.3 and three hours) [111]. Potential influence factors include age [112], food [113] and alterations in the gastrointestinal tract such as gastrectomy [88]. The distribution of capecitabine is a highly discussed topic. So far, there are only hints that it might be a substrate for ATP-binding cassette transporters [39, 114–116]. Capecitabine is sequentially converted to 5'-deoxy-5-fluorocytidine (DFCR) by hepatic carboxylesterase and then metabolized to 5'-deoxy-5-fluorouridine (DFUR) by cytidine deaminase. The intermediate metabolite DFUR is finally converted to 5FU by the enzyme thymidine phosphorylase, particularly in tumor cells [111]. Potential drug-drug interactions between capecitabine and CYP2C9 substrates, particularly warfarin, have been reported with a significant increase in warfarin exposure [117]. As mentioned in chapter 1.1.4, drug-drug interactions involving capecitabine were explored in chapter 4 of this thesis. Half-life of capecitabine was reported to be short (< one hour) and the majority of the capecitabine dose is renally excreted as fluoro- β -alanine [111].

Toxicity

The formation of 5FU inside the tumor cells leads to less systemic toxic effects of capecitabine compared to intravenous 5FU [111]. For example, myelosuppression occurs less frequently than under 5FU therapy [104]. However, capecitabine causes a higher incidence of HFS which is the main dose-limiting toxicity and is observed in up to 77% of patients [118–123]. Although not life-threatening, HFS may negatively impact patients' quality of life [124, 125] and may lead to dose reductions or treatment discontinuations [126, 127]. However, studies showed a significant correlation between the occurrence of capecitabine-induced HFS and therapy efficacy [128, 129]. The exact pathophysiology is still not well understood but reports suggested that inhibition of the main metabolizing enzyme of 5FU, DPD, decreases the incidence of HFS [130]. Notably, a randomized phase III study by Kwakman et al. compared HFS incidence in patients under capecitabine therapy with patients treated with S-1, a drug combination consisting of tegafur (another oral prodrug of 5FU), gimeracil (a DPD inhibitor) and oteracil (prevents the phosphorylation of 5FU in the digestive tract). The study revealed that S-1 patients had a significantly lower HFS incidence [127].

1.2.3 Regorafenib

Regorafenib (Fig. 4) was an important part of the population pharmacokinetic analysis in the project presented in chapter 4 where its influence on capecitabine pharmacokinetics was investigated. Therefore, it is introduced in this chapter. Regorafenib is an orally administered multikinase inhibitor approved as monotherapy for second- or third-line treatment of advanced colorectal cancer, hepatocellular carcinoma and gastrointestinal stromal tumors at a dose of 160 mg once daily [131].

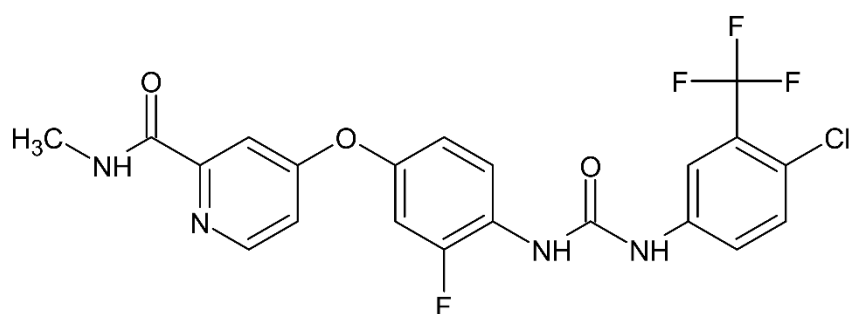


Fig. 4 Chemical structure of regorafenib [73]

Pharmacokinetics

Absorption of regorafenib is highly variable as maximum plasma concentrations are reached between one and six hours after administration. Additionally, food intake was reported to have a pronounced effect on regorafenib exposure as a low-fat meal and a high-fat meal increased mean regorafenib AUC

by 48% and 36%, respectively [132]. Regorafenib is highly bound to plasma proteins (99.5%) [132] and was reported to be a clinically relevant inhibitor of the breast cancer resistance protein drug transporter [133]. It is predominantly metabolized in the liver with a low hepatic extraction ratio [134], mainly by CYP3A4 and UDP-glucuronosyltransferase 1A9 [135]. As a substrate for CYP3A4, regorafenib is prone for drug-drug interactions. Indeed, the administration of the strong CYP3A4 inhibitor ketoconazole and the strong CYP3A4 inducer rifampicin substantially altered regorafenib exposure [136]. Whereas eight metabolites of regorafenib could be identified, only two of these metabolites, M-2 (regorafenib N-oxide) and M-5 (N-desmethyl-regorafenib), are of particular interest since they are pharmacologically active as well [135]. The exposure of both metabolites is also dependent on a food effect. Whereas a low-fat meal increased mean M-2 and M-5 AUC by 40% and 23%, respectively, a high-fat meal decreased mean AUC by 20% and 51%, respectively [132]. Elimination of regorafenib is predominantly biliary with 71.2% of a regorafenib dose recovered in feces. Only 19.3% of the total dose was recovered in urine as water-soluble metabolites. Unchanged regorafenib was the most prominent compound found in feces (47.2% of total dose) [135]. In addition, regorafenib and the metabolites M-2 and M-5 were reported to undergo enterohepatic circulation as multiple plasma concentration peaks were observed six to eight and 24 hours after administration [135, 137]. Mean elimination half-lives of regorafenib, M-2 and M-5 were reported to be 28, 25 and 51 hours, respectively [136].

Pharmacodynamics and exposure-response relationships

As a multikinase inhibitor, regorafenib has a broad mechanism of action, targeting several protein kinases, including tyrosine kinases. It interacts with multiple pathways including tumor angiogenesis by inhibiting VEGFR subtypes 1-3 and TIE2, oncogenesis (inhibition of KIT, PDGFR, RET and BRAF) and tumor microenvironment (inhibition of PDGFR- β and FGFR) [138].

The exposure-response relationship does not exhibit a clear picture. Whereas plasma sVEGFR-2 concentrations decline with increasing regorafenib exposure, overall plasma concentrations of sVEGFRs increase [139]. However, a recent study in 34 Japanese cancer patients identified associations between the sum of regorafenib, M-2 and M-5 trough concentrations in the first therapy cycle and progression-free survival. A cut-off value of 2.9 $\mu\text{g}/\text{mL}$ was suggested [140].

Toxicity

Similar to many tyrosine kinase-targeting drugs, the most prominent dose-limiting adverse events of regorafenib are skin rash, hypertension, diarrhea and HFS [136, 137]. Whereas a relationship between regorafenib exposure and response could not be reliably established, a link between exposure and toxicity was identified in two studies in Japanese cancer patients [140, 141]. Fukudo et al. identified

that patients above a cut-off value of 4.3 $\mu\text{g}/\text{mL}$ (sum of regorafenib, M-2 and M-5 trough concentrations) had a significantly higher risk for HFS grade ≥ 2 according to CTCAE [140].

2. Aim and objectives

The overall aim of this work was to develop, evaluate and apply pharmacokinetic and pharmacodynamic/clinical outcome models in order to gain new insights and a better understanding of the pharmacokinetic-pharmacodynamic behavior of the fluoropyrimidine drugs 5FU and capecitabine. Since these models were developed in exploratory settings, it was further intended to investigate if such models were generally suitable for application to new scenarios (chapters 4 and 5) and new clinical endpoints from a pharmacometric perspective (chapter 6). A further objective was to assess the general suitability of pharmacometric modeling approaches as elements of precision medicine of 5FU. Specific objectives of the individual projects are described below.

Therapeutic drug monitoring of fluorouracil

This project (chapter 3) aimed to review the current evidence on TDM as a method for precision dosing of infusional 5FU, especially in comparison to BSA-based dosing. An important objective of this research work was to further assess the future perspectives for 5FU-TDM. In particular, the usefulness of pharmacometric modeling approaches for combination with 5FU-TDM should be investigated.

Population pharmacokinetics of combinedly administered regorafenib and capecitabine in patients with locally advanced rectal cancer

The aim of this project, presented in chapter 4, was to develop population pharmacokinetic models of regorafenib and its metabolites M-2 and M-5 as well as capecitabine and its metabolites DFUR and DFUR. It was intended to investigate if there are any potential drug-drug interactions between both drugs as they have not been administered combinedly so far. In the case of an identified drug-drug interaction, its impact should be further quantified.

Influence of skeletal muscle index on fluorouracil pharmacokinetics and toxicity

This project (chapter 5) was designed to retrospectively evaluate the relationship between the skeletal muscle index as a measure of sarcopenia and pharmacokinetics as well as toxicity of 5FU. A major aim was to extend an initially developed population pharmacokinetic model by investigating the potential influence of different skeletal muscle indices on 5FU pharmacokinetics in a covariate analysis.

Markov model of patient-reported hand-foot syndrome under capecitabine

The project described in chapter 6 was intended to develop a Markov modeling and simulation framework to describe and predict patient-reported severity of hand-foot syndrome (HFS) in patients treated with capecitabine. It was further aimed to investigate the impact of potential covariates on HFS severity. In general, based on this example, the suitability of Markov models for the simulation of the time course of patient-reported adverse event severity was assessed as this kind of clinical endpoint has not been yet investigated in a pharmacometric model in cancer patients.

3. Current status and future outlooks on therapeutic drug monitoring of fluorouracil

Eduard Schmulenson (1), Nigina Zimmermann (1), Gerd Mikus (1, 2, 3), Markus Joerger (4), Ulrich Jaehde (1)

Expert Opin Drug Metabol Toxicol 2021; 17: 1407 – 1422. DOI: 10.1080/17425255.2021.2029403

- (1) Department of Clinical Pharmacy, Institute of Pharmacy, University of Bonn, Bonn, Germany
- (2) Department of Clinical Pharmacy and Biochemistry, Institute of Pharmacy, Freie Universität Berlin, Berlin, Germany
- (3) Department of Clinical Pharmacology and Pharmacoepidemiology, University Hospital Heidelberg, Heidelberg, Germany
- (4) Department of Medical Oncology and Hematology, Cantonal Hospital St. Gallen, St. Gallen, Switzerland

Contribution: I designed the outline of the review, performed the literature search, analyzed the results of the literature search, and finally wrote the manuscript.

Introduction: Despite its use for many decades, dosing of the anticancer drug fluorouracil (5FU) is still suboptimal, as the traditionally applied body surface area (BSA)-based dosing exhibits a wide range of pharmacokinetic (PK) inter-individual variability (IIV). This IIV might be partially explained by the status of the main metabolizing enzyme dihydropyridimidine dehydrogenase (DPD). Consequently, BSA-based dosing may lead to reduced efficacy and increased risk in toxicity in a substantial proportion of patients [7, 9, 82]. Therapeutic drug monitoring (TDM) is an important tool to overcome these issues as it provides the possibility to continuously adjust a drug dose on an individual patient level. Therefore, it is potentially useful to further advance precision medicine. However, whereas the benefits of TDM of anticancer drugs are often emphasized in literature [5, 142], its implementation in routine care is still unsatisfactorily. 5FU-TDM has been investigated for over 30 years [143] but clinical implementation is similarly lacking despite manifold evidence [82]. To date, only preemptive pharmacogenetic testing of DPD status is routinely performed [96]. The aim of this review was to evaluate the current status of TDM of infusional 5FU and to highlight the latest evidence as well as the future role for 5FU-TDM as a part of precision medicine in anticancer therapy.

Methods: A comprehensive literature search was conducted in PubMed between June and September 2021. The following search terms were used: “fluorouracil” in conjunction with “therapeutic drug monitoring”, “pharmacokinetics”, “variability”, “covariate”, “pharmacodynamics”, “pharmacogenetics”, “pharmacogenomics”, “analytical methodology”, “toxicity”, “personalized medicine” and “precision medicine”. Reference sections of included articles were further screened for relevant articles. Randomized controlled trials, systematic and narrative reviews as well as prospective and retrospective observational trials were included.

Results: 5FU PK is highly variable between patients, including dose- and time-dependent elimination [89, 144, 145] in combination with a presumable DPD saturation [89, 90, 146]. BSA-based dosing led to an up to 10-fold variability in 5FU plasma concentrations [144] and even though limited influence of BSA on 5FU PK have been reported [89, 93, 147], its influence is not large enough to justify BSA-based dosing only. These circumstances are the main reasons to perform 5FU-TDM and an exposure-response/-toxicity relationship was successfully established, targeting an area under the concentration-time curve (AUC) range of 20 – 30 mg·h/L for the most commonly used 5FU-based chemotherapy regimens [82]. However, various studies showed that up to 64% of patients are underdosed, i.e. below the recommended AUC range [98, 100–102, 148–152] and about 15% are overdosed, thus frequently experiencing severe toxicity [82]. Regarding the routinely performed, pre-

therapeutic genotyping of the DPD-encoding gene, *DPYD*, four genotypes are particularly associated with severe toxicity [95]. However, they only explain a part of the genetic contribution of DPD activity-based toxicity as DPD phenotypes were poorly predicted by the four well-studied genotypes [153]. Thus, DPD phenotyping is of particular interest, but studies reported inconsistent results regarding correlations to 5FU PK and toxicity [144, 154–162], presumably due to different saturation statuses of DPD [162, 163]. Current evidence of 5FU-TDM has been comprehensively demonstrated. Still, it plays only a minor role in clinical guidelines [164–168]. Only the 2019 Guideline of the International Association of Therapeutic Drug Monitoring and Clinical Toxicology (IATDMCT) systematically summarized relevant studies and pointed out the advantages of 5FU-TDM [82]. Studies which were published after the IATDMCT guideline further strengthen the evidence for 5FU-TDM, reporting that dose adjustments according to measured 5FU plasma concentrations led to a higher proportion of patients being within the recommended AUC range [100] and patients below or above this range had a weaker response or higher incidence of toxicity, respectively [102]. Another study reported that preemptive DPD phenotyping resulted in a higher proportion of patients being underdosed, suggesting that phenotyping has to be combined with TDM in order to avoid decreased 5FU efficacy [155]. Implementation of 5FU-TDM into clinical routine still faces manifold obstacles, including availability of proper analytical methods [169], time and sampling management [82] as well as handling of plasma samples [82]. However, commercial analytical kits with sample stabilizers have been established which contribute to overcome most of these issues [98, 170]. While simple 5FU-TDM dosing algorithms for clinicians do exist [97–99, 101, 171], model-informed precision dosing has the potential to further advance 5FU therapy into the digitalized precision medicine area. By developing and applying pharmacometric models with Bayesian estimation approaches, dose adaptation during the whole course of therapy can be supported [172]. 5FU-TDM would be able to inform these models with unique patient information, i.e. measured plasma concentrations. However, the proper identification of covariates influencing 5FU PK would be crucial for such models. So far, published 5FU models could only include a very heterogeneous set of covariates [89, 92–94, 173–176]. Particularly, *DPYD* genotypes could not be successfully implemented. Only one of these studies included the measured DPD activity [173].

Discussion: Clinical uptake of 5FU-TDM is still limited. The collected evidence in this review, however, further highlights the advantages of performing 5FU-TDM compared to BSA-based dosing. As preemptive genotyping/phenotyping approaches are only able to identify a proportion of patients at risk while potentially deteriorating efficacy, a combination with TDM is of high importance. A further implementation of 5FU-TDM within a pharmacometric modeling framework has the potential to

provide additional support for clinicians in dose finding, even before initiating therapy. For that purpose, a larger patient cohort would be needed for model development and validation.

4. Population pharmacokinetic analyses of regorafenib and capecitabine in patients with locally advanced rectal cancer (SAKK 41/16 RECAP)

Eduard Schmulenson (1), Cédric Bovet (2), Regula Theurillat (2), Laurent Arthur Decosterd (3), Carlo R. Largiadèr (2), Jean-Christophe Prost (2), Chantal Csajka (4), Daniela Bärtschi (5), Matthias Guckenberger (6), Roger von Moos (7), Sara Bastian (7)*, Markus Joerger (8)*, Ulrich Jaehde (1)*

Br J Clin Pharmacol 2022; 88: 5336 – 5347. DOI: 10.1111/bcp.15461

1. Institute of Pharmacy, Department of Clinical Pharmacy, University of Bonn, Bonn, Germany
2. Department of Clinical Chemistry, Inselspital, Bern University Hospital and University of Bern, Bern, Switzerland
3. Laboratory of Clinical Pharmacology, Lausanne University Hospital and University of Lausanne, Lausanne, Switzerland
4. Clinical Pharmaceutical Sciences, Lausanne University, Lausanne, Switzerland
5. SAKK Coordinating Center, Bern, Switzerland
6. Department of Radiation Oncology, University Hospital Zurich, University of Zurich, Zurich, Switzerland
7. Cantonal Hospital Graubünden, Chur, Switzerland
8. Department of Medical Oncology and Hematology, Cantonal Hospital St. Gallen, St. Gallen, Switzerland

*contributed equally

This is an open access article under the terms of the Creative Commons Attribution-NonCommercial License: <http://creativecommons.org/licenses/by-nc/4.0/>

Contribution: I prepared the datasets used for modeling and simulation, respectively. I developed two parent drug-metabolite models, evaluated covariates including model-generated drug exposure parameters, performed simulations in order to investigate the quantitative impact of the identified drug-drug interaction, and finally wrote the manuscript.

Introduction: Patients with locally advanced rectal cancer (LARC) often experience low treatment responses as the rate of complete pathological response is reported to be 10 – 25% [177, 178]. Furthermore, about one third of these patients relapse after fluoropyrimidine-based chemoradiotherapy and surgery [179]. Therefore, there is a high medical need for this indication and in recent studies investigating tyrosine kinase inhibitors (TKI) as add-on to standard neoadjuvant chemoradiotherapy, treatment response was reported to be improved while adequate toxicity was maintained [180, 181]. In trial SAKK 41/16, the multi-TKI regorafenib was added to a capecitabine-based, neoadjuvant chemoradiotherapy for the first time. This trial included a pharmacokinetic (PK) part in order to investigate potential drug-drug interactions (DDI) between both oral anticancer drugs. Although they are metabolized by different enzymes [111, 137], a DDI analysis is nevertheless important due to overlapping toxicity, including hand-foot syndrome and diarrhea [138, 182]. Aim of this project was to develop population PK models of capecitabine, regorafenib and their metabolites (5'-deoxy-5-fluorocytidine [DFCR], 5'-deoxy-5-fluorouridine [DFUR] for capecitabine as well as M-2 [regorafenib N-oxide] and M-5 [N-desmethyl-regorafenib] for regorafenib) in LARC patients and to use these models for investigations of DDI.

Methods: SAKK 41/16 (clinicaltrials.gov number NCT02910843) was an open-label, multicentric and non-randomized phase Ib trial where the recommended dose and pathological response to regorafenib which was added to capecitabine-based chemoradiotherapy, was explored. 25 patients were recruited between March 2017 and April 2021 of which 12 patients were part of a dose-escalation cohort and the remaining patients were enrolled in an expansion cohort after dose finding. As PK sampling was only conducted in the dose-escalation cohort, data from these 12 patients was used for model development. Patients received oral capecitabine 825 mg/m² bidaily on days 1 to 38. Regorafenib was administered at three dose levels (40/80/120 mg) once daily on days 1 to 14 and days 22 to 35. Local radiotherapy was given in all patients at a total dose of 50.4 Gy. Plasma samples for analysis of regorafenib, capecitabine and their metabolites were collected on day 1 (0.5, 1, 2, 3, 4 and 6 h after dosing) followed by post-dose sampling on days 2, 4, 8, 15, 22, 29 and 36. Population PK analysis of the concentration-time data was performed using the nonlinear mixed-effect modeling software NONMEM® [183]. Separate parent-metabolite models for regorafenib and capecitabine, respectively, were developed in a sequential manner [184]. The established base models were used

to generate drug exposure parameters. In a covariate analysis, generated concentrations over time and cumulative area under the curve (AUC) over time of regorafenib, M-2 and M-5 were tested on the clearance of capecitabine and its metabolites, and the same PK parameters of capecitabine and metabolites were also tested on the clearance of regorafenib and its metabolites. Demographic data (sex, age, body weight, body surface area), bilirubin and hemoglobin were tested as covariates as well. Goodness-of-fit plots, prediction-corrected visual predictive checks [185] and bootstrap analysis were used for model evaluation. The final population PK models were used for simulation analyses. Here, the quantitative impact of potential covariates including DDIs on the PK of capecitabine, regorafenib or their metabolites were analyzed.

Results: Plasma concentrations of capecitabine, DFCR and DFUR were best characterized by one-compartment models and absorption was described by parallel first- and zero-order processes. Flip-flop PK was observed for all three compounds as well. Apparent capecitabine clearance was 286 L/h (relative standard error [RSE] 14.9%, inter-individual variability [IIV] 40.1%). The covariate analysis revealed that capecitabine clearance was significantly reduced by regorafenib cumulative AUC (median reduction of 45.6%) as exponential covariate (estimate $-4.10 \cdot 10^{-4}$, RSE 17.8%). Regorafenib, M-2 and M-5 plasma concentrations were best described by two-compartment models with transit compartment absorption [186]. Apparent regorafenib clearance was 1.94 L/h (RSE 12.1%, IIV 38.1%). Here, no covariates were identified. Simulation analyses revealed significantly negative associations between capecitabine clearance and regorafenib exposure. While capecitabine exposure was reduced with higher regorafenib dosage, DFCR and DFUR exposures were similar across the dose range.

Discussion: This is the first study which evaluated the combined administration of regorafenib and capecitabine in LARC patients. Both developed population PK models were structurally similar to previously published models from literature [112, 187–189]. However, the established capecitabine absorption model differed from published ones as its absorption is highly variable in general [88, 112, 188, 189] and may occur from different sites [113] which may be an explanation for the two identified absorption processes. Moreover, an implementation of a reported enterohepatic circulation of regorafenib and its metabolites [187] was not supported by the data from this study, presumably due to model overparametrization and inadequate sampling times [137]. The negative influence of regorafenib cumulative AUC on capecitabine clearance would translate into a reduced formation of active metabolites of capecitabine, presumably due to drug transporter inhibition [114, 133]. However, as DFCR and DFUR exposure remained unaffected, the same should be assumed for fluorouracil which is formed by DFUR. In conclusion, the developed models and the identified covariate effect demonstrated a negligible DDI between both regorafenib and capecitabine.

5. Influence of the skeletal muscle index on pharmacokinetics and toxicity of fluorouracil

Eduard Schmulenson (1)*, Nigina Zimmermann (1)*, Lothar Müller (2), Stefanie Kapsa (1), Iryna Sihinevich (1), Ulrich Jaehde (1)

Cancer Med 2023; 12: 2580 – 2589. DOI: 10.1002/cam4.5118

1. Department of Clinical Pharmacy, Institute of Pharmacy, University of Bonn, Bonn, Germany
2. Onkologie UnterEms, Leer, Germany

*contributed equally

This is an open access article under the terms of the Creative Commons Attribution License:
<https://creativecommons.org/licenses/by/4.0/>

Contribution: I prepared the dataset used for modeling, extended and externally validated an existing population pharmacokinetic model, evaluated covariates, evaluated the final model, performed logistic regression analyses, and finally wrote the manuscript. Nigina Zimmermann shared this publication as a co-first author due to her contributions towards quantification of skeletal muscle indices, dataset preparation, and statistical analyses.

Introduction: The body composition of patients has been associated with tolerability and effectiveness of anticancer therapy. In particular, sarcopenia in cancer patients was reported to be associated with low overall survival and higher toxicity [19–23]. Sarcopenia is usually defined by a reduction in skeletal muscle index (SMI) which is calculated by the total muscle cross-sectional area at the third lumbar vertebra (L3) normalized to the squared patient's height (cm^2/m^2) [24]. As a hydrophilic drug, the volume of distribution of 5FU is highly correlated with lean body mass (LBM) which includes muscle mass [25]. 5FU is usually dosed according to the patient's body surface area (BSA) which, however, does not account for changes in muscle status. Therefore, there is a particular interest in assessing the patient's body composition [32]. In fact, different measures of body composition (total body water, fat-free mass, dose per kg LBM) revealed associations to 5FU pharmacokinetics (PK) and toxicity [26, 30, 31]. The aim of this study was to assess the influence of the SMI as a metric for sarcopenia on the PK and toxicity of 5FU.

Methods: Patients under a 5FU-based, infusional chemotherapy from the oncological practice UnterEms in Leer, Germany, were retrospectively analyzed. Patients with documented therapeutic drug monitoring (TDM) of 5FU and at least one computed tomography (CT) scan of the L3 area were included. 5FU plasma concentrations were obtained at steady-state and abdominal skeletal muscle areas were quantified in Hounsfield units for the psoas major muscle, back and total skeletal muscle to determine the SMI. For the latter, an automated segmentation method was used additionally. CT image analysis was performed with the software sliceOmatic® [190]. The influence of the different SMI measures on 5FU PK was analyzed in an initially developed population PK model of 5FU, which was based on data from Wilhelm et al. [98]. Different covariates, including age, sex, BSA and infusion time were tested on 5FU clearance and volume of distribution after development of the base model. This final covariate model was then applied to the dataset of this study. SMI measures were individually tested as covariates on PK parameters of 5FU. Model development was performed in NONMEM® [183]. For model evaluation, goodness-of-fit plots, prediction-corrected visual predictive checks [185] and bootstrap analyses were used. Furthermore, regression analyses were performed to analyze the influence of SMI measures on the probability of clinically relevant adverse events (Common Terminology Criteria for Adverse Events [CTCAE] grades ≥ 2). Here, odds ratios were

calculated to assess the relative probability to develop an adverse event grade ≥ 2 when the SMI increases by one unit.

Results: A total of 111 patients with available CT images and 5FU-TDM were included for analysis. First, an initial population PK model based on data from the study of Wilhelm et al. [98] was developed which consisted of a one-compartment model with linear elimination. Due to model instabilities, estimates of the volume of distribution and its inter-individual variability (IIV) had to be fixed to previously estimated values which were based on analyses of rich PK data [92, 191, 192]. Therefore, volume of distribution could not be used for covariate analysis and all covariates were tested on clearance only. BSA was found to be the only significant covariate on 5FU clearance. The subsequent application of this model on the dataset from this study revealed that all four SMI parameters showed a significant improvement of the model fit. However, IIV of 5FU clearance was only slightly reduced whereas the SMI of the back muscle showed the largest reduction (-1.1 percentage points). As the inclusion of the SMI of the back muscle also showed the best model fit, this parameter was chosen for the final model. The logistic regression analysis showed that lower SMI values of the back muscle increased the probability for polyneuropathy and lower SMI of the psoas increased the probability for fatigue. An increase of the respective SMI by $1 \text{ cm}^2/\text{m}^2$ decreased the probability of developing the identified adverse event \geq grade 2 by 48% and 85%, respectively.

Discussion: This is the first study evaluating the influence of different SMI measures on 5FU pharmacokinetics and toxicity. The developed population PK model described the observed data well even though it was not possible to estimate the volume of distribution. The inclusion of the SMI of the back muscle led to the largest improvement of the model fit which deserves further investigation on physiological plausibility. While this finding gives additional hints that body composition may influence PK of 5FU and other anticancer drugs [26–29] the minor reduction of the IIV of 5FU clearance revealed that the usage of SMI for dose adjustment purposes may be of limited value. In fact, the inclusion of BSA had a higher impact on 5FU clearance in the present model. The findings of the logistic regression analysis were generally in accordance with previous studies [30, 31, 148]. The identified higher probability of the occurrence of clinically relevant polyneuropathy with decreasing SMI of the back muscle, however, deserves further investigation. As the psoas muscle is necessary for everyday movement, the reduction of its SMI may be an explanation for the identified increase in the probability of clinically relevant fatigue. In conclusion, this study gives first hints that the SMI as a measure of body composition may be associated with PK and toxicity of 5FU.

6. Evaluation of patient-reported severity of hand–foot syndrome under capecitabine using a Markov modeling approach

Eduard Schmulenson (1), Linda Krolop (1), Sven Simons (1), Susanne Ringsdorf (1), Yon-Dschun Ko (2), Ulrich Jaehde (1)

Cancer Chemother Pharmacol 2020; 86: 435 – 444. DOI: 10.1007/s00280-020-04128-7

1. Institute of Pharmacy, Department of Clinical Pharmacy, University of Bonn, Bonn, Germany
2. Department of Internal Medicine, Evangelische Kliniken Bonn gGmbH, Johanniter Hospital, Bonn, Germany

This is an open access article under the terms of the Creative Commons Attribution License:
<https://creativecommons.org/licenses/by/4.0/>

Contribution: I prepared the datasets used for modeling and simulation, respectively. I developed a population Markov model based on patient-reported severity of hand-foot syndrome over time, evaluated covariates, performed simulations in order to investigate the impact of dose adjustments on adverse event severity, and finally wrote the manuscript.

Introduction: As reports of diverging assessments of adverse events between cancer patients and clinicians have become more numerous [51, 52, 54] the patient's perspective has gained a higher importance in managing toxicity of anticancer drug therapy. This was a motivation for developing a patient-reported outcomes (PRO) version of the widely used Common Terminology Criteria for Adverse Events (CTCAE) [48, 55] where toxicity is reported on a categorical scale. One possibility to establish a relationship between drug exposure and such categorical toxicity data are pharmacometric Markov models which aim to estimate the probability for the respective adverse event grade. Markov models are widely applied in the field of pharmacometrics nowadays [59, 62–65, 193]. In this work, the severity of hand-foot syndrome (HFS) under treatment with capecitabine was modeled using a Markov approach as HFS is reported to be the main dose-limiting toxicity under this therapy [119, 194]. Although a Markov model for capecitabine-associated HFS was already established [195], this model could only consider clinician-based CTCAE grades. Therefore, it was meaningful to provide an extension towards PRO. The aim of this project was to develop a modeling and simulation framework to describe and predict patient-reported HFS severity in patients treated with capecitabine. Based on this example, the general suitability of Markov models to simulate the time course of patient-reported toxic symptoms should be assessed.

Methods: For model development, raw data from two prospective, observational studies which included 150 capecitabine-naïve patients [196, 197] were used. HFS severity was assessed by patients using an in-house questionnaire where HFS severity grades (0 to 3) were described based on CTCAE grades version 3.0 [198]. After each conducted cycle patients were asked to fill out the questionnaire. They were observed up to six three-week therapy cycles. A minimal continuous-time Markov model (mCTMM) [66] was applied to analyze the HFS time course using the nonlinear mixed effects modeling software NONMEM [183]. The developed mCTMM consisted of a compartmental structure with each compartment representing one HFS grade. Probabilities of experiencing one of the grades were modeled as compartment amounts and described by differential equations consisting of transition rate constants between adjacent grades. The Markov property was introduced by setting the compartment amount of the observed grade to 1 and the other amounts to 0 before the next observation. A feature of the mCTMM is the assumption that the transition rates are independent of the grade, only the mean equilibration time (MET) was introduced as additional parameter which characterizes transition rates across different grades [66]. The calculation of probabilities was similar

to a proportional odds model combined with logit transformation in order to conveniently estimate model parameters describing HFS severity (logit intercepts, linear covariate functions, inter-individual variability) [58, 66]. After establishing the base mCTMM, a covariate analysis was conducted. Effects of dose and time as well as patient-related covariates (age, sex, overall adherence, combination therapy, tumor entity) were tested on MET and the logit intercept parameter. Model evaluation included visual predictive checks (VPC) [199] and bootstrap analysis. Model applicability was evaluated by performing a simulation study to assess the appropriateness of the commonly applied capecitabine dose adjustment strategy from the summary of product characteristics (SmPC) [200]. Probabilities of HFS grade 0 to 3 in virtual patients at a starting dose of 1250 mg/m² capecitabine with and without dose adjustments were simulated and compared. Lastly, the predictive performance of the developed model was assessed by simulating HFS severity based on Bayesian estimates of inter-individual variability for each conducted therapy cycle. The simulated grades were then compared to the observed ones by calculating positive and negative predictive values (PPV, NPV) which indicated the predictability of HFS grades 2/3 and 0/1, respectively.

Results: A mCTMM was successfully developed and applied on the dataset. A linear effect of the absolute daily dose of capecitabine was found to be the only statistically significant covariate on the logit intercept, indicating higher HFS severity probability with a higher dose. The VPC showed an accurate description of the observed data by the model whereas the bootstrap indicated a robust estimation of model parameters. The simulation study demonstrated a reduction of severe HFS (grade 3) while increasing the probabilities of HFS grades 0 and 1 using the dose adjustment strategy according to the SmPC. Calculated PPV and NPV values were rather low, indicating a poor predictive performance on an individual patient level.

Discussion: This is the first study evaluating the time course of patient-reported adverse event severity in clinical routine during anticancer therapy with a Markov modeling approach. By using the mCTMM as a parsimonious version of the standard continuous-time Markov models, a robust and well-performing model was developed despite the sparse-data situation. The identification of the absolute daily capecitabine dose as predictor of HFS severity was in line with previous studies [201, 202]. Whereas population-based recommendations can be supported using this model, predictive performance on an individual level was rather poor. Possible limitations which contributed to this circumstance are the low grading frequency by the patients [67], the overall limited number of observations per patient, the limited number of covariates and the assumption that the observed, patient-reported grade equaled the “true” grade [68]. In conclusion, mCTMM can be set up using PRO data. This modeling framework may assist in the optimization of dosage regimens on the population level aiming at minimizing symptom burden during anticancer drug therapy.

7. Conclusions

The main objective of this thesis was to develop and apply various pharmacometric modeling approaches in order to improve anticancer therapy with the fluoropyrimidines 5FU and capecitabine by assessing their pharmacokinetic and pharmacodynamic behavior. Population pharmacokinetic modeling was successfully applied as it was able to explore drug-drug interactions of a new drug combination consisting of capecitabine and regorafenib and the potential influence of the skeletal muscle index on pharmacokinetics of 5FU. Markov modeling was successfully applied as well in order to link capecitabine dosage to the time course of drug-induced, patient-reported hand-foot syndrome. In addition, it was aimed to review the current evidence and future perspectives on therapeutic drug monitoring of 5FU as a tool for dose individualization and how pharmacometric models may help to achieve individualized 5FU therapy. The performed analyses as well as the literature review should be seen as complimentary approaches to contribute to increasing efficacy and safety for cancer patients under therapy with fluoropyrimidines. Overall, an integrated pharmacometric framework which is continuously improved by constantly providing routinely measured drug plasma concentrations and real-world patient data would be the ultimate goal. Using such a framework would allow for a strong clinical decision support by performing simulations for individual patients. The major results and conclusions of the individual projects are summarized below.

Therapeutic drug monitoring of fluorouracil

Although the use of 5FU is well-established for treatment of various solid tumors, dosing has been suboptimal with a substantial proportion of patients being over- or underdosed. The literature review conducted in this project showed that therapeutic drug monitoring (TDM) of 5FU is a powerful tool to individualize therapy in clinical routine. As for several decades, studies demonstrated the advantages of 5FU-TDM and new studies further revealed significant benefits regarding 5FU therapy response and safety. Whereas pharmacogenetic testing for risk variants of the main metabolizing enzyme dihydropyrimidine dehydrogenase (DPD) is a well-established part of precision medicine of 5FU, the results of this review strongly support that TDM should also be a vital part of this area. Our review demonstrated that genotyping is only able to explain parts of variability in 5FU pharmacokinetics. As there is a clear relationship between 5FU exposure and response, accounting for this variability is a crucial task which can only be satisfactorily solved in conjunction with TDM. The topic of precision dosing in oncology is gaining more attention in the recent years as an emerging number of studies has assessed the benefits of TDM, especially for oral anticancer drugs [4, 142, 203–206]. Furthermore, it was shown that pharmacometric modeling approaches have a great potential to significantly contribute towards precision dosing of 5FU. However, the currently published population

pharmacometric models exhibit very heterogeneous 5FU pharmacokinetics, presumably due to different administration schedules, tumor entities, genotyping/phenotyping methods of DPD as well as small patient cohorts. Choosing a proper population size, modern continuous infusion regimens of 5FU, consistent DPD testing methods as well as coupling the developed model to electronic health records would provide a basis for a valuable pharmacometric framework. Such a model would also be able to suggest a proper starting dose for initiation of 5FU therapy while continuously improving individual patient predictions via TDM.

Population pharmacokinetics of combinedly administered regorafenib and capecitabine in patients with locally advanced rectal cancer

Current treatment options for locally advanced rectal cancer result in rather low response rates and a high proportion of relapses. This emphasizes the need for new treatment strategies. In the present study, two oral drugs which are approved for the use in colorectal cancer, capecitabine and regorafenib, were combinedly administered for the first time in a clinical study. By developing population pharmacokinetic models for both drugs and their main metabolites, a significant negative influence of regorafenib exposure, expressed as cumulative area under the plasma concentration-time curve over time, on capecitabine clearance was identified. Theoretically, this would result in a higher capecitabine exposure and a reduced formation of its metabolites, potentially reducing drug efficacy as the investigated metabolites are precursors of 5FU. However, a subsequently conducted simulation analysis revealed that this drug-drug interaction was of negligible clinical relevance as the exposure of the capecitabine metabolites remained virtually unaffected. This translates into an unchanged exposure of 5FU which should ultimately result in unchanged efficacy. Since capecitabine-associated adverse events are mainly attributed to its metabolites [207], a reduced capecitabine clearance and hence a higher exposure is expected to be of negligible relevance as well. It should be noted, however, that a pharmacodynamic analysis regarding efficacy and safety of this drug combination has not been conducted by the time of publication of this project. Therefore, the clinical implications of the present analysis are yet to be investigated for the analyzed patient cohort.

So far, the underlying mechanisms of the identified interaction are unknown as both drugs do not share the same metabolizing enzymes. It is however possible that the breast cancer resistance protein (BCRP) which is an active drug transporter of the ATP-binding cassette (ABC) family might be involved. It has been reported that regorafenib inhibits BCRP [133] and there are potential hints that capecitabine is an ABC transporter substrate [114–116]. These developed models could serve as a basis for a future double-arm study. One study arm would consist of capecitabine monotherapy and the other arm of the combination of capecitabine and regorafenib in order to further investigate the

clinical relevance of the present finding. Such a study should also include the approved regorafenib dosage of 160 mg daily.

Influence of skeletal muscle index on fluorouracil pharmacokinetics and toxicity

Whereas the nutrition and muscle statuses and thus, the body composition of cancer patients are widely recognized as cornerstones of a successful anticancer therapy and good prognosis, their influence on dosing of anticancer drugs has not been comprehensively researched so far. Most importantly, the widely performed body surface area (BSA)-based dosing of anticancer drugs such as 5FU does not account for changes in body composition. As there have been hints that different measures of body composition were potential predictors of 5FU pharmacokinetics and toxicity [26, 30, 31], it was expected that the skeletal muscle index (SMI) exhibited similar influences. In fact, this retrospective study revealed that all investigated SMI measures were significant predictors for 5FU pharmacokinetics in a population pharmacokinetic model. Whereas the most significant SMI influence on 5FU clearance was identified by including the SMI of the back muscle, it could only explain a tiny portion of inter-individual variability of 5FU clearance. BSA was able to explain a much larger portion of this variability in this study. A prospective study, in which 5FU pharmacokinetics and SMI measures are analyzed, along with more extensive 5FU sampling (in order to obtain plasma concentrations before steady-state for estimating 5FU volume of distribution), should provide additional insights. The SMI of the back muscle was a predictor for clinically relevant polyneuropathy and lower SMI of the psoas increased the probability for fatigue. Whereas development of polyneuropathy deserves further investigation, the decrease of the psoas SMI can indeed be linked to fatigue as the psoas muscle is important for everyday movement. However, the performed logistic regression analysis was focused on evaluating the general susceptibility of experiencing clinically relevant adverse events depending on muscle status in patients treated with a 5FU-based chemotherapy. Concomitant chemotherapy may contribute to the identified adverse events. However, only qualitative information of the administration of other drugs was available. By assessing the influence of individual drug pharmacokinetics on adverse event development in a future study, it would be possible to distinguish between the respective individual contributions of these drugs.

Even in the case that the findings of this study are confirmed in future prospective studies, the overall translatability of the results into clinical practice remains a crucial aspect. In fact, CT imaging of cancer patients is frequently performed in clinical routine, e.g. for tumor staging, in contrast to assessments of muscle status. Nevertheless, the availability of such longitudinally collected data would allow for the continuous assessment of the patient's body composition. 5FU-TDM and adverse event grading could be integrated into these assessments, ideally within a pharmacometric modeling framework. Such a framework could consist of a population pharmacokinetic model in combination with an

adverse event grade model, e.g. a proportional odds model [58] or a Markov model (as presented in chapter 6). It could be used for predicting individual 5FU concentration-time courses and adverse event severity depending on SMI.

Markov model of patient-reported hand-foot syndrome under capecitabine

Hand-foot syndrome (HFS) is one of the major causes for dose reductions or treatment interruptions as well as discontinuations under capecitabine. As patient-reported symptom burden significantly differs from the clinician's assessment, a model-based approach which specifically describes the patient's perspective would be of high interest. To date, this is the first study in which cancer patient-reported adverse event severity was analyzed with a Markov modeling approach. A significant influence of absolute daily capecitabine dose on the probability of higher adverse event grades was identified. Whereas this finding was rather predictable [201, 202], it was nonetheless an important study to demonstrate that Markov models are suitable to describe patient-reported burden of HFS in a clinical setting. The developed model described the observed adverse event severity data well and was suitable to confirm population-based recommendations of dose adjustments as shown in the conducted simulation study. However, the individual prediction performance of the developed model was rather poor, particularly due to the low number of observations per patient along with long time intervals between these observations (grading was performed once per three-week cycle). It is conceivable that such models can be implemented into a pharmacometric framework which is coupled to the patient's electronic health record as described in chapter 3 of this thesis. In order to apply pharmacometric Markov models to real-world patients, it is important to consider the continuous-time structure of these models. As time intervals between patient-reported observations may vary in clinical routine, choosing a discrete-time Markov model would be suboptimal. These models generally assume equal time intervals between two neighboring observations, regardless of the actual time periods [66]. Whereas such models can be used in a regulated setting of a clinical trial, they may potentially lack important information in a real-world scenario. Nevertheless, it should be aimed towards a more frequent grading of symptom burden. By combining such a pharmacometric framework with a recommended weekly grading [208] which can now be conveniently performed with electronic questionnaires [56, 209, 210], the potential of continuous-time Markov models can be vastly increased in the future.

8. Summary

The fluoropyrimidine drugs fluorouracil (5FU) and capecitabine are widely used for the treatment of various solid tumors. Despite the long-term clinical experience with these drugs a substantial proportion of patients is suboptimally dosed, leading to a highly variable treatment outcome and toxicity, respectively. Pharmacometric modeling is potentially useful to address these issues and to provide optimal dose regimens for individual patients. The aim of this work was to develop and apply pharmacometric models to gain a better understanding of the pharmacokinetics (PK) and pharmacodynamics of 5FU and capecitabine in order to improve anticancer therapy. These models were used for simulation of different dosing regimens investigating the influence of various sources of variability.

A comprehensive literature review on the current status and future outlooks on therapeutic drug monitoring (TDM) of 5FU was performed. It revealed strong supporting evidence for conducting a 5FU-TDM to enable optimal therapy response and safety, particularly in combination with routine pharmacogenetic testing. Incorporating pharmacometric models into clinical routine can potentially assist clinicians in finding a proper 5FU dose even before starting therapy.

Population PK models of capecitabine, the tyrosine kinase inhibitor regorafenib and their respective metabolites were developed to investigate potential drug-drug interactions between both drugs. The impact of the interaction was quantified via simulation analyses. Covariate analyses of the successfully developed models revealed that the cumulative area under the curve of regorafenib reduced capecitabine clearance estimates. Simulations showed significantly negative associations between regorafenib exposure and capecitabine clearance. However, the effect on the exposure of capecitabine metabolites was negligible.

The muscle status, expressed as skeletal muscle index (SMI), was assessed as covariate in a population PK model of 5FU as well as its influence on the development of 5FU-associated adverse events by regression analyses. The SMI of the back muscle was found to be a significant covariate on 5FU clearance. However, it was only able to explain a small portion of variability. Lower SMI values of the back muscle increased the probability for polyneuropathy and lower SMI of the psoas increased the probability for fatigue.

Capecitabine-induced and patient-reported severity of hand-foot syndrome (HFS) was analyzed with a Markov modeling approach. Different covariates were investigated as potential predictors on symptom burden. Simulations were performed to assess the influence of dose adjustments on the time course of HFS. The successfully developed Markov model revealed that the absolute capecitabine

dose was a significant predictor for HFS. Simulations showed a reduction of severe HFS when dose adjustments were performed according to HFS severity.

In conclusion, this work demonstrated the potential of pharmacometric models assisting in dose adjustment strategies under therapy with 5FU and capecitabine.

9. References

1. National Cancer Institute. Precision Medicine. Available at: <https://www.cancer.gov/publications/dictionaries/cancer-terms/def/precision-medicine>. Accessed 27 Jan 2022.
2. Food and Drug Administration. Precision Medicine 2018. Available at: <https://www.fda.gov/medical-devices/in-vitro-diagnostics/precision-medicine>. Accessed 27 Jan 2022.
3. Karapetis CS, Khambata-Ford S, Jonker DJ, et al. K-ras mutations and benefit from cetuximab in advanced colorectal cancer. *N Engl J Med* 2008; 359: 1757–1765.
4. Groenland SL, Mathijssen RHJ, Beijnen JH, et al. Individualized dosing of oral targeted therapies in oncology is crucial in the era of precision medicine. *Eur J Clin Pharmacol* 2019; 75: 1309–1318.
5. Paci A, Veal G, Bardin C, et al. Review of therapeutic drug monitoring of anticancer drugs part 1--cytotoxics. *Eur J Cancer* 2014; 50: 2010–2019.
6. Du Bois D, Du Bois EF. A formula to estimate the approximate surface area if height and weight be known. *Arch Intern Med* 1916; 17: 863–871.
7. Mathijssen RHJ, Jong FA de, Loos WJ, et al. Flat-fixed dosing versus body surface area based dosing of anticancer drugs in adults: does it make a difference? *Oncologist* 2007; 12: 913–923.
8. Felici A, Verweij J, Sparreboom A. Dosing strategies for anticancer drugs: the good, the bad and body-surface area. *Eur J Cancer* 2002; 38: 1677–1684.
9. Beumer JH, Chu E, Salamone SJ. Body-surface area-based chemotherapy dosing: appropriate in the 21st century? *J Clin Oncol* 2012; 30: 3896–3897.
10. Baker SD, Verweij J, Rowinsky EK, et al. Role of body surface area in dosing of investigational anticancer agents in adults, 1991-2001. *J Natl Cancer Inst* 2002; 94: 1883–1888.
11. Rousseau A, Marquet P. Application of pharmacokinetic modelling to the routine therapeutic drug monitoring of anticancer drugs. *Fundam Clin Pharmacol* 2002; 16: 253–262.
12. Wicha SG, Kees MG, Solms A, et al. TDMx: a novel web-based open-access support tool for optimising antimicrobial dosing regimens in clinical routine. *Int J Antimicrob Agents* 2015; 45: 442–444.
13. Lis CG, Gupta D, Lammersfeld CA, et al. Role of nutritional status in predicting quality of life outcomes in cancer—a systematic review of the epidemiological literature. *Nutr J* 2012; 11: 27.
14. Ravasco P, Monteiro-Grillo I, Camilo ME. Does nutrition influence quality of life in cancer patients undergoing radiotherapy? *Radiother Oncol* 2003; 67: 213–220.

15. Schwedhelm C, Boeing H, Hoffmann G, et al. Effect of diet on mortality and cancer recurrence among cancer survivors: a systematic review and meta-analysis of cohort studies. *Nutr Rev* 2016; 74: 737–748.
16. Cruz-Jentoft AJ, Bahat G, Bauer J, et al. Sarcopenia: revised European consensus on definition and diagnosis. *Age Ageing* 2019; 48: 16–31.
17. Prado CM, Purcell SA, Laviano A. Nutrition interventions to treat low muscle mass in cancer. *J Cachexia Sarcopenia Muscle* 2020; 11: 366–380.
18. Haehling S von, Morley JE, Anker SD. An overview of sarcopenia: facts and numbers on prevalence and clinical impact. *J Cachexia Sarcopenia Muscle* 2010; 1: 129–133.
19. Martin L, Birdsell L, Macdonald N, et al. Cancer cachexia in the age of obesity: skeletal muscle depletion is a powerful prognostic factor, independent of body mass index. *J Clin Oncol* 2013; 31: 1539–1547.
20. Prado CMM, Lieffers JR, McCargar LJ, et al. Prevalence and clinical implications of sarcopenic obesity in patients with solid tumours of the respiratory and gastrointestinal tracts: a population-based study. *The Lancet Oncology* 2008; 9: 629–635.
21. Ryan AM, Prado CM, Sullivan ES, et al. Effects of weight loss and sarcopenia on response to chemotherapy, quality of life, and survival. *Nutrition* 2019; 67-68: 110539.
22. Caan BJ, Cespedes Feliciano EM, Prado CM, et al. Association of Muscle and Adiposity Measured by Computed Tomography With Survival in Patients With Nonmetastatic Breast Cancer. *JAMA Oncol* 2018; 4: 798–804.
23. Shachar SS, Williams GR, Muss HB, et al. Prognostic value of sarcopenia in adults with solid tumours: A meta-analysis and systematic review. *Eur J Cancer* 2016; 57: 58–67.
24. Baracos VE, Arribas L. Sarcopenic obesity: hidden muscle wasting and its impact for survival and complications of cancer therapy. *Annals of Oncology* 2018; 29: ii1-ii9.
25. Morgan DJ, Bray KM. Lean body mass as a predictor of drug dosage. Implications for drug therapy. *Clin Pharmacokinet* 1994; 26: 292–307.
26. Gusella M, Toso S, Ferrazzi E, et al. Relationships between body composition parameters and fluorouracil pharmacokinetics. *Br J Clin Pharmacol* 2002; 54: 131–139.
27. Mir O, Coriat R, Blanchet B, et al. Sarcopenia predicts early dose-limiting toxicities and pharmacokinetics of sorafenib in patients with hepatocellular carcinoma. *PLoS One* 2012; 7: e37563.
28. Massicotte M-H, Borget I, Broutin S, et al. Body composition variation and impact of low skeletal muscle mass in patients with advanced medullary thyroid carcinoma treated with

- vandetanib: results from a placebo-controlled study. *J Clin Endocrinol Metab* 2013; 98: 2401–2408.
29. Prado CMM, Lima ISF, Baracos VE, et al. An exploratory study of body composition as a determinant of epirubicin pharmacokinetics and toxicity. *Cancer Chemother Pharmacol* 2011; 67: 93–101.
 30. Ali R, Baracos VE, Sawyer MB, et al. Lean body mass as an independent determinant of dose-limiting toxicity and neuropathy in patients with colon cancer treated with FOLFOX regimens. *Cancer Med* 2016; 5: 607–616.
 31. Prado CMM, Baracos VE, McCargar LJ, et al. Body composition as an independent determinant of 5-fluorouracil-based chemotherapy toxicity. *Clin Cancer Res* 2007; 13: 3264–3268.
 32. Prado CMM, Maia YLM, Ormsbee M, et al. Assessment of nutritional status in cancer—the relationship between body composition and pharmacokinetics. *Anticancer Agents Med Chem* 2013; 13: 1197–1203.
 33. Mould DR, Upton RN. Basic concepts in population modeling, simulation, and model-based drug development. *CPT Pharmacometrics Syst Pharmacol* 2012; 1: e6.
 34. Mould DR, Upton RN. Basic concepts in population modeling, simulation, and model-based drug development-part 2: introduction to pharmacokinetic modeling methods. *CPT Pharmacometrics Syst Pharmacol* 2013; 2: e38.
 35. Owen JS, Fiedler-Kelly J. *Introduction to Population Pharmacokinetic / Pharmacodynamic Analysis with Nonlinear Mixed Effects Models*. Hoboken, New Jersey: John Wiley & Sons, Inc; 2014.
 36. Shore N, Zurth C, Fricke R, et al. Evaluation of Clinically Relevant Drug-Drug Interactions and Population Pharmacokinetics of Darolutamide in Patients with Nonmetastatic Castration-Resistant Prostate Cancer: Results of Pre-Specified and Post Hoc Analyses of the Phase III ARAMIS Trial. *Target Oncol* 2019; 14: 527–539.
 37. Imbs D-C, Diéras V, Bachelot T, et al. Pharmacokinetic interaction between pazopanib and cisplatin regimen. *Cancer Chemother Pharmacol* 2016; 77: 385–392.
 38. Biomarkers Definitions Working Group. Biomarkers and surrogate endpoints: preferred definitions and conceptual framework. *Clin Pharmacol Ther* 2001; 69: 89–95.
 39. Sáez-Belló M, Mangas-Sanjuán V, Martínez-Gómez MA, et al. Evaluation of ABC gene polymorphisms on the pharmacokinetics and pharmacodynamics of capecitabine in colorectal patients: Implications for dosing recommendations. *Br J Clin Pharmacol* 2021; 87: 905–915.

40. Yin A, Ettaieb MHT, Swen JJ, et al. Population Pharmacokinetic and Pharmacogenetic Analysis of Mitotane in Patients with Adrenocortical Carcinoma: Towards Individualized Dosing. *Clin Pharmacokinet* 2021; 60: 89–102.
41. Klopp-Schulze L, Mueller-Schoell A, Neven P, et al. Integrated Data Analysis of Six Clinical Studies Points Toward Model-Informed Precision Dosing of Tamoxifen. *Front Pharmacol* 2020; 11: 283.
42. Puzkiel A, Arellano C, Vachoux C, et al. Model-Based Quantification of Impact of Genetic Polymorphisms and Co-Medications on Pharmacokinetics of Tamoxifen and Six Metabolites in Breast Cancer. *Clin Pharmacol Ther* 2021; 109: 1244–1255.
43. Schindler E, Amantea MA, Karlsson MO, et al. A Pharmacometric Framework for Axitinib Exposure, Efficacy, and Safety in Metastatic Renal Cell Carcinoma Patients. *CPT Pharmacometrics Syst Pharmacol* 2017; 6: 373–382.
44. Hansson EK, Amantea MA, Westwood P, et al. PKPD Modeling of VEGF, sVEGFR-2, sVEGFR-3, and sKIT as Predictors of Tumor Dynamics and Overall Survival Following Sunitinib Treatment in GIST. *CPT Pharmacometrics Syst Pharmacol* 2013; 2: e84.
45. Diekstra MH, Fritsch A, Kanefendt F, et al. Population Modeling Integrating Pharmacokinetics, Pharmacodynamics, Pharmacogenetics, and Clinical Outcome in Patients With Sunitinib-Treated Cancer. *CPT Pharmacometrics Syst Pharmacol* 2017; 6: 604–613.
46. Netterberg I, Li C-C, Molinero L, et al. A PK/PD Analysis of Circulating Biomarkers and Their Relationship to Tumor Response in Atezolizumab-Treated non-small Cell Lung Cancer Patients. *Clin Pharmacol Ther* 2019; 105: 486–495.
47. Marshall SF, Burghaus R, Cosson V, et al. Good Practices in Model-Informed Drug Discovery and Development: Practice, Application, and Documentation. *CPT Pharmacometrics Syst Pharmacol* 2016; 5: 93–122.
48. National Cancer Institute. Common Terminology Criteria for Adverse Events (CTCAE). Available at: https://ctep.cancer.gov/protocoldevelopment/electronic_applications/ctc.htm. Accessed 27 Jan 2022.
49. Basch E, Jia X, Heller G, et al. Adverse symptom event reporting by patients vs clinicians: relationships with clinical outcomes. *J Natl Cancer Inst* 2009; 101: 1624–1632.
50. Pakhomov SV, Jacobsen SJ, Chute CG, et al. Agreement between patient-reported symptoms and their documentation in the medical record. *Am J Manag Care* 2008; 14: 530–539.
51. Galizia D, Milani A, Geuna E, et al. Self-evaluation of duration of adjuvant chemotherapy side effects in breast cancer patients: A prospective study. *Cancer Med* 2018; 7: 4339–4344.

52. Veitch ZW, Shepshelovich D, Gallagher C, et al. Underreporting of Symptomatic Adverse Events in Phase I Clinical Trials. *J Natl Cancer Inst* 2021; 113: 980–988.
53. Moon DH, Chera BS, Deal AM, et al. Clinician-observed and patient-reported toxicities and their association with poor tolerance to therapy in older patients with head and neck or lung cancer treated with curative radiotherapy. *J Geriatr Oncol* 2019; 10: 42–47.
54. Atkinson TM, Ryan SJ, Bennett AV, et al. The association between clinician-based common terminology criteria for adverse events (CTCAE) and patient-reported outcomes (PRO): a systematic review. *Support Care Cancer* 2016; 24: 3669–3676.
55. Basch E, Reeve BB, Mitchell SA, et al. Development of the National Cancer Institute’s patient-reported outcomes version of the common terminology criteria for adverse events (PRO-CTCAE). *J Natl Cancer Inst* 2014; 106: dju244.
56. Absolom K, Warrington L, Hudson E, et al. Phase III Randomized Controlled Trial of eRAPID: eHealth Intervention During Chemotherapy. *J Clin Oncol* 2021; 39: 734–747.
57. Friberg LE, Henningson A, Maas H, et al. Model of chemotherapy-induced myelosuppression with parameter consistency across drugs. *J Clin Oncol* 2002; 20: 4713–4721.
58. Sheiner LB. A new approach to the analysis of analgesic drug trials, illustrated with bromfenac data. *Clin Pharmacol Ther* 1994; 56: 309–322.
59. Karlsson MO, Schoemaker RC, Kemp B, et al. A pharmacodynamic Markov mixed-effects model for the effect of temazepam on sleep. *Clin Pharmacol Ther* 2000; 68: 175–188.
60. Bergstrand M, Söderlind E, Weitschies W, et al. Mechanistic modeling of a magnetic marker monitoring study linking gastrointestinal tablet transit, in vivo drug release, and pharmacokinetics. *Clin Pharmacol Ther* 2009; 86: 77–83.
61. Keizer RJ, Gupta A, Mac Gillavry MR, et al. A model of hypertension and proteinuria in cancer patients treated with the anti-angiogenic drug E7080. *J Pharmacokinet Pharmacodyn* 2010; 37: 347–363.
62. Lacroix BD, Karlsson MO, Friberg LE. Simultaneous Exposure-Response Modeling of ACR20, ACR50, and ACR70 Improvement Scores in Rheumatoid Arthritis Patients Treated With Certolizumab Pegol. *CPT Pharmacometrics Syst Pharmacol* 2014; 3: e143.
63. Xu C, Ravva P, Dang JS, et al. A continuous-time multistate Markov model to describe the occurrence and severity of diarrhea events in metastatic breast cancer patients treated with lumretuzumab in combination with pertuzumab and paclitaxel. *Cancer Chemother Pharmacol* 2018; 82: 395–406.

64. Pilla Reddy V, Petersson KJ, Suleiman AA, et al. Pharmacokinetic-pharmacodynamic modeling of severity levels of extrapyramidal side effects with markov elements. *CPT Pharmacometrics Syst Pharmacol* 2012; 1: e1.
65. Suleiman AA, Frechen S, Scheffler M, et al. A Modeling and Simulation Framework for Adverse Events in Erlotinib-Treated Non-Small-Cell Lung Cancer Patients. *AAPS J* 2015; 17: 1483–1491.
66. Schindler E, Karlsson MO. A Minimal Continuous-Time Markov Pharmacometric Model. *AAPS J* 2017; 19: 1424–1435.
67. Brekkan A, Jönsson S, Karlsson MO, et al. Handling underlying discrete variables with bivariate mixed hidden Markov models in NONMEM. *J Pharmacokinet Pharmacodyn* 2019; 46: 591–604.
68. Perez-Pitarch A, Gottipati G, Uppoor R, et al. An Innovative Pharmacometric Approach for the Simultaneous Analysis of Frequency, Duration and Severity of Migraine Events. *Pharm Res* 2020; 37: 189.
69. Plan EL, Karlsson KE, Karlsson MO. Approaches to simultaneous analysis of frequency and severity of symptoms. *Clin Pharmacol Ther* 2010; 88: 255–259.
70. Lu T, Yang Y, Jin JY, et al. Analysis of Longitudinal-Ordered Categorical Data for Muscle Spasm Adverse Event of Vismodegib: Comparison Between Different Pharmacometric Models. *CPT Pharmacometrics Syst Pharmacol* 2020; 9: 96–105.
71. Heidelberger C, Chaudhuri NK, Danneberg P, et al. Fluorinated pyrimidines, a new class of tumour-inhibitory compounds. *Nature* 1957; 179: 663–666.
72. Wilson PM, Danenberg PV, Johnston PG, et al. Standing the test of time: targeting thymidylate biosynthesis in cancer therapy. *Nat Rev Clin Oncol* 2014; 11: 282–298.
73. Wishart DS, Knox C, Guo AC, et al. DrugBank: a comprehensive resource for in silico drug discovery and exploration. *Nucleic Acids Res* 2006; 34: D668-72.
74. Argilés G, Tabernero J, Labianca R, et al. Localised colon cancer: ESMO Clinical Practice Guidelines for diagnosis, treatment and follow-up. *Ann Oncol* 2020; 31: 1291–1305.
75. van Cutsem E, Cervantes A, Nordlinger B, et al. Metastatic colorectal cancer: ESMO Clinical Practice Guidelines for diagnosis, treatment and follow-up. *Ann Oncol* 2014; 25 Suppl 3: iii1-9.
76. Pfister DG, Spencer S, Adelstein D, et al. Head and Neck Cancers, Version 2.2020, NCCN Clinical Practice Guidelines in Oncology. *J Natl Compr Canc Netw* 2020; 18: 873–898.
77. Smyth EC, Verheij M, Allum W, et al. Gastric cancer: ESMO Clinical Practice Guidelines for diagnosis, treatment and follow-up. *Ann Oncol* 2016; 27: v38-v49.

78. Tempero MA, Malafa MP, Al-Hawary M, et al. Pancreatic Adenocarcinoma, Version 2.2021, NCCN Clinical Practice Guidelines in Oncology. *J Natl Compr Canc Netw* 2021; 19: 439–457.
79. Lee JJ, Beumer JH, Chu E. Therapeutic drug monitoring of 5-fluorouracil. *Cancer Chemother Pharmacol* 2016; 78: 447–464.
80. Modest DP, Karthaus M, Fruehauf S, et al. Panitumumab Plus Fluorouracil and Folinic Acid Versus Fluorouracil and Folinic Acid Alone as Maintenance Therapy in RAS Wild-Type Metastatic Colorectal Cancer: The Randomized PANAMA Trial (AIO KRK 0212). *J Clin Oncol* 2022; 40: 72–82.
81. Heinemann V, von Weikersthal LF, Decker T, et al. FOLFIRI plus cetuximab or bevacizumab for advanced colorectal cancer: final survival and per-protocol analysis of FIRE-3, a randomised clinical trial. *Br J Cancer* 2021; 124: 587–594.
82. Beumer JH, Chu E, Allegra C, et al. Therapeutic Drug Monitoring in Oncology: International Association of Therapeutic Drug Monitoring and Clinical Toxicology Recommendations for 5-Fluorouracil Therapy. *Clin Pharmacol Ther* 2019; 105: 598–613.
83. Dekker E, Tanis PJ, Vleugels JLA, et al. Colorectal cancer. *Lancet* 2019; 394: 1467–1480.
84. Tepper J, Krasna MJ, Niedzwiecki D, et al. Phase III trial of trimodality therapy with cisplatin, fluorouracil, radiotherapy, and surgery compared with surgery alone for esophageal cancer: CALGB 9781. *J Clin Oncol* 2008; 26: 1086–1092.
85. Pietrantonio F, Morano F, Corallo S, et al. Maintenance Therapy With Panitumumab Alone vs Panitumumab Plus Fluorouracil-Leucovorin in Patients With RAS Wild-Type Metastatic Colorectal Cancer: A Phase 2 Randomized Clinical Trial. *JAMA Oncol* 2019; 5: 1268–1275.
86. de Gramont A, Figer A, Seymour M, et al. Leucovorin and fluorouracil with or without oxaliplatin as first-line treatment in advanced colorectal cancer. *J Clin Oncol* 2000; 18: 2938–2947.
87. Thirion P, Michiels S, Pignon JP, et al. Modulation of fluorouracil by leucovorin in patients with advanced colorectal cancer: an updated meta-analysis. *J Clin Oncol* 2004; 22: 3766–3775.
88. Jacobs BAW, Deenen MJ, Joerger M, et al. Pharmacokinetics of Capecitabine and Four Metabolites in a Heterogeneous Population of Cancer Patients: A Comprehensive Analysis. *CPT Pharmacometrics Syst Pharmacol* 2019; 8: 940–950.
89. Terret C, Erdociain E, Guimbaud R, et al. Dose and time dependencies of 5-fluorouracil pharmacokinetics. *Clin Pharmacol Ther* 2000; 68: 270–279.
90. Goirand F, Lemaitre F, Launay M, et al. How can we best monitor 5-FU administration to maximize benefit to risk ratio? *Expert Opin Drug Metab Toxicol* 2018; 14: 1303–1313.

91. Milano G, Etienne MC, Cassuto-Viguier E, et al. Influence of sex and age on fluorouracil clearance. *J Clin Oncol* 1992; 10: 1171–1175.
92. Mueller F, Büchel B, Köberle D, et al. Gender-specific elimination of continuous-infusional 5-fluorouracil in patients with gastrointestinal malignancies: results from a prospective population pharmacokinetic study. *Cancer Chemother Pharmacol* 2013; 71: 361–370.
93. Arshad U, Ploylearmsaeng S-A, Karlsson MO, et al. Prediction of exposure-driven myelotoxicity of continuous infusion 5-fluorouracil by a semi-physiological pharmacokinetic-pharmacodynamic model in gastrointestinal cancer patients. *Cancer Chemother Pharmacol* 2020; 85: 711–722.
94. Climente-Martí M, Merino-Sanjuán M, Almenar-Cubells D, et al. A Bayesian method for predicting 5-fluorouracil pharmacokinetic parameters following short-term infusion in patients with colorectal cancer. *J Pharm Sci* 2003; 92: 1155–1165.
95. Meulendijks D, Henricks LM, Sonke GS, et al. Clinical relevance of DPYD variants c.1679T>G, c.1236G>A/HapB3, and c.1601G>A as predictors of severe fluoropyrimidine-associated toxicity: a systematic review and meta-analysis of individual patient data. *Lancet Oncol* 2015; 16: 1639–1650.
96. European Medicines Agency. EMA recommendations on DPD testing prior to treatment with fluorouracil, capecitabine, tegafur and flucytosine. Available at: https://www.ema.europa.eu/en/documents/referral/fluorouracil-fluorouracil-related-substances-article-31-referral-ema-recommendations-dpd-testing_en.pdf. Accessed 13 Jul 2021.
97. Gamelin E, Delva R, Jacob J, et al. Individual fluorouracil dose adjustment based on pharmacokinetic follow-up compared with conventional dosage: results of a multicenter randomized trial of patients with metastatic colorectal cancer. *J Clin Oncol* 2008; 26: 2099–2105.
98. Wilhelm M, Mueller L, Miller MC, et al. Prospective, Multicenter Study of 5-Fluorouracil Therapeutic Drug Monitoring in Metastatic Colorectal Cancer Treated in Routine Clinical Practice. *Clin Colorectal Cancer* 2016; 15: 381–388.
99. Kaldate RR, Haregewoin A, Grier CE, et al. Modeling the 5-fluorouracil area under the curve versus dose relationship to develop a pharmacokinetic dosing algorithm for colorectal cancer patients receiving FOLFOX6. *Oncologist* 2012; 17: 296–302.
100. Macaire P, Morawska K, Vincent J, et al. Therapeutic drug monitoring as a tool to optimize 5-FU-based chemotherapy in gastrointestinal cancer patients older than 75 years. *Eur J Cancer* 2019; 111: 116–125.

101. Denda T, Kanda M, Morita Y, et al. Pharmacokinetic dose adjustment of 5-FU in modified FOLFOX7 plus bevacizumab for metastatic colorectal cancer in Japanese patients: a-JUST phase II clinical trial. *Cancer Chemother Pharmacol* 2016; 78: 1253–1261.
102. Yang Q, Bi Y, Li X, et al. A retrospective analysis of plasma concentration monitoring of fluorouracil in patients with advanced colorectal cancer. *Eur J Hosp Pharm* 2020; 27: e36-e40.
103. Electronic Medicines Compendium. Fluorouracil 50 mg/ml injection: Summary of product characteristics 2021. Available at: <https://www.medicines.org.uk/emc/product/3791/smpc>. Accessed 27 Jan 2022.
104. Kadoyama K, Miki I, Tamura T, et al. Adverse event profiles of 5-fluorouracil and capecitabine: data mining of the public version of the FDA Adverse Event Reporting System, AERS, and reproducibility of clinical observations. *Int J Med Sci* 2012; 9: 33–39.
105. Lévy E, Piedbois P, Buyse M, et al. Toxicity of fluorouracil in patients with advanced colorectal cancer: effect of administration schedule and prognostic factors. *J Clin Oncol* 1998; 16: 3537–3541.
106. Electronic Medicines Compendium. Capecitabine 500 mg film-coated tablets: Summary of product characteristics 2021. Available at: <https://www.medicines.org.uk/emc/product/9939/smpc>. Accessed 27 Jan 2022.
107. Skof E, Rebersek M, Hlebanja Z, et al. Capecitabine plus Irinotecan (XELIRI regimen) compared to 5-FU/LV plus Irinotecan (FOLFIRI regimen) as neoadjuvant treatment for patients with unresectable liver-only metastases of metastatic colorectal cancer: a randomised prospective phase II trial. *BMC Cancer* 2009; 9: 120.
108. O’Shaughnessy J, Miles D, Vukelja S, et al. Superior survival with capecitabine plus docetaxel combination therapy in anthracycline-pretreated patients with advanced breast cancer: phase III trial results. *J Clin Oncol* 2002; 20: 2812–2823.
109. Cassidy J, Clarke S, Díaz-Rubio E, et al. Randomized phase III study of capecitabine plus oxaliplatin compared with fluorouracil/folinic acid plus oxaliplatin as first-line therapy for metastatic colorectal cancer. *J Clin Oncol* 2008; 26: 2006–2012.
110. Man FM de, Veerman GDM, Oomen-de Hoop E, et al. Comparison of toxicity and effectiveness between fixed-dose and body surface area-based dose capecitabine. *Ther Adv Med Oncol* 2019; 11: 1758835919838964.
111. Reigner B, Blesch K, Weidekamm E. Clinical pharmacokinetics of capecitabine. *Clin Pharmacokinet* 2001; 40: 85–104.

112. Daher Abdi Z, Lavau-Denes S, Prémaud A, et al. Pharmacokinetics and exposure-effect relationships of capecitabine in elderly patients with breast or colorectal cancer. *Cancer Chemother Pharmacol* 2014; 73: 1285–1293.
113. Reigner B, Verweij J, Dirix L, et al. Effect of food on the pharmacokinetics of capecitabine and its metabolites following oral administration in cancer patients. *Clin Cancer Res* 1998; 4: 941–948.
114. Zhang J, Zhang L, Yan Y, et al. Are capecitabine and the active metabolite 5-Fu CNS penetrable to treat breast cancer brain metastasis? *Drug Metab Dispos* 2015; 43: 411–417.
115. Varma A, Mathaiyan J, Shewade D, et al. Influence of ABCB-1, ERCC-1 and ERCC-2 gene polymorphisms on response to capecitabine and oxaliplatin (CAPOX) treatment in colorectal cancer (CRC) patients of South India. *J Clin Pharm Ther* 2020; 45: 617–627.
116. Lou Y, Wang Q, Zheng J, et al. Possible Pathways of Capecitabine-Induced Hand-Foot Syndrome. *Chem Res Toxicol* 2016; 29: 1591–1601.
117. Camidge R, Reigner B, Cassidy J, et al. Significant effect of capecitabine on the pharmacokinetics and pharmacodynamics of warfarin in patients with cancer. *J Clin Oncol* 2005; 23: 4719–4725.
118. Twelves C, Wong A, Nowacki MP, et al. Capecitabine as adjuvant treatment for stage III colon cancer. *N Engl J Med* 2005; 352: 2696–2704.
119. Twelves C, Scheithauer W, McKendrick J, et al. Capecitabine versus 5-fluorouracil/folinic acid as adjuvant therapy for stage III colon cancer: final results from the X-ACT trial with analysis by age and preliminary evidence of a pharmacodynamic marker of efficacy. *Ann Oncol* 2012; 23: 1190–1197.
120. Tebbutt NC, Wilson K, GebSKI VJ, et al. Capecitabine, bevacizumab, and mitomycin in first-line treatment of metastatic colorectal cancer: results of the Australasian Gastrointestinal Trials Group Randomized Phase III MAX Study. *J Clin Oncol* 2010; 28: 3191–3198.
121. O’Shaughnessy JA, Blum J, Moiseyenko V, et al. Randomized, open-label, phase II trial of oral capecitabine (Xeloda) vs. a reference arm of intravenous CMF (cyclophosphamide, methotrexate and 5-fluorouracil) as first-line therapy for advanced/metastatic breast cancer. *Ann Oncol* 2001; 12: 1247–1254.
122. Fumoleau P, Largillier R, Clippe C, et al. Multicentre, phase II study evaluating capecitabine monotherapy in patients with anthracycline- and taxane-pretreated metastatic breast cancer. *Eur J Cancer* 2004; 40: 536–542.
123. Blum JL, Dieras V, Lo Russo PM, et al. Multicenter, Phase II study of capecitabine in taxane-pretreated metastatic breast carcinoma patients. *Cancer* 2001; 92: 1759–1768.

124. Lassere Y, Hoff P. Management of hand-foot syndrome in patients treated with capecitabine (Xeloda). *Eur J Oncol Nurs* 2004; 8 Suppl 1: S31-40.
125. Urakawa R, Tarutani M, Kubota K, et al. Hand Foot Syndrome Has the Strongest Impact on QOL in Skin Toxicities of Chemotherapy. *J Cancer* 2019; 10: 4846–4851.
126. Leicher LW, Graaf JC de, Coers W, et al. Tolerability of Capecitabine Monotherapy in Metastatic Colorectal Cancer: A Real-World Study. *Drugs R D* 2017; 17: 117–124.
127. Kwakman JJM, Simkens LHJ, van Rooijen JM, et al. Randomized phase III trial of S-1 versus capecitabine in the first-line treatment of metastatic colorectal cancer: SALTO study by the Dutch Colorectal Cancer Group. *Ann Oncol* 2017; 28: 1288–1293.
128. Azuma Y, Hata K, Sai K, et al. Significant association between hand-foot syndrome and efficacy of capecitabine in patients with metastatic breast cancer. *Biol Pharm Bull* 2012; 35: 717–724.
129. Müller V, Fuxius S, Steffens C-C, et al. Quality of life under capecitabine (Xeloda®) in patients with metastatic breast cancer: data from a german non-interventional surveillance study. *Oncol Res Treat* 2014; 37: 748–755.
130. Yen-Revollo JL, Goldberg RM, McLeod HL. Can inhibiting dihydropyrimidine dehydrogenase limit hand-foot syndrome caused by fluoropyrimidines? *Clin Cancer Res* 2008; 14: 8–13.
131. Electronic Medicines Compendium. Stivarga 40 mg film-coated tablets: Summary of product characteristics 2022. Available at: <https://www.medicines.org.uk/emc/product/1263/smpc>. Accessed 2 Feb 2022.
132. Solimando DA, Waddell JA. Drug monographs: bosutinib and regorafenib. *Hosp Pharm* 2013; 48: 190–194.
133. Strumberg D, Al-Batran S-E, Takacs I, et al. A phase I study to determine the effect of regorafenib (REG) on the pharmacokinetics (PK) of substrates of P-glycoprotein (P-gp; digoxin) and breast cancer resistant protein (BCRP; rosuvastatin) in patients with advanced solid tumors. *Annals of Oncology* 2016; 27: vi156.
134. Pang YY, Tan YL, Ho HK. Investigation of the effect of plasma albumin levels on regorafenib-induced hepatotoxicity using a validated liquid chromatography-tandem mass spectrometry method. *J Chromatogr B Analyt Technol Biomed Life Sci* 2017; 1061-1062: 220–224.
135. Gerisch M, Hafner F-T, Lang D, et al. Mass balance, metabolic disposition, and pharmacokinetics of a single oral dose of regorafenib in healthy human subjects. *Cancer Chemother Pharmacol* 2018; 81: 195–206.
136. Rey J-B, Launay-Vacher V, Tournigand C. Regorafenib as a single-agent in the treatment of patients with gastrointestinal tumors: an overview for pharmacists. *Target Oncol* 2015; 10: 199–213.

137. Mross K, Frost A, Steinbild S, et al. A phase I dose-escalation study of regorafenib (BAY 73-4506), an inhibitor of oncogenic, angiogenic, and stromal kinases, in patients with advanced solid tumors. *Clin Cancer Res* 2012; 18: 2658–2667.
138. Strumberg D, Schultheis B. Regorafenib for cancer. *Expert Opin Investig Drugs* 2012; 21: 879–889.
139. Food and Drug Administration. Regorafenib Clinical Pharmacology and Biopharmaceutics Review. Available at: https://www.accessdata.fda.gov/drugsatfda_docs/nda/2012/203085Orig1s000ClinPharmR.pdf. Accessed 20 Mar 2022.
140. Fukudo M, Asai K, Tani C, et al. Pharmacokinetics of the oral multikinase inhibitor regorafenib and its association with real-world treatment outcomes. *Invest New Drugs* 2021; 39: 1422–1431.
141. Suzuki T, Sukawa Y, Imamura CK, et al. A Phase II Study of Regorafenib With a Lower Starting Dose in Patients With Metastatic Colorectal Cancer: Exposure-Toxicity Analysis of Unbound Regorafenib and Its Active Metabolites (RESET Trial). *Clin Colorectal Cancer* 2020; 19: 13-21.e3.
142. Mueller-Schoell A, Groenland SL, Scherf-Clavel O, et al. Therapeutic drug monitoring of oral targeted antineoplastic drugs. *Eur J Clin Pharmacol* 2021; 77: 441–464.
143. Santini J, Milano G, Thyss A, et al. 5-FU therapeutic monitoring with dose adjustment leads to an improved therapeutic index in head and neck cancer. *Br J Cancer* 1989; 59: 287–290.
144. Gamelin E, Boisdron-Celle M, Guérin-Meyer V, et al. Correlation between uracil and dihydrouracil plasma ratio, fluorouracil (5-FU) pharmacokinetic parameters, and tolerance in patients with advanced colorectal cancer: A potential interest for predicting 5-FU toxicity and determining optimal 5-FU dosage. *J Clin Oncol* 1999; 17: 1105.
145. Ibrahim T, Di Paolo A, Amatori F, et al. Time-dependent pharmacokinetics of 5-fluorouracil and association with treatment tolerability in the adjuvant setting of colorectal cancer. *J Clin Pharmacol* 2012; 52: 361–369.
146. van Groeningen CJ, Pinedo HM, Heddes J, et al. Pharmacokinetics of 5-fluorouracil assessed with a sensitive mass spectrometric method in patients on a dose escalation schedule. *Cancer Res* 1988; 48: 6956–6961.
147. Port RE, Daniel B, Ding RW, et al. Relative importance of dose, body surface area, sex, and age for 5-fluorouracil clearance. *Oncology* 1991; 48: 277–281.

148. Williams GR, Deal AM, Shachar SS, et al. The impact of skeletal muscle on the pharmacokinetics and toxicity of 5-fluorouracil in colorectal cancer. *Cancer Chemother Pharmacol* 2018; 81: 413–417.
149. Saam J, Critchfield GC, Hamilton SA, et al. Body surface area-based dosing of 5-fluorouracil results in extensive interindividual variability in 5-fluorouracil exposure in colorectal cancer patients on FOLFOX regimens. *Clin Colorectal Cancer* 2011; 10: 203–206.
150. Patel JN, O’Neil BH, Deal AM, et al. A community-based multicenter trial of pharmacokinetically guided 5-fluorouracil dosing for personalized colorectal cancer therapy. *Oncologist* 2014; 19: 959–965.
151. Braitheh FS, Salamone SJ, Li Y, et al. Pharmacokinetic (PK)-guided optimization of 5-fluorouracil (5FU) exposure in colorectal cancer (CRC) patients: U.S.-based clinical practices experience. *J Clin Oncol* 2014; 32: 3574.
152. Mindt S, Aida S, Merx K, et al. Therapeutic drug monitoring (TDM) of 5-fluorouracil (5-FU): new preanalytic aspects. *Clin Chem Lab Med* 2019; 57: 1012–1016.
153. Pallet N, Hamdane S, Garinet S, et al. A comprehensive population-based study comparing the phenotype and genotype in a pretherapeutic screen of dihydropyrimidine dehydrogenase deficiency. *Br J Cancer* 2020; 123: 811–818.
154. Fleming RA, Milano G, Thyss A, et al. Correlation between dihydropyrimidine dehydrogenase activity in peripheral mononuclear cells and systemic clearance of fluorouracil in cancer patients. *Cancer Res* 1992; 52: 2899–2902.
155. Tron C, Lemaitre F, Boisteau E, et al. When helping the minority of patients may hurt the majority: The case for DPD phenotyping and 5-fluorouracil therapeutic drug monitoring. *Dig Liver Dis* 2021; 53: 258–260.
156. Dolat M, Macaire P, Goirand F, et al. Association of 5-FU Therapeutic Drug Monitoring to DPD Phenotype Assessment May Reduce 5-FU Under-Exposure. *Pharmaceuticals (Basel)* 2020.
157. Meulendijks D, Henricks LM, Jacobs BAW, et al. Pretreatment serum uracil concentration as a predictor of severe and fatal fluoropyrimidine-associated toxicity. *Br J Cancer* 2017; 116: 1415–1424.
158. Boisdron-Celle M, Remaud G, Traore S, et al. 5-Fluorouracil-related severe toxicity: a comparison of different methods for the pretherapeutic detection of dihydropyrimidine dehydrogenase deficiency. *Cancer Lett* 2007; 249: 271–282.
159. Burns KE, Chavani O, Jeong SH, et al. Comparison of a thymine challenge test and endogenous uracil-dihydrouracil levels for assessment of fluoropyrimidine toxicity risk. *Cancer Chemother Pharmacol* 2021; 87: 711–716.

160. Ciccolini J, Mercier C, Evrard A, et al. A rapid and inexpensive method for anticipating severe toxicity to fluorouracil and fluorouracil-based chemotherapy. *Ther Drug Monit* 2006; 28: 678–685.
161. Zhou ZW, Wang GQ, Wan DS, et al. The dihydrouracil/uracil ratios in plasma and toxicities of 5-fluorouracil-based adjuvant chemotherapy in colorectal cancer patients. *Chemotherapy* 2007; 53: 127–131.
162. Sistonen J, Büchel B, Froehlich TK, et al. Predicting 5-fluorouracil toxicity: DPD genotype and 5,6-dihydrouracil:uracil ratio. *Pharmacogenomics* 2014; 15: 1653–1666.
163. van Staveren MC, van Kuilenburg ABP, Guchelaar H-J, et al. Evaluation of an oral uracil loading test to identify DPD-deficient patients using a limited sampling strategy. *Br J Clin Pharmacol* 2016; 81: 553–561.
164. Wörmann B, Bokemeyer C, Burmeister T, et al. Dihydropyrimidine Dehydrogenase Testing prior to Treatment with 5-Fluorouracil, Capecitabine, and Tegafur: A Consensus Paper. *Oncol Res Treat* 2020; 43: 628–636.
165. Hamzic S, Aebi S, Joerger M, et al. Fluoropyrimidine chemotherapy: recommendations for DPYD genotyping and therapeutic drug monitoring of the Swiss Group of Pharmacogenomics and Personalised Therapy. *Swiss Med Wkly* 2020; 150: w20375.
166. Lunenburg CATC, van der Wouden CH, Nijenhuis M, et al. Dutch Pharmacogenetics Working Group (DPWG) guideline for the gene-drug interaction of DPYD and fluoropyrimidines. *Eur J Hum Genet* 2020; 28: 508–517.
167. Loriot M-A, Ciccolini J, Thomas F, et al. Dépistage du déficit en dihydropyrimidine déshydrogénase (DPD) et sécurisation des chimiothérapies à base de fluoropyrimidines : mise au point et recommandations nationales du GPCO-Uncancer et du RNPGx [Dihydropyrimidine déshydrogénase (DPD) deficiency screening and securing of fluoropyrimidine-based chemotherapies: Update and recommendations of the French GPCO-Uncancer and RNPGx networks]. *Bull Cancer* 2018; 105: 397–407. French.
168. Amstutz U, Henricks LM, Offer SM, et al. Clinical Pharmacogenetics Implementation Consortium (CPIC) Guideline for Dihydropyrimidine Dehydrogenase Genotype and Fluoropyrimidine Dosing: 2017 Update. *Clin Pharmacol Ther* 2018; 103: 210–216.
169. Schneider JJ, Galettis P, Martin JH. Overcoming barriers to implementing precision dosing with 5-fluorouracil and capecitabine. *Br J Clin Pharmacol* 2021; 87: 317–325.
170. Moloney M, Faulkner D, Link E, et al. Feasibility of 5-fluorouracil pharmacokinetic monitoring using the My-5FU PCM™ system in a quaternary oncology centre. *Cancer Chemother Pharmacol* 2018; 82: 865–876.

171. Saif MW, Choma A, Salamone SJ, et al. Pharmacokinetically guided dose adjustment of 5-fluorouracil: a rational approach to improving therapeutic outcomes. *J Natl Cancer Inst* 2009; 101: 1543–1552.
172. Kluwe F, Michelet R, Mueller-Schoell A, et al. Perspectives on Model-Informed Precision Dosing in the Digital Health Era: Challenges, Opportunities, and Recommendations. *Clin Pharmacol Ther* 2021; 109: 29–36.
173. Etienne M-C, Chatelut E, Pivot X, et al. Co-variables influencing 5-fluorouracil clearance during continuous venous infusion. A NONMEM analysis. *Eur J Cancer* 1998; 34: 92–97.
174. Woloch C, Di Paolo A, Marouani H, et al. Population pharmacokinetic analysis of 5-FU and 5-FDHU in colorectal cancer patients: search for biomarkers associated with gastro-intestinal toxicity. *Curr Top Med Chem* 2012; 12: 1713–1719.
175. Bressolle F, Joulia JM, Pinguet F, et al. Circadian rhythm of 5-fluorouracil population pharmacokinetics in patients with metastatic colorectal cancer. *Cancer Chemother Pharmacol* 1999; 44: 295–302.
176. Kuwahara A, Kobuchi S, Tamura T. Association between circadian and chemotherapeutic cycle effects on plasma concentration of 5-fluorouracil and the clinical outcome following definitive 5-fluorouracil/cisplatin-based chemoradiotherapy in patients with esophageal squamous cell carcinoma. *Oncol Lett* 2019; 17: 668–675.
177. Gérard J-P, Azria D, Gourgou-Bourgade S, et al. Comparison of two neoadjuvant chemoradiotherapy regimens for locally advanced rectal cancer: results of the phase III trial ACCORD 12/0405-Prodige 2. *J Clin Oncol* 2010; 28: 1638–1644.
178. Park J, Yoon SM, Yu CS, et al. Randomized phase 3 trial comparing preoperative and postoperative chemoradiotherapy with capecitabine for locally advanced rectal cancer. *Cancer* 2011; 117: 3703–3712.
179. Bosset J-F, Collette L, Calais G, et al. Chemotherapy with preoperative radiotherapy in rectal cancer. *N Engl J Med* 2006; 355: 1114–1123.
180. Marti FEM, Jayson GC, Manoharan P, et al. Novel phase I trial design to evaluate the addition of cediranib or selumetinib to preoperative chemoradiotherapy for locally advanced rectal cancer: the DREAMtherapy trial. *Eur J Cancer* 2019; 117: 48–59.
181. von Moos R, Koeberle D, Schacher S, et al. Neoadjuvant radiotherapy combined with capecitabine and sorafenib in patients with advanced KRAS-mutated rectal cancer: A phase I/II trial (SAKK 41/08). *Eur J Cancer* 2018; 89: 82–89.
182. Saif MW, Katirtzoglou NA, Syrigos KN. Capecitabine: an overview of the side effects and their management. *Anticancer Drugs* 2008; 19: 447–464.

183. Beal S, Sheiner LB, Boeckmann A, Bauer RJ. NONMEM User's Guides (1989-2018). Gaithersburg, MD, USA: Icon Development Solutions; 2018.
184. Stroh M, Hutmacher MM, Pang J, et al. Simultaneous pharmacokinetic model for rolofylline and both M1-trans and M1-cis metabolites. *AAPS J* 2013; 15: 498–504.
185. Bergstrand M, Hooker AC, Wallin JE, et al. Prediction-corrected visual predictive checks for diagnosing nonlinear mixed-effects models. *AAPS J* 2011; 13: 143–151.
186. Lindauer A, Siepman T, Oertel R, et al. Pharmacokinetic/pharmacodynamic modelling of venlafaxine: pupillary light reflex as a test system for noradrenergic effects. *Clin Pharmacokinet* 2008; 47: 721–731.
187. Keunecke A, Hoefman S, Drenth H-J, et al. Population pharmacokinetics of regorafenib in solid tumours: Exposure in clinical practice considering enterohepatic circulation and food intake. *Br J Clin Pharmacol* 2020; 86: 2362–2376.
188. Urien S, Rezaí K, Lokiec F. Pharmacokinetic modelling of 5-FU production from capecitabine— a population study in 40 adult patients with metastatic cancer. *J Pharmacokinet Pharmacodyn* 2005; 32: 817–833.
189. Lunar N, Etienne-Grimaldi M-C, Macaire P, et al. Population pharmacokinetic and pharmacodynamic modeling of capecitabine and its metabolites in breast cancer patients. *Cancer Chemother Pharmacol* 2021; 87: 229–239.
190. Popuri K, Cobzas D, Esfandiari N, et al. Body Composition Assessment in Axial CT Images Using FEM-Based Automatic Segmentation of Skeletal Muscle. *IEEE Trans Med Imaging* 2016; 35: 512–520.
191. Streit M, Jaehde U, Stremetzne S, et al. Five-day continuous infusion of 5-fluorouracil and pulsed folinic acid in patients with metastatic colorectal carcinoma: an effective second-line regimen. *Ann Oncol* 1997; 8: 163–165.
192. Hendrayana T, Kurth V, Krolop L, et al. Variability in fluorouracil exposure during continuous intravenous infusion. *Int J Clin Pharmacol Ther* 2012; 50: 82–84.
193. Niebecker R, Maas H, Staab A, et al. Modeling Exposure-Driven Adverse Event Time Courses in Oncology Exemplified by Afatinib. *CPT Pharmacometrics Syst Pharmacol* 2019; 8: 230–239.
194. Cassidy J, Twelves C, van Cutsem E, et al. First-line oral capecitabine therapy in metastatic colorectal cancer: A favorable safety profile compared with intravenous 5-fluorouracil/leucovorin. *Ann Oncol* 2002; 13: 566–575.
195. Hénin E, You B, VanCutsem E, et al. A dynamic model of hand-and-foot syndrome in patients receiving capecitabine. *Clin Pharmacol Ther* 2009; 85: 418–425.

196. Simons S, Ringsdorf S, Braun M, et al. Enhancing adherence to capecitabine chemotherapy by means of multidisciplinary pharmaceutical care. *Support Care Cancer* 2011; 19: 1009–1018.
197. Krolop L, Ko Y-D, Schwindt PF, et al. Adherence management for patients with cancer taking capecitabine: A prospective two-arm cohort study. *BMJ Open* 2013; 3: e003139.
198. National Cancer Institute. Common Terminology Criteria for Adverse Events v3.0 (CTCAE) 2006. Available at: <http://ctep.cancer.gov/>. Accessed 6 Jan 2020.
199. Karlsson MO, Holford N. A tutorial on visual predictive checks 2008. Available at: <http://www.page-meeting.org/?abstract=1434>. Accessed 2 Apr 2022.
200. Electronic Medicines Compendium. Capecitabine 500 mg film-coated tablets: Summary of Product Characteristics, September 2018. Available at: <https://www.medicines.org.uk/emc/product/9939>. Accessed 6 Jan 2020.
201. Scheithauer W, Blum J. Coming to grips with hand-foot syndrome. Insights from clinical trials evaluating capecitabine. *Oncology (Williston Park, N Y)* 2004; 18: 1161-8, 1173; discussion 1173-6, 1181-4.
202. Kara IO, Sahin B, Erkisi M. Palmar-plantar erythrodysesthesia due to docetaxel-capecitabine therapy is treated with vitamin E without dose reduction. *Breast* 2006; 15: 414–424.
203. Groenland SL, Verheijen RB, Joerger M, et al. Precision Dosing of Targeted Therapies Is Ready for Prime Time. *Clin Cancer Res* 2021; 27: 6644–6652.
204. IJzerman NS, Groenland SL, Koenen AM, et al. Therapeutic drug monitoring of imatinib in patients with gastrointestinal stromal tumours - Results from daily clinical practice. *Eur J Cancer* 2020; 136: 140–148.
205. Braal CL, Jager A, Hoop EO, et al. Therapeutic Drug Monitoring of Endoxifen for Tamoxifen Precision Dosing: Feasible in Patients with Hormone-Sensitive Breast Cancer. *Clin Pharmacokinet* 2021.
206. Mc Laughlin AM, Schmulenson E, Teplytska O, et al. Developing a Nationwide Infrastructure for Therapeutic Drug Monitoring of Targeted Oral Anticancer Drugs: The ON-TARGET Study Protocol. *Cancers (Basel)* 2021; 13: 6281.
207. Ma WW, Saif MW, El-Rayes BF, et al. Emergency use of uridine triacetate for the prevention and treatment of life-threatening 5-fluorouracil and capecitabine toxicity. *Cancer* 2017; 123: 345–356.
208. Mendoza TR, Dueck AC, Bennett AV, et al. Evaluation of different recall periods for the US National Cancer Institute’s PRO-CTCAE. *Clin Trials* 2017; 14: 255–263.

209. Scarfò L, Karamanidou C, Doubek M, et al. MyPal ADULT study protocol: a randomised clinical trial of the MyPal ePRO-based early palliative care system in adult patients with haematological malignancies. *BMJ Open* 2021; 11: e050256.
210. Basch E, Schrag D, Henson S, et al. Effect of Electronic Symptom Monitoring on Patient-Reported Outcomes Among Patients With Metastatic Cancer. *JAMA* 2022; 327: 2413–2422.

Further information on assistance received and resources used

General

Introduction to pharmacometric modeling, statistical software and software packages (including coding), i.e. NONMEM®, R, Piraña, Pearl-speaks-NONMEM, assisted by: Patricia Egidi, Dr. Achim Fritsch, previous PhD and MSc theses of Dr. Stefanie Kapsa (née Kraff) and Iryna Sihinevich, respectively.

Chapter 3: Current status and future outlooks on therapeutic drug monitoring of fluorouracil

Nigina Zimmermann, Prof. Dr. Gerd Mikus and Prof. Dr. Ulrich Jaehde assisted in outlining the literature review. Nigina Zimmermann assisted in literature search. All co-authors assisted in analysis of the results of the literature search and contributed to writing the manuscript.

Chapter 4: Population pharmacokinetic analyses of regorafenib and capecitabine in patients with locally advanced rectal cancer (SAKK 41/16 RECAP)

This study was designed and conducted by network members of the Swiss Group for Clinical Cancer Research (SAKK). The SAKK provided the study data for pharmacometric analysis.

Prof. Dr. Dr. Markus Jörger and Prof. Dr. Ulrich Jaehde assisted in pharmacometric analysis.

All co-authors contributed to writing the manuscript.

Chapter 5: Influence of the skeletal muscle index on pharmacokinetics and toxicity of fluorouracil

Nigina Zimmermann, Dr. Lothar Müller and Prof. Dr. Ulrich Jaehde assisted in designing the research. Study data was provided by Dr. Lothar Müller (Onkologie UnterEms, Leer).

Nigina Zimmermann analyzed the computed tomography images. Nigina Zimmermann and Prof. Dr. Ulrich Jaehde assisted in data analysis. The previous population pharmacokinetic model of fluorouracil was developed by Dr. Stefanie Kapsa (née Kraff) and Iryna Sihinevich.

All co-authors contributed to writing the manuscript.

Chapter 6: Evaluation of patient-reported severity of hand–foot syndrome under capecitabine using a Markov modeling approach

The studies were designed and conducted by the co-authors Dr. Linda Krolop, Dr. Sven Simons, Dr. Susanne Ringsdorf, Prof. Dr. Yon-Dschun Ko (Johanniter-Krankenhaus, Bonn) and Prof. Dr. Ulrich Jaehde.

Prof. Dr. Ulrich Jaehde assisted in pharmacometric analysis.

All co-authors contributed to writing the manuscript.



Appendix

Full-text publications and supplementary materials

Due to legal reasons the journal article “Current status and future outlooks on therapeutic drug monitoring of fluorouracil” (Chapter 3) cannot be printed in this thesis. Please refer to the following link: <https://doi.org/10.1080/17425255.2021.2029403>

ORIGINAL ARTICLE

Population pharmacokinetic analyses of regorafenib and capecitabine in patients with locally advanced rectal cancer (SAKK 41/16 RECAP)

Eduard Schmulenson¹  | Cédric Bovet² | Regula Theurillat² |
Laurent Arthur Decosterd³ | Carlo R. Largiadèr² | Jean-Christophe Prost² |
Chantal Csajka⁴ | Daniela Bärtschi⁵ | Matthias Guckenberger⁶ |
Roger von Moos⁷ | Sara Bastian⁷ | Markus Joerger⁸ | Ulrich Jaehde¹ 

¹Institute of Pharmacy, Department of Clinical Pharmacy, University of Bonn, Bonn, Germany

²Department of Clinical Chemistry, Inselspital, Bern University Hospital and University of Bern, Bern, Switzerland

³Laboratory of Clinical Pharmacology, Lausanne University Hospital and University of Lausanne, Lausanne, Switzerland

⁴Clinical Pharmaceutical Sciences, Lausanne University, Lausanne, Switzerland

⁵SAKK Coordinating Center, Bern, Switzerland

⁶Department of Radiation Oncology, University Hospital Zurich, University of Zurich, Zurich, Switzerland

⁷Cantonal Hospital Graubünden, Chur, Switzerland

⁸Department of Medical Oncology and Hematology, Cantonal Hospital St. Gallen, St. Gallen, Switzerland

Correspondence

Prof. Dr. Ulrich Jaehde, Institute of Pharmacy,
University of Bonn, An der Immenburg
4, 53121 Bonn, Germany.
Email: u.jaehde@uni-bonn.de

Funding information

The trial was supported by Bayer and research agreements with the following institutions: Swiss State Secretariat for Education, Research and Innovation (SERI), Swiss Cancer Research Foundation (SCS) and Swiss Cancer League (SCL).

Aims: Locally advanced rectal cancer (LARC) is an area of unmet medical need with one third of patients dying from their disease. With response to neoadjuvant chemoradiotherapy being a major prognostic factor, trial SAKK 41/16 assessed potential benefits of adding regorafenib to capecitabine-amplified neoadjuvant radiotherapy in LARC patients.

Methods: Patients received regorafenib at three dose levels (40/80/120 mg once daily) combined with capecitabine 825 mg/m² bidaily and local radiotherapy. We developed population pharmacokinetic models from plasma concentrations of capecitabine and its metabolites 5'-deoxy-5-fluorocytidine and 5'-deoxy-5-fluorouridine as well as regorafenib and its metabolites M-2 and M-5 as implemented into SAKK 41/16 to assess potential drug–drug interactions (DDI). After establishing parent-metabolite base models, drug exposure parameters were tested as covariates within the respective models to investigate for potential DDI. Simulation analyses were conducted to quantify their impact.

Results: Plasma concentrations of capecitabine, regorafenib and metabolites were characterized by one and two compartment models and absorption was described by

Sara Bastian, Markus Joerger and Ulrich Jaehde shared senior authorship.

The authors confirm that the Principal Investigator for this paper is Sara Bastian and that she had direct clinical responsibility for patients.

This is an open access article under the terms of the [Creative Commons Attribution-NonCommercial](https://creativecommons.org/licenses/by-nc/4.0/) License, which permits use, distribution and reproduction in any medium, provided the original work is properly cited and is not used for commercial purposes.

© 2022 The Authors. *British Journal of Clinical Pharmacology* published by John Wiley & Sons Ltd on behalf of British Pharmacological Society.

parallel first- and zero-order processes and transit compartments, respectively. Apparent capecitabine clearance was 286 L/h (relative standard error [RSE] 14.9%, interindividual variability [IIV] 40.1%) and was reduced by regorafenib cumulative area under the plasma concentration curve (median reduction of 45.6%) as exponential covariate (estimate -4.10×10^{-4} , RSE 17.8%). Apparent regorafenib clearance was 1.94 L/h (RSE 12.1%, IIV 38.1%). Simulation analyses revealed significantly negative associations between capecitabine clearance and regorafenib exposure.

Conclusions: This work informs the clinical development of regorafenib and capecitabine combination treatment and underlines the importance of studying potential DDI with new anticancer drug combinations.

KEYWORDS

capecitabine, drug–drug interaction, population pharmacokinetics, rectal cancer, regorafenib

1 | INTRODUCTION

Colorectal cancer (CRC) is the third most common cause of cancer cases worldwide and ranks second in cancer deaths.¹ While the overall incidence of CRC declined in many high-income countries in recent years, CRC incidence in adults younger than 50 years increased substantially,^{1,2} mainly driven by rising cases of rectal cancer.³ Rectal cancer comprises about one third of the total colorectal cancer cases.^{4,5} Neoadjuvant chemo-radiotherapy followed by potentially curative surgery is standard of care in patients with locally advanced rectal cancer (LARC). Alternatively, the watchful waiting strategy after complete pathological response of neoadjuvant chemo-radiotherapy is another approach in LARC patients, requiring intensification of therapy.⁶ Response to neoadjuvant chemo-radiotherapy is an important independent prognostic factor,⁷ still the rate of complete pathological response is only 10–25%,^{8,9} and one third of patients with LARC relapse after chemo-radiotherapy and surgery.¹⁰ Recent studies added tyrosine kinase inhibitors (TKI) such as sorafenib¹¹ or cediranib¹² to capecitabine-based chemo-radiotherapy in LARC to improve clinical outcome. Trial SAKK 41/16 added the second-generation multi-TKI regorafenib to capecitabine-based chemo-radiotherapy, and this trial included a pharmaco-translational part with extensive pharmacokinetic (PK) analysis of both anticancer drugs to assess for potential drug–drug interactions (DDI).

Neoadjuvant chemo-radiation with capecitabine has been shown to be tolerated both alone and in combination with irinotecan¹³ or oxaliplatin.¹⁴ Optimal dosing of oral capecitabine in combination with radiotherapy has been established at 825 mg/m² bidaily given throughout the course of radiotherapy.¹⁵ Regorafenib is an oral multi-TKI with broad activity, including inhibition of angiogenesis (VEGFR1–3, TIE2), impact on the tumour microenvironment (PDGFR- β , FGFR) and oncogenesis (KIT, PDGFR and RET).¹⁶ Regorafenib has been approved as monotherapy in patients with advanced CRC, hepatocellular carcinoma and gastrointestinal stromal tumours at a daily dose of 160 mg. Regorafenib has a bioavailability of 69%¹⁷ and is metabolized to active metabolites M-2 (regorafenib N-oxide) and M-5 (N-

What is already known about this subject

- Patients with locally advanced rectal cancer suffer from frequent locoregional and systemic relapse.
- The addition of the tyrosine kinase inhibitor regorafenib to capecitabine-augmented local radiotherapy is a promising strategy to improve pathological response rates.

What this study adds

- Our population pharmacokinetic models show a negative impact of regorafenib cumulative area under the plasma concentration curve on capecitabine clearance.
- The drug–drug interaction between regorafenib and capecitabine seems to be of negligible clinical relevance.

desmethyl-regorafenib) by CYP3A4 and UGT1A9.¹⁸ Mean elimination half-life of M-2 and M-5 is 24 and 51–64 hours, respectively. Excretion of regorafenib is mainly via faeces (50%) and less via the kidneys (19%).¹⁷ Capecitabine is sequentially converted to 5'-deoxy-5-fluorocytidine (DFCR) by hepatic carboxylesterase and to 5'-deoxy-5-fluorouridine (DFUR) by cytidine deaminase. The intermediate DFUR is converted to fluorouracil by the enzyme thymidine phosphorylase in the final activating step. Capecitabine is a known inhibitor of CYP2C9, but potential DDI based on CYP2C9 are not expected as regorafenib is not metabolized by this enzyme. However, as regorafenib and capecitabine have overlapping toxicity, including palmar-plantar erythrodysesthesia and diarrhoea,^{16,19} it is important to identify potential DDI.

The aim of this study was to implement population PK models of regorafenib, capecitabine and their metabolites in LARC patients, and to investigate potential interactions between both drugs.

2 | METHODS

2.1 | Patients and data

This open-label, multi-centre, non-randomized phase IB trial explored the recommended dose of and pathological response to regorafenib when added to capecitabine-augmented neoadjuvant chemo-radiotherapy in patients with AJCC stage II/III rectal cancer (mT3/4 N0, mTx N1–2 cM0). SAKK 41/16 recruited 25 patients from six Swiss sites between March 2017 and April 2021. The trial includes a dose-escalation part and an expansion cohort after establishing the recommended phase-2 dose. All patients were tested for mutations of the dihydropyrimidine dehydrogenase gene (*DPYD*), and patients harbouring one of four dysfunctional *DPYD* mutations (*DPYD* c.1679T>G [rsrs55886062], c.1905+1G>A [rsrs3918290], c.2846A>T [rs67376798], c.1129-5923C>G [rs75017182]) were excluded from SAKK 41/16.^{20,21} Furthermore, only patients between 18 and 75 years with adequate renal (creatinine clearance >50 mL/min) and hepatic function (markers such as bilirubin, alanine/aspartate aminotransferase $\leq 1.5 \times$ the upper limit of normal) were included. The study was conducted according to the Declaration of Helsinki and patients provided written informed consent before participation. The study protocol was approved by the respective regulatory authorities and registered under clinicaltrials.gov number NCT02910843.

PK data from 12 patients enrolled into the dose-escalation cohort were used for the development of the population PK models as no blood samples were obtained from patients belonging to the expansion cohort. Patients received oral capecitabine 825 mg/m² bidaily on Days 1 to 38. Regorafenib was administered at three dose levels (40, 80 and 120 mg) once daily on Days 1 to 14 and Days 22 to 35. Local radiotherapy was given in all patients at 1.8 Gy per day in 28 fractions (5.6 weeks) for a total dose of 50.4 Gy. Patients underwent rectal cancer surgery 6–12 weeks (± 1 week) after completion of chemo-radiotherapy. Plasma samples for analysis of regorafenib, capecitabine and their metabolites were collected on Day 1 (0.5, 1, 2, 3, 4 and 6 h after dosing) followed by post-dose sampling on Days 2, 4, 8, 15, 22, 29 and 36. PK sampling after Day 1 occurred at the time of the patient's appointment and was not bound to a specific time point. Patient characteristics are outlined in Table 1.

2.2 | Quantification of drug concentrations

Plasma concentrations of regorafenib and its active metabolites M-2 and M-5 were quantified using a validated liquid chromatography coupled to tandem mass spectrometry assay as previously described.²² Plasma concentrations of capecitabine and its metabolites DFCR and DFUR were quantified using a second validated assay by liquid chromatography coupled to tandem mass spectrometry between 0.5 and 10 μ g/mL plasma. This assay was validated according to the US Food and Drug Administration and C62-A of the Clinical and Laboratory Standards Institute Guidelines.^{23,24} Validation parameters fulfilled the acceptance criteria of these guidelines. The results of

TABLE 1 Summary of patient characteristics at baseline ($N = 12$)

Characteristic	<i>n</i> or median (range)
Number of males/females	7/5
Number of patients with regorafenib dose of 40/80/120 mg	3/6/3
<i>AJCC tumour staging</i>	
Tumour stage (T1/T2/T3)	0/0/12
Nodal status (N0/N1/N2/Nx)	1/4/6/1
Metastases (M0/M1)	12/0
Age (years)	57 (48–75)
Weight (kg)	71.7 (55.9–96.0)
Body surface area (m ²)	1.86 (1.59–2.16)
Body mass index (kg/m ²)	24.4 (20.4–33.2)
Bilirubin concentration (μ mol/L)	6 (2–14)
Alanine aminotransferase (U/L)	16 (10–34)
Aspartate aminotransferase (U/L)	20 (13–30)
Haemoglobin concentration (g/L)	138 (127–157)
Absolute neutrophil count ($10^3/\mu$ L)	4.76 (4.03–7.98)
Creatinine clearance (mL/min)	98 (63–118)

the validation parameters are shown in Tables S1.1 to S1.4 in the Supporting Information. The lower limit of quantification for the assay was 0.25 μ g/mL. Reference standards for capecitabine and DFCR/DFUR were obtained from Santa Cruz Biotechnology, Inc. (Heidelberg, Germany) and TCI Deutschland GmbH (Eschborn, Germany), respectively. The isotope-labelled internal standards capecitabine ²H₁₁, DFCR ¹³C¹⁵N₂, DFUR ¹³C¹⁵N₂ were obtained from Toronto Research Chemicals (Toronto, Canada). Stock solutions and dilutions were prepared in acetonitrile:water 1:1 (v/v). Calibrators (0.5–10 μ g/mL) and quality controls (1.5, 5 and 9 μ g/mL) were prepared in pooled plasma (Dunn Labortechnik GmbH). After thawing the plasma samples at 4 °C, 10 μ L acetonitrile:water 1:1 (v/v) (for calibrators and QCs the corresponding standard dilution) and 140 μ L acetonitrile:ethanol 1:1 (v/v) containing the internal standards were added to 50 μ L of plasma in a 96-well plate. The plate was sealed and shaken on a plate shaker at 1000 rpm and room temperature for 5 minutes. After centrifugation (4000 relative centrifugal force, room temperature, 20 minutes), 20 μ L of the supernatant was diluted with 300 μ L of water in a new 96-well plate with a pipetting robot (Liquid Handling Station LHS, Brand, Germany). Finally, the plate was sealed and shaken on a plate shaker at room temperature at 1000 rpm for 5 minutes. 3 μ L of the extracted samples was analysed by reversed-phase chromatography (Acquity UPLC HSS T3 column, 2.1 \times 50 mm, 1.7 μ M, Waters) on a triple quadrupole mass spectrometer (Xevo TQ-S, Waters) coupled to an UPLC Acquity I-Class system (Waters). Capecitabine, DFCR and DFUR were separated at 0.4 mL/min with a gradient using water (A) and methanol (B) acidified with 0.05% (v/v) formic acid as mobile phases (0.0–1.0 min, 1% B; 1.0–4.5 min, 1–95% B; held for 1 min, then switched back to 1% B and equilibrated from 5.1–7.0 min). The source offset and transition parameters were

optimized for each analyte. The raw data were processed with TargetLynx available in the MassLynx software (version 4.1, Waters).

2.3 | Population pharmacokinetic models

Population PK analysis of the concentration–time data of regorafenib and capecitabine was performed using the nonlinear mixed-effect modelling software NONMEM version 7.5 (double precision, level 1.1).²⁵ NONMEM uses a maximum likelihood criterion to simultaneously estimate population values of fixed-effects variables (e.g. drug clearance) and values of random-effects variables (e.g., interindividual, interoccasion and residual variability). The likelihood-ratio test was used to discriminate between nested models. The inclusion of an extra parameter required a statistically significant reduction ($P < .05$) of the objective function value (OFV) provided by NONMEM®. Non-nested models were compared by the Akaike Information Criterion (AIC). Implemented scripts in PsN (version 5.0.0)^{26,27} were used for model development and R (version 4.1.0)²⁸ was used for graphical purposes. Piraña (version 2.9.7)²⁹ served as front interface.

2.3.1 | Structural model development of the capecitabine-metabolite model

In order to describe the absorption process of capecitabine, different absorption models were tested (first-, zero-order absorption, combined zero- and first-order absorption, transit absorption models). Additionally, we tested absorption models as described previously for oral capecitabine,^{30–32} as the corresponding plasma concentrations supported a fast initial absorption phase (Figure S2.1 in the Supporting Information).

The population PK parent-metabolite model was developed in three sequential steps. After establishing the parent drug model, its structural parameters were fixed and the subsequent metabolites were included in a stepwise fashion. Eventually, all parameters were estimated simultaneously.³⁴ One- and two-compartment models were evaluated for the description of the plasma concentration–time course of capecitabine and its metabolites. Since the bioavailability F of capecitabine and the fractions converted to the metabolites were structurally unidentifiable, model parameters were estimated relative to these values (e.g. clearance/ F). Overall, plasma concentrations below the lower limit of quantification (0.25 µg/mL for capecitabine and metabolites, 0.02 µg/mL for regorafenib and metabolites) were included for model development.³⁵

2.3.2 | Structural model development of the regorafenib-metabolite model

Model development steps for regorafenib, M-2 and M-5 were identical to the procedure for capecitabine and its metabolites. Besides one- and two-compartment models, three-compartment models were

investigated for the description of the plasma concentrations of the respective compounds as well. In addition, different enterohepatic circulation (EHC) models as described previously^{36–38} were additionally investigated.

2.3.3 | Statistical model development

Population PK parameters were assumed to be log-normally distributed and interindividual variability (IIV) was implemented as an exponential function.³⁹ We tested different error models (additive, proportional, combined additive/proportional) to describe residual PK variability.³⁹ Interoccasion variability (IOV) was explored on clearance and absorption parameters as well.³⁹

2.3.4 | Covariate analysis

The resulting capecitabine- and regorafenib-metabolite base models were used to generate drug exposure parameters. In a covariate analysis, concentrations over time and cumulative area under the curve (AUC) over time of regorafenib, M-2 and M-5 were tested on the clearance of capecitabine and its metabolites, and the same PK parameters were also tested on the clearance of regorafenib and its metabolites. Laboratory parameters were preselected as covariates if they were associated with a Common Terminology Criteria for Adverse Events (CTCAE) grade >0 ⁴⁰ in at least 15% of total measurements. Covariates were implemented into the model in a stepwise forward inclusion and backward elimination approach using the *scm* script implemented in PsN.^{26,27} In the forward selection process, covariates which led to a significant decrease of the OFV ($P < .05$) were kept for further evaluation. The final forward model was re-evaluated by backward elimination of each covariate with a significance level of $P < .01$. If a covariate was still significant in this step, the plausibility of its effect as well as a successful model convergence was assessed and eventually kept in the model. Exponential and linear parameter-covariate relations were tested for continuous and categorical covariates, respectively.

For covariate analysis, the above-mentioned drug exposure parameters as well as demographic data (sex, age, weight, height, body surface area, body mass index), bilirubin and haemoglobin concentration were preselected. Even though bilirubin concentration exhibited a rather narrow range at baseline (Table 1), it was nevertheless included as the number of CTCAE grades >0 increased during the course of therapy (concentration range 2–32 µmol/L).

2.3.5 | Model evaluation

The precision of model parameter estimates defined as the relative standard error (RSE) assisted in model evaluation. Models which converged with a successful covariance step, were considered for further analysis. In order to assess the model fit, goodness-of-fit plots⁴¹ as

well as prediction-corrected visual predictive checks (pcVPC) were used. For the development of a pcVPC 5th, 50th and 95th percentiles with the respective 95% confidence intervals (CI) were generated from 1000 simulated datasets based on the observed dataset and superimposed by the observed plasma concentrations over time. Both simulated and observed plasma concentrations were normalized with respect to the median prediction.⁴² pcVPC were constructed in R using a modified code originally provided by the PMX Solutions website.⁴³ In addition, model robustness as well as precision and bias of parameter estimates were evaluated by non-parametric bootstrap analysis without stratification. Median and 95% CI of parameter estimates were derived from 1000 replicate datasets obtained from sampling individuals from the original dataset with replacement.

2.4 | Simulation study

The final population PK and covariate models were forwarded to extensive simulation studies. Here, the impact of potential covariates including drug interactions on the PK of capecitabine, regorafenib or their metabolites were analysed. The PK model of capecitabine containing the identified exposure parameter of regorafenib as covariate was therefore simulated. Values of this regorafenib drug exposure parameter were previously generated via simulation of its PK model. For Days 1, 8, 15, 22, 29 and 36, geometric mean drug clearances of capecitabine were calculated, along with their respective 95% CI.

3 | RESULTS

3.1 | Model building

For the development of the population PK parent-metabolite models, 86 capecitabine, 126 DFCR and 132 DFUR plasma concentration measurements were included as well as 151 regorafenib, 141 M-2 and 113 M-5 plasma concentration measurements (Figures S2.1–S2.6 in the Supporting Information).

3.1.1 | Capecitabine and metabolites

The observed plasma concentration–time course of capecitabine, DFCR and DFUR were best described by a one-compartment model (Figure 1). Model parameter estimates and bootstrap results are presented in Table 2. Residual variability was modelled using a proportional error model. Implementation of IOV was not successful due to run errors. In order to describe capecitabine absorption, a parallel first- and zero-order absorption model was most appropriate (Table S3.1 in the Supporting Information). The relatively slow first-order absorption process of capecitabine in combination with a rapid elimination indicated a flip-flop PK for capecitabine. Estimating the volume of distribution of the metabolite DFUR resulted in values close to the boundary of zero. This finding in combination with a

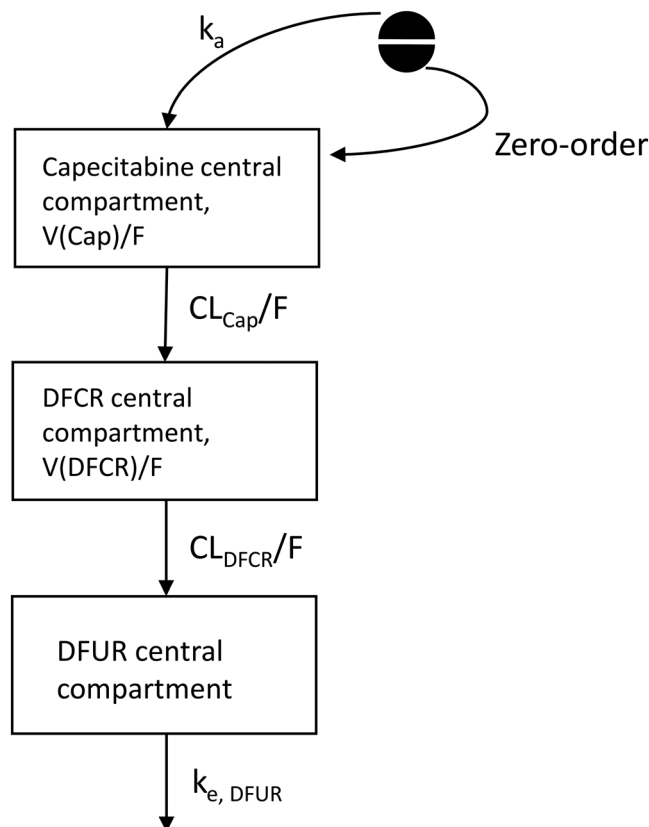


FIGURE 1 Model structure of the capecitabine-metabolite model. DFCR: 5'-deoxy-5-fluorocytidine; DFUR: 5'-deoxy-5-fluorouridine; CL_{Cap}/F , CL_{DFCR}/F : apparent capecitabine/DFCR clearance; V_{Cap}/F , V_{DFCR}/F : apparent capecitabine/DFCR volume of distribution; $k_{e, DFUR}$: elimination rate constant for DFUR; k_a : first-order absorption rate constant.

similar decay of DFCR and DFUR plasma concentrations (Figures S2.2 and S2.3 in the Supporting Information) indicated a flip-flop PK for DFUR as well.³² Therefore, only an elimination rate constant for DFUR ($k_{e, DFUR}$) was estimated and an IIV term on this rate constant was implemented.

The covariate analysis for the capecitabine-metabolite model is presented in Table S3.2 in the Supporting Information. The final model included regorafenib cumulative AUC as a covariate on capecitabine clearance, which led to a stable model along with a significant drop in OFV compared to the base model (-33.918 , $P < .00001$).

The identified exponential covariate led to a reduction of capecitabine clearance estimates:

$$CL_{Cap} = CL_{Cap, pop} \times e^{(-\theta \times AUC_{Reg, cum})} \times e^{\eta_i \cdot CL_{Cap, pop}} \quad (1)$$

where CL_{Cap} denotes the individual capecitabine clearance estimate, $CL_{Cap, pop}$ the population estimate of capecitabine clearance, θ is the covariate effect estimate, $AUC_{Reg, cum}$ is the cumulative AUC over time of regorafenib and $\eta_i \cdot CL_{Cap, pop}$ represents the IIV term for the capecitabine population clearance of the i^{th} individual with a mean of 0 and a variance of ω^2 . The median reduction of capecitabine clearance was

TABLE 2 Parameter estimates of the capecitabine-metabolite model

Parameter	Estimate (relative standard error, %)	Shrinkage [%]	Bootstrap median (95% confidence intervals)
CL _{Cap} /F [L/h]	286 (14.9)		296 (173–418)
V _{Cap} /F [L]	179 (17.8)		187 (101–273)
k _a [1/h]	0.0714 (23.2)		0.0828 (0.0387–0.336)
Duration zero-order absorption [h]	0.250 (2.5)		0.336 (0.0910–0.658)
Fraction of the first-order absorption process [%]	21.4 (11.8)		20.2 (13.0–36.1)
CL _{DFCR} /F [L/h]	123 (10.5)		122 (93.5–151)
V _{DFCR} /F [L]	71.9 (17.5)		67.2 (37.3–96.7)
k _{e, DFUR} [1/h]	99.2 (9.6)		100 (82.4–125)
Regorafenib cumulative AUC effect on CL _{Cap} /F	-4.10×10^{-4} (17.8)		-4.06×10^{-4} (-1.00×10^{-3} – (-3.02×10^{-5}))
<i>Interindividual variability</i>			
CL _{Cap} /F [%]	40.1 (26.4)	5.3	39.2 (13.9–91.9)
V _{Cap} /F [%]	39.7 (36.7)	20.6	43.9 (12.0–110)
CL _{DFCR} /F [%]	32.2 (25.5)	3.2	32.6 (3.83–63.2)
V _{DFCR} /F [%]	47.6 (35.5)	13.4	50.1 (19.2–96.3)
k _{e, DFUR} [%]	29.3 (25.9)	4.6	27.5 (16.7–40.6)
<i>Residual variability</i>			
Capecitabine [%]	60.1 (10.9)	3.9	58.8 (43.4–77.5)
DFCR [%]	46.1 (8.1)	4.7	45.1 (34.2–56.2)
DFUR [%]	45.2 (7.8)	4.7	42.9 (32.2–52.4)

CL_{Cap}/F, CL_{DFCR}/F: apparent capecitabine/DFCR clearance; V_{Cap}/F, V_{DFCR}/F: apparent capecitabine/DFCR volume of distribution; k_{e, DFUR}: elimination rate constant for DFUR; k_a: first-order absorption rate constant.

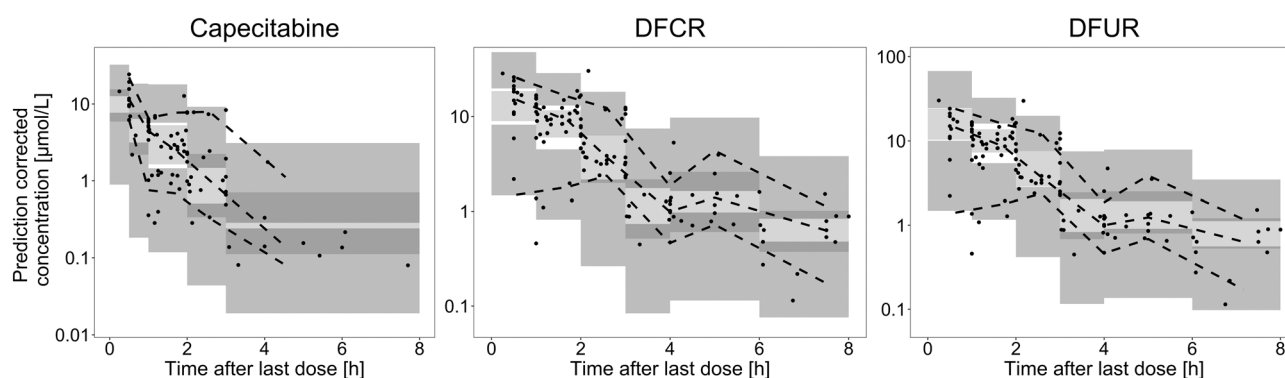


FIGURE 2 Prediction-corrected visual predictive checks of capecitabine, DFCR and DFUR. Black dots: Prediction-corrected observations; dashed lines: 90% interval and median of the prediction-corrected observations; dark grey shaded area: 95% confidence intervals of the 5th and 95th prediction interval; light grey shaded area: 95% confidence interval of median prediction.

45.6% at Day 36 (derived from a median regorafenib cumulative AUC from Day 0 to Day 36 of 1458.5 µmol-h/L).

Bootstrap estimates were in accordance with estimates from the final model. The models correctly described the observed data as depicted in the pcVPC (Figure 2) and in the goodness-of-fit plots (Figures S3.1–S3.3 in the Supporting Information). The pcVPC additionally indicated flip-flop PK for capecitabine, DFCR and DFUR due to a slow absorption or formation process.

3.1.2 | Regorafenib and metabolites

Plasma concentrations of regorafenib, M-2 and M-5 were best described by two-compartment models with a proportional error model. Due to a non-significant reduction in OFV, IOV was not incorporated. A summary of the model parameter estimates including the bootstrap results is presented in Table 3. A transit compartment model with Erlang distribution as previously described by Lindauer et al.⁴⁴ and Rousseau et al.⁴⁵ was

TABLE 3 Parameter estimates of the regorafenib-metabolite model.

Parameter	Estimate (relative standard error, %)	Shrinkage [%]	Bootstrap median (95% confidence intervals)
$CL_{\text{Regorafenib}}/F$ [L/h]	1.94 (12.1)		1.91 (1.47–2.46)
V_c/F [L]	10.4 (33.2)		9.83 (2.37–23.2)
$MAT_{\text{Regorafenib}}$ [h]	3.01 (9.6)		3.05 (2.03–4.05)
V_p/F [L]	63.9 (8.7)		64.4 (50.3–85.2)
Q/F [L/h]	13.5 (10.8)		13.7 (9.64–17.7)
CL_{M-2}/F [L/h]	0.936 (10.8)		0.932 (0.731–1.19)
$k_{g,\text{met}}$ [1/h]	0.265 (12.8)		0.267 (0.168–0.449)
MAT_{M-2} [h]	1.90 (14.1)		1.91 (1.31–2.96)
CL_{M-5}/F [L/h]	2.01 (21.7)		2.02 (1.14–3.16)
<i>Interindividual variability</i>			
$CL_{\text{Regorafenib}}/F$ [%]	38.1 (23.6)	3.1	34.5 (14.8–48.0)
V_c/F [%]	131.5 (24.2)	3.7	126.9 (82.3–238.7)
MAT (Regorafenib) [%]	21.7 (24.7)	4.4	19.9 (5.92–30.0)
CL_{M-2}/F [%]	25.2 (33.6)	11.6	23.7 (6.15–37.9)
CL_{M-5}/F [%]	75.6 (22.3)	0.1	72.6 (50.1–99.3)
<i>Residual variability</i>			
Regorafenib [%]	52.6 (7.4)	3.6	51.2 (42.5–59.0)
M-2 [%]	57.9 (8.1)	1.5	57.9 (52.2–63.6)
M-5 [%]	54.1 (9.1)	4.7	53.6 (48.1–59.4)

$CL_{\text{Regorafenib}}/F$, CL_{M-2}/F , CL_{M-5}/F : apparent regorafenib/M-2/M-5 clearance; V_c/F : apparent shared central volume of distribution; V_p/F : apparent shared peripheral volume of distribution; Q/F : apparent shared intercompartmental clearance; $MAT_{\text{Regorafenib}}/MAT_{M-2}$: mean absorption time of regorafenib/M-2 defined as n transit compartments/transit constant k_{tr} ; $k_{g,\text{met}}$: presystemic metabolic rate constant.

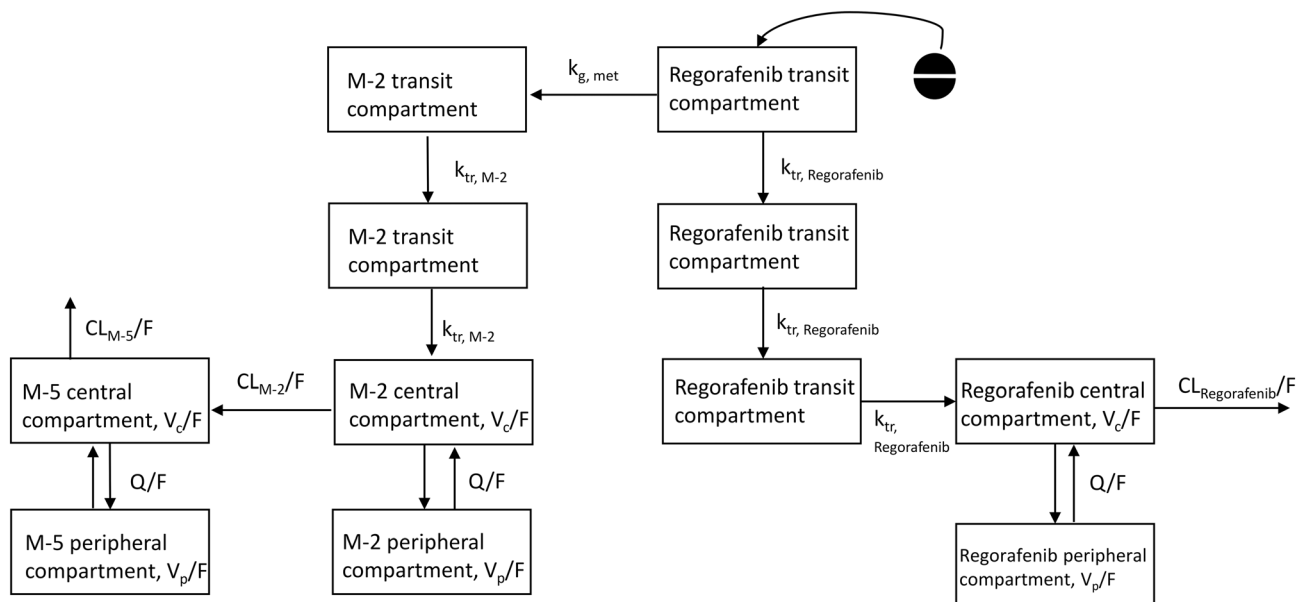


FIGURE 3 Model structure of the regorafenib-metabolite model. $CL_{\text{Regorafenib}}/F$, CL_{M-2}/F , CL_{M-5}/F : apparent regorafenib/M-2/M-5 clearance; V_c/F : apparent shared central volume of distribution; V_p/F : apparent shared peripheral volume of distribution; Q/F : apparent shared intercompartmental clearance; $k_{tr, \text{Regorafenib}}/k_{tr, M-2}$: transfer rate constants defined as n transit compartments/mean absorption time; $k_{g,\text{met}}$: presystemic metabolic rate constant

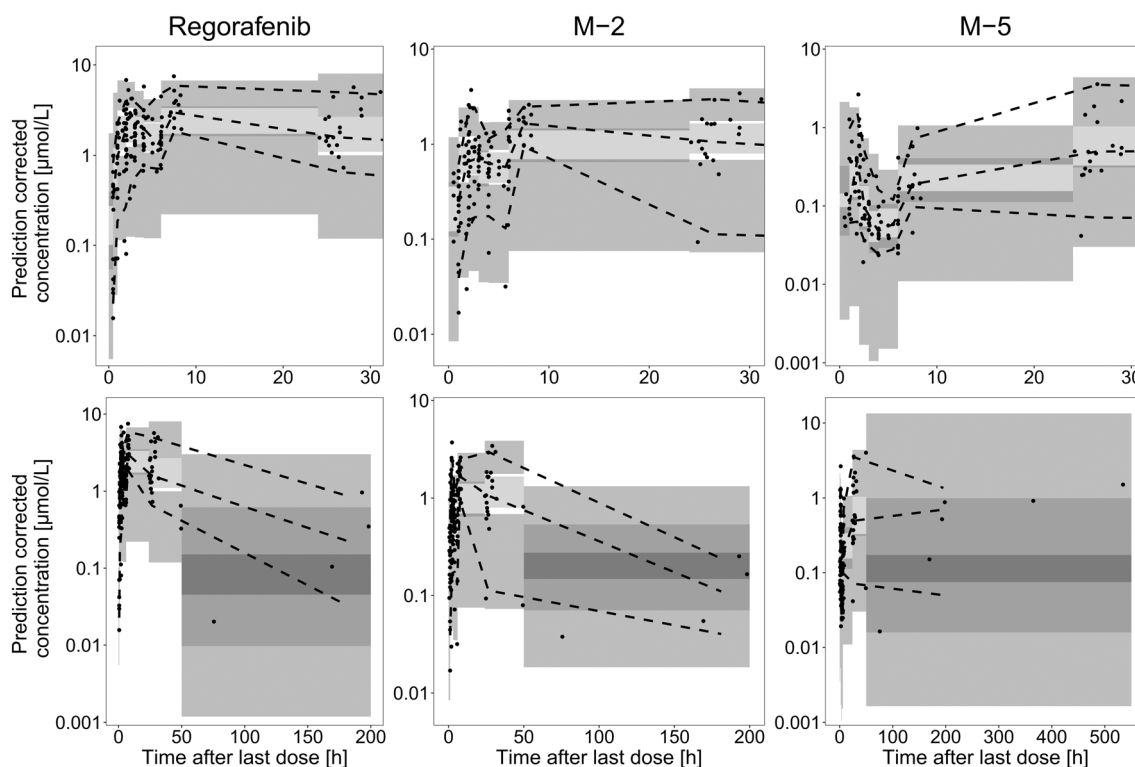


FIGURE 4 Prediction-corrected visual predictive checks of regorafenib, M-2 and M-5 from 0 to 30 hours (upper panel) and from 0 to 200 hours (regorafenib, M-2, lower panel) as well as from 0 to 550 hours (M-5, lower panel). Black dots: Prediction-corrected observations; dashed lines: 90% interval and median of the prediction-corrected observations; dark grey shaded area: 95% confidence intervals of the 5th and 95th prediction interval; light grey shaded area: 95% confidence interval of the median prediction.

the most suitable in order to describe regorafenib absorption (Table S3.3 in the Supporting Information). Mean absorption time (MAT) was estimated and a transfer rate constant (k_{tr}) between these compartments was calculated as follows:

$$k_{tr} = \frac{\text{Number of transit compartments}}{\text{MAT}} \quad (2)$$

The formation of M-2 and M-5 is outlined in Figure 3. M-2 metabolism was best described by presystemic formation occurring from the first transit compartment of regorafenib. A series of transit compartments was chosen for the description of M-2 absorption as well. Since PK data after direct administration of M-2 and M-5 were not available and the conversion percentages were unknown, the volumes of distribution of M-2 and M-5 could not be estimated. Therefore, it was assumed that their volumes of distribution as well as the intercompartmental clearances were the same as that of regorafenib. IIV terms on the clearances of all three compounds, the shared volume of distribution and the mean absorption time of regorafenib were successfully included. Available plasma concentration data of regorafenib and its metabolites did not support the implementation of EHC models.

Covariate analyses of regorafenib-metabolite base models are presented in Table S3.4 in the Supporting Information. None of the identified covariates remained in the final model. The pcVPC (Figure 4) as well as the goodness-of-fit plots (Figures S3.4–S3.6 in

the Supporting Information) showed an adequate description of the observed data although the depiction of the observed data versus the population predictions of M-2 and M-5 revealed a tendency towards an underprediction of higher plasma concentration values.

3.2 | Simulation study

The impact of regorafenib cumulative AUC on capecitabine clearance was submitted to simulation analysis as described above. The final regorafenib-metabolite model was used to simulate 1000 subjects for each regorafenib dose level (40/80/120 mg once daily) until Day 36. The treatment schedule was the same as the schedule from the study (2 weeks of treatment, 7-day break, another 2 weeks of treatment). A capecitabine dose of 1500 mg bidaily (corresponding to 825 mg/m² bidaily) was chosen and simulation was subsequently performed including the regorafenib cumulative AUC as covariate for the same time period. In addition, 1000 patients without regorafenib were simulated. The simulation results are depicted in Figure 5 (from 792–864 hours) and Figure S4.1 in the Supporting Information (total simulation time period). Calculated capecitabine clearance values are presented for various time points in Table S4.1 in the Supporting Information. A higher regorafenib dose and subsequent cumulative AUC was associated with a lower capecitabine clearance (Table S4.1) and hence reduced capecitabine metabolism to active metabolites. Whereas capecitabine

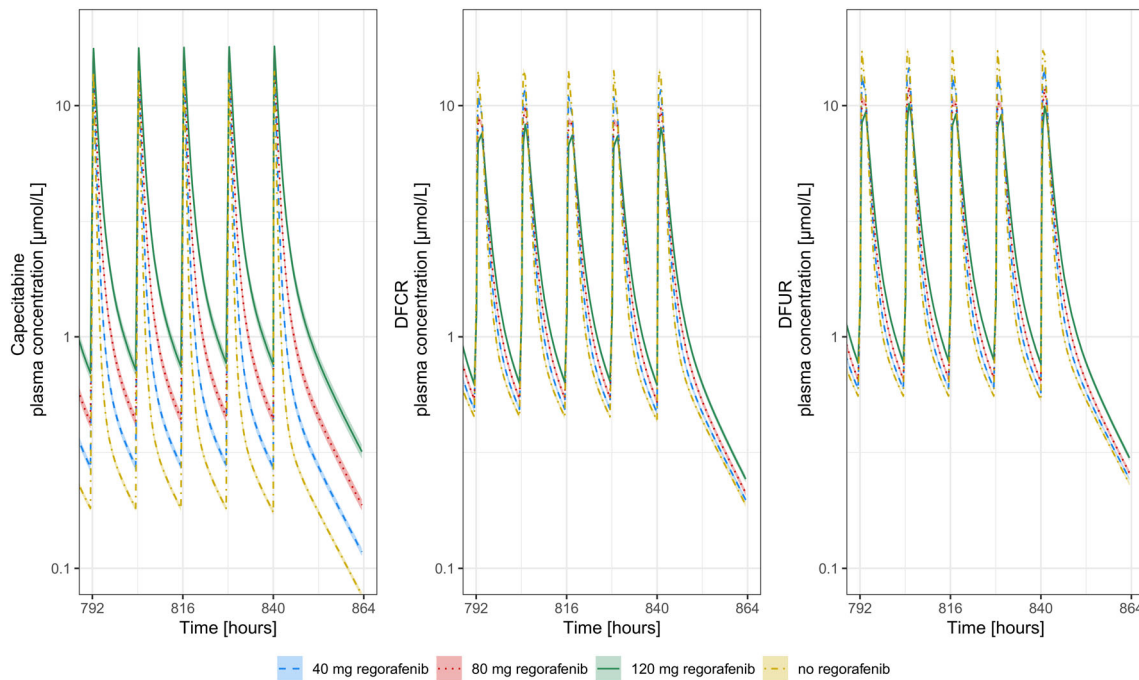


FIGURE 5 Simulated plasma concentrations of capecitabine, DFCR and DFUR depending on regorafenib dosage from 792 to 864 hours.

clearance was comparable between regorafenib dose levels on Day 1, the impact of regorafenib on capecitabine clearance increased with increasing cumulative regorafenib exposure (Table S4.1). With decreasing capecitabine clearance, formation of DFCR and DFUR was expected to decrease likewise. Like for capecitabine, CIs of the concentration–time curves of DFCR and DFUR overlapped in the beginning as well, whereas they diverged more with increasing cumulative regorafenib exposure. However, the differences in metabolite exposure were negligible between the different regorafenib dose levels including simulations with 0 mg regorafenib. The respective plots are presented in Figure 5 as well as in Figures S4.2 and S4.3 in the Supporting Information.

4 | DISCUSSION

This is the first study to evaluate the addition of the multi-TKI regorafenib to capecitabine-augmented local radiotherapy in LARC patients. We successfully developed population PK and covariate parent-metabolite models of regorafenib and capecitabine in patients of trial SAKK 41/16 RECAP. The description of capecitabine absorption by parallel first- and zero-order processes differed from the absorption models of published capecitabine models in which parallel first-order,³³ transit compartments³² or first-order absorption with lag time^{30,31} were established. In fact, capecitabine absorption is highly variable due to, for example, double peaks,³³ the impact of age,³¹ food⁴⁶ or alterations in the gastrointestinal tract including potential gastrectomy in patients with gastro-oesophageal cancer, for example.³² One possible explanation for the identification of a dual absorption process may be the reflection of different absorption sites,

namely the small intestine and the stomach.^{33,46} The slow first-order absorption process as well as comparatively slower metabolite formations were presumably responsible for the occurrence of flip-flop PK for capecitabine, DFCR, and DFUR in our model. This was also indicated by biphasic declines of the concentration–time curves despite using one-compartment models.⁴⁷ It should, however, be noted that the patients' first observations were almost exclusively those with the highest plasma concentrations. An additional sample could be drawn between 0 and 0.5 hours post dose intake, e.g. after 15 minutes, as observed in the model of Jacobs et al.³² to gain more certainty about capecitabine absorption. The establishment of one-compartment models for capecitabine, DFCR and DFUR was in accordance with several published population PK models.^{30,31,33} Additionally, the identified flip-flop PK of DFUR could also be observed in the model of Jacobs et al.³²

The population PK model structure and parameters of the regorafenib-metabolite model were similar to the published model of Keunecke et al.³⁸ However, in our model the formation of M-5 from M-2 was established, whereas Keunecke et al. assumed that M-5 is directly formed by regorafenib.³⁸ The proposed metabolic pathway of Gerisch et al. indicated that M-5 is indeed formed by M-2⁴⁸ and our population PK model did not allow us to distinguish between both proposed pathways (Table S3.3 in the Supporting Information). The implementation of covariates was not successful either since the inclusion of additional parameters led to model instabilities presumably due to overparameterization. The inclusion of identified covariates from the study of Keunecke et al.³⁸ (sex on clearance of regorafenib, M-2 and M-5, respectively, as well as BMI on regorafenib clearance) led to estimated covariate parameters with large RSE ($\geq 58\%$) and a non-significant drop in OFV compared to the base model

(-6.052 , $P = .20$). Furthermore, the establishment of an EHC could not be supported by the underlying data of this study. Besides a presumed overparameterization of the model, the sampling time of regorafenib and its metabolites should be adjusted in order to account for the identification of EHC-caused concentration peaks. Secondary and tertiary peaks were found to be at about 6 to 8 as well as 24 hours after dose intake,¹⁸ hence additional sampling of regorafenib and its metabolites should be considered, as in this trial the last sample was drawn at 6 hours.

The covariate analysis in this study revealed a significant negative influence of regorafenib cumulative AUC over time on the formation of capecitabine active metabolites. Already 1 week after regorafenib intake, capecitabine clearance values were significantly reduced depending on regorafenib dose levels (Table S4.1). This should lead to a reduced formation of its metabolites DFUR, DFUR as well as fluorouracil, which is finally converted to active metabolites. However, DFUR and DFUR exposure remained unaffected by the reduced capecitabine clearance (Figures S4.2 and S4.3), which translates to an unaffected exposure of fluorouracil. Accordingly, we assume a negligible clinical relevance of this DDI since capecitabine-associated adverse events are mainly attributed to its metabolites.⁴⁹ However, fluorouracil was not quantified in this study since its formation occurs intracellularly and thus it exhibits very low plasma concentrations after capecitabine administration. A possible explanation for the identified DDI could be the inhibition of the ATP-binding cassette (ABC) transporters P-glycoprotein (Pgp) or breast cancer resistance protein (BCRP) by regorafenib^{50,51} since there have been hints that capecitabine might be a substrate for ABC transporters.^{52–54} However, a clinical study with regorafenib and the Pgp substrate digoxin as well as the BCRP substrate rosuvastatin showed no influence on digoxin PK but on rosuvastatin exposure by regorafenib.⁵¹ In addition, similar effects on capecitabine exposure were observed in two clinical trials in which capecitabine was administered in combination with sorafenib which is the defluorinated form of regorafenib. Both studies reported moderately increased capecitabine AUC while co-administering sorafenib compared to control groups with capecitabine monotherapy.^{55,56} From published population PK models of capecitabine, bilirubin concentration as a linear covariate on capecitabine clearance was tested³⁰ but resulted in a failure of the covariance step. Since only patients with adequate hepatic and renal function (see “Methods” section) were included in this study, covariate analysis of elimination parameters for all compounds was impeded as the respective laboratory parameters exhibited a rather narrow range. It should be noted that our identified covariate effect should be carefully interpreted due to the small number of patients in this analysis. Furthermore, regorafenib was administered in lower doses than the approved dose of 160 mg daily. Therefore, the impact of the usual daily dose of regorafenib could not be evaluated in our study. In order to assess the clinical relevance of our finding, a future double-arm study which investigates patients under capecitabine monotherapy and patients under the combination of capecitabine and regorafenib should be conducted in a larger number of study participants. Intracellular concentrations of active metabolites of fluorouracil such as

5-fluorouridine 5'-triphosphate as predictor for capecitabine toxicity⁵⁷ could be additionally quantified.

In conclusion, the developed population PK models suggest a negligible effect of regorafenib cumulative AUC on the metabolic activation of capecitabine. Our models may serve as a basis for future DDI studies in patients under therapy with both oral anticancer drugs.

ACKNOWLEDGEMENT

Open Access funding enabled and organized by Projekt DEAL.

COMPETING INTERESTS

All authors declare that they have no conflicts of interest that are relevant to the content of this manuscript.

CONTRIBUTORS

C.R.L., C.C., D.B., R.v.M., S.B. and M.J. designed the study. E.S., C.B., R.T., L.A.D., C.R.L., J.-C.P., M.G., R.v.M., S.B. and M.J. performed the research. E.S., M.J. and U.J. analysed the data. E.S., C.B., R.T., C.R.L., J.-C.P., D.B., M.G., R.v.M., S.B., M.J. and U.J. wrote or contributed to the writing of the manuscript.

DATA AVAILABILITY STATEMENT

The modelling codes are provided in the Supporting Information available online. Data are available from the Swiss Group for Clinical Cancer Research (SAKK) upon reasonable request.

ORCID

Eduard Schmulenson  <https://orcid.org/0000-0002-8026-609X>

Ulrich Jaehde  <https://orcid.org/0000-0002-2493-7370>

REFERENCES

- Sung H, Ferlay J, Siegel RL, et al. Global Cancer Statistics 2020: GLOBOCAN estimates of incidence and mortality worldwide for 36 cancers in 185 countries. *CA Cancer J Clin*. 2021;71(3):209-249. doi:10.3322/caac.21660
- Araghi M, Soerjomataram I, Bardot A, et al. Changes in colorectal cancer incidence in seven high-income countries: a population-based study. *Lancet Gastroenterol Hepatol*. 2019;4(7):511-518. doi:10.1016/S2468-1253(19)30147-5
- Saad el Din K, Loree JM, Sayre EC, et al. Trends in the epidemiology of young-onset colorectal cancer: a worldwide systematic review. *BMC Cancer*. 2020;20(1):288. doi:10.1186/s12885-020-06766-9
- Glynne-Jones R, Wyrwicz L, Tiret E, et al. Rectal cancer: ESMO clinical practice guidelines for diagnosis, treatment and follow-up. *Ann Oncol*. 2017;28(suppl_4):iv22-iv40. doi:10.1093/annonc/mdx224
- Siegel RL, Miller KD, Goding Sauer A, et al. Colorectal cancer statistics, 2020. *CA Cancer J Clin*. 2020;70(3):145-164. doi:10.3322/caac.21601
- López-Campos F, Martín-Martín M, Fornell-Pérez R, et al. Watch and wait approach in rectal cancer: current controversies and future directions. *World J Gastroenterol*. 2020;26(29):4218-4239. doi:10.3748/wjg.v26.i29.4218
- Karagkounis G, Thai L, Mace AG, et al. Prognostic implications of pathological response to neoadjuvant chemoradiation in pathologic stage III rectal cancer. *Ann Surg*. 2019;269(6):1117-1123. doi:10.1097/SLA.0000000000002719

8. Gérard J-P, Azria D, Gourgou-Bourgade S, et al. Comparison of two neoadjuvant chemoradiotherapy regimens for locally advanced rectal cancer: results of the phase III trial ACCORD 12/0405-Prodigie 2. *J Clin Oncol*. 2010;28(10):1638-1644. doi:10.1200/JCO.2009.25.8376
9. Park J, Yoon SM, Yu CS, Kim JH, Kim TW, Kim JC. Randomized phase 3 trial comparing preoperative and postoperative chemoradiotherapy with capecitabine for locally advanced rectal cancer. *Cancer*. 2011;117(16):3703-3712. doi:10.1002/cncr.25943
10. Bosset J-F, Collette L, Calais G, et al. Chemotherapy with preoperative radiotherapy in rectal cancer. *N Engl J Med*. 2006;355(11):1114-1123. doi:10.1056/NEJMoa060829
11. von Moos R, Koeberle D, Schacher S, et al. Neoadjuvant radiotherapy combined with capecitabine and sorafenib in patients with advanced KRAS-mutated rectal cancer: a phase I/II trial (SAKK 41/08). *Eur J Cancer*. 2018;89:82-89. doi:10.1016/j.ejca.2017.11.005
12. Marti FEM, Jayson GC, Manoharan P, et al. Novel phase I trial design to evaluate the addition of cediranib or selumetinib to preoperative chemoradiotherapy for locally advanced rectal cancer: the DREAMtherapy trial. *Eur J Cancer*. 2019;117:48-59. doi:10.1016/j.ejca.2019.04.029
13. Willeke F, Horisberger K, Kraus-Tiefenbacher U, et al. A phase II study of capecitabine and irinotecan in combination with concurrent pelvic radiotherapy (CapIri-RT) as neoadjuvant treatment of locally advanced rectal cancer. *Br J Cancer*. 2007;96(6):912-917. doi:10.1038/sj.bjc.6603645
14. Koeberle D, Burkhard R, von Moos R, et al. Phase II study of capecitabine and oxaliplatin given prior to and concurrently with preoperative pelvic radiotherapy in patients with locally advanced rectal cancer. *Br J Cancer*. 2008;98(7):1204-1209. doi:10.1038/sj.bjc.6604297
15. Krishnan S, Janjan NA, Skibber JM, et al. Phase II study of capecitabine (Xeloda) and concomitant boost radiotherapy in patients with locally advanced rectal cancer. *Int J Radiat Oncol Biol Phys*. 2006;66(3):762-771. doi:10.1016/j.ijrobp.2006.05.063
16. Strumberg D, Schultheis B. Regorafenib for cancer. *Expert Opin Investig Drugs*. 2012;21(6):879-889. doi:10.1517/13543784.2012.684752
17. Solimando DA, Waddell JA. Drug monographs: bosutinib and regorafenib. *Hosp Pharm*. 2013;48(3):190-194. doi:10.1310/hpj4803-190
18. Mross K, Frost A, Steinbild S, et al. A phase I dose-escalation study of regorafenib (BAY 73-4506), an inhibitor of oncogenic, angiogenic, and stromal kinases, in patients with advanced solid tumors. *Clin Cancer Res*. 2012;18(9):2658-2667. doi:10.1158/1078-0432.CCR-11-1900
19. Saif MW, Katirtzoglou NA, Syrigos KN. Capecitabine: an overview of the side effects and their management. *Anticancer Drugs*. 2008;19(5):447-464. doi:10.1097/CAD.0b013e3282f945aa
20. Hamzic S, Aebi S, Joerger M, et al. Fluoropyrimidine chemotherapy: recommendations for DPYD genotyping and therapeutic drug monitoring of the Swiss Group of Pharmacogenomics and Personalised Therapy. *Swiss Med Wkly*. 2020;150:w20375. doi:10.4414/smww.2020.20375
21. Amstutz U, Henricks LM, Offer SM, et al. Clinical Pharmacogenetics Implementation Consortium (CPIC) guideline for dihydropyrimidine dehydrogenase genotype and fluoropyrimidine dosing: 2017 update. *Clin Pharmacol Ther*. 2018;103(2):210-216. doi:10.1002/cpt.911
22. Cardoso E, Mercier T, Wagner AD, et al. Quantification of the next-generation oral anti-tumor drugs dabrafenib, trametinib, vemurafenib, cobimetinib, pazopanib, regorafenib and two metabolites in human plasma by liquid chromatography-tandem mass spectrometry. *J Chromatogr B Analyt Technol Biomed Life Sci*. 2018;1083:124-136. doi:10.1016/j.jchromb.2018.02.008
23. US Food and Drug Administration. Bioanalytical Method Validation. Guidance for Industry; 2018.
24. CLSI. *Liquid Chromatography-Mass Spectrometry Methods; Approved Guidelines*. CLSI document C62-A. Wayne, PA: Clinical and Laboratory Standard Institute; 2014.
25. Bauer RJ. *NONMEM Users Guide*. Gaithersburg, MD: Icon Development Solutions; 2021.
26. Lindbom L, Pihlgren P, Jonsson EN, et al. PsN-Toolkit—a collection of computer intensive statistical methods for non-linear mixed effect modeling using NONMEM. *Comput Methods Programs Biomed*. 2005;79(3):241-257. doi:10.1016/j.cmpb.2005.04.005
27. Lindbom L, Ribbing J, Jonsson EN. Perl-speaks-NONMEM (PsN)—a Perl module for NONMEM related programming. *Comput Methods Programs Biomed*. 2004;75(2):85-94. doi:10.1016/j.cmpb.2003.11.003
28. R Core Team. R: A Language and Environment for Statistical Computing. Vienna, Austria: R Foundation for Statistical Computing; 2021. <http://www.R-project.org/>. Accessed December 22, 2021.
29. Keizer RJ, Karlsson MO, Hooker A. Modeling and simulation workbench for NONMEM: tutorial on Pirana, PsN, and Xpose. *CPT Pharmacometrics Syst Pharmacol*. 2013;2(6):e50. doi:10.1038/psp.2013.24
30. Urien S, Zezai K, Lokiec F. Pharmacokinetic modelling of 5-FU production from capecitabine—a population study in 40 adult patients with metastatic cancer. *J Pharmacokinetic Pharmacodyn*. 2005;32(5-6):817-833. doi:10.1007/s10928-005-0018-2
31. Daher Abdi Z, Lavau-Denes S, Prémaud A, et al. Pharmacokinetics and exposure-effect relationships of capecitabine in elderly patients with breast or colorectal cancer. *Cancer Chemother Pharmacol*. 2014;73(6):1285-1293. doi:10.1007/s00280-014-2466-0
32. Jacobs BAW, Deenen MJ, Joerger M, et al. Pharmacokinetics of capecitabine and four metabolites in a heterogeneous population of cancer patients: a comprehensive analysis. *CPT Pharmacometrics Syst Pharmacol*. 2019;8(12):940-950. doi:10.1002/psp4.12474
33. Lunar N, Etienne-Grimaldi M-C, Maccuire P, et al. Population pharmacokinetic and pharmacodynamic modeling of capecitabine and its metabolites in breast cancer patients. *Cancer Chemother Pharmacol*. 2021;87(2):229-239. doi:10.1007/s00280-020-04208-8
34. Stroh M, Hutmacher MM, Pang J, Lutz R, Magara H, Stone J. Simultaneous pharmacokinetic model for rolofylline and both M1-trans and M1-cis metabolites. *AAPS J*. 2013;15(2):498-504. doi:10.1208/s12248-012-9443-5
35. Keizer RJ, Jansen RS, Rosing H, et al. Incorporation of concentration data below the limit of quantification in population pharmacokinetic analyses. *Pharmacol Res Perspect*. 2015;3(2):e00131. doi:10.1002/prp2.131
36. Jain L, Woo S, Gardner ER, et al. Population pharmacokinetic analysis of sorafenib in patients with solid tumours. *Br J Clin Pharmacol*. 2011;72(2):294-305. doi:10.1111/j.1365-2125.2011.03963.x
37. NUsers (NONMEM UsersNet Archive). Adaptation of multiple-dose enterohepatic circulation model suggested by Luann Phillips (after Stuart Beal) 2002. <https://cognigen.com/nonmem/nm/98may312002.html>. Accessed December 22, 2021.
38. Keunecke A, Hoefman S, Drenth H-J, Zisowsky J, Cleton A, Ploeger BA. Population pharmacokinetics of regorafenib in solid tumours: exposure in clinical practice considering enterohepatic circulation and food intake. *Br J Clin Pharmacol*. 2020;86(12):2362-2376. doi:10.1111/bcp.14334
39. Mould DR, Upton RN. Basic concepts in population modeling, simulation, and model-based drug development—part 2: introduction to pharmacokinetic modeling methods. *CPT Pharmacometrics Syst Pharmacol*. 2013;2(4):e38. doi:10.1038/psp.2013.14
40. National Cancer Institute. Common terminology criteria for adverse events. <https://ctep.cancer.gov>. Accessed April 20, 2022.
41. Nguyen THT, Mouksassi M-S, Holford N, et al. Model evaluation of continuous data pharmacometric models: metrics and graphics. *CPT Pharmacometrics Syst Pharmacol*. 2017;6(2):87-109. doi:10.1002/psp4.12161
42. Bergstrand M, Hooker AC, Wallin JE, Karlsson MO. Prediction-corrected visual predictive checks for diagnosing nonlinear mixed-effects models. *AAPS J*. 2011;13(2):143-151. doi:10.1208/s12248-011-9255-z

43. PMX Solutions. A step-by-step guide to prediction corrected visual predictive checks (VPC) of NONMEM models. <https://www.pmxsolutions.com/2018/09/21/a-step-by-step-guide-to-prediction-corrected-visual-predictive-checks-vpc-of-nonmem-models/> Accessed December 22, 2021.
44. Lindauer A, Siepmann T, Oertel R, et al. Pharmacokinetic/pharmacodynamic modelling of venlafaxine: pupillary light reflex as a test system for noradrenergic effects. *Clin Pharmacokinet*. 2008;47(11):721-731. doi:10.2165/00003088-200847110-00003
45. Rousseau A, Léger F, Le Meur Y, et al. Population pharmacokinetic modeling of oral cyclosporin using NONMEM: comparison of absorption pharmacokinetic models and design of a Bayesian estimator. *Ther Drug Monit*. 2004;26(1):23-30. doi:10.1097/00007691-200402000-00006
46. Reigner B, Verweij J, Dirix L, et al. Effect of food on the pharmacokinetics of capecitabine and its metabolites following oral administration in cancer patients. *Clin Cancer Res*. 1998;4(4):941-948.
47. Neyens M, Crauwels HM, Perez-Ruixo JJ, Rossenu S. Population pharmacokinetics of the rilpivirine long-acting formulation after intramuscular dosing in healthy subjects and people living with HIV. *J Antimicrob Chemother*. 2021;76(12):3255-3262. doi:10.1093/jac/dkab338
48. Gerisch M, Hafner F-T, Lang D, et al. Mass balance, metabolic disposition, and pharmacokinetics of a single oral dose of regorafenib in healthy human subjects. *Cancer Chemother Pharmacol*. 2017;81(1):195-206. doi:10.1007/s00280-017-3480-9
49. Ma WW, Saif MW, El-Rayes BF, et al. Emergency use of uridine triacetate for the prevention and treatment of life-threatening 5-fluorouracil and capecitabine toxicity. *Cancer*. 2017;123(2):345-356. doi:10.1002/cncr.30321
50. Wang Y-J, Zhang Y-K, Zhang G-N, et al. Regorafenib overcomes chemotherapeutic multidrug resistance mediated by ABCB1 transporter in colorectal cancer: in vitro and in vivo study. *Cancer Lett*. 2017;396:145-154. doi:10.1016/j.canlet.2017.03.011
51. Strumberg D, Al-Batran S-E, Takacs I, et al. A phase I study to determine the effect of regorafenib (REG) on the pharmacokinetics (PK) of substrates of P-glycoprotein (P-gp; digoxin) and breast cancer resistant protein (BCRP; rosuvastatin) in patients with advanced solid tumors. *Ann Oncol*. 2016;27:V1156. doi:10.1093/annonc/mdw370.23
52. Zhang J, Zhang L, Yan Y, et al. Are capecitabine and the active metabolite 5-Fu CNS penetrable to treat breast cancer brain metastasis? *Drug Metab Dispos*. 2015;43(3):411-417. doi:10.1124/dmd.114.061820
53. Lou Y, Wang Q, Zheng J, et al. Possible pathways of capecitabine-induced hand-foot syndrome. *Chem Res Toxicol*. 2016;29(10):1591-1601. doi:10.1021/acs.chemrestox.6b00215
54. Varma A, Mathaiyan J, Shewade D, Dubashi B, Sunitha K. Influence of ABCB-1, ERCC-1 and ERCC-2 gene polymorphisms on response to capecitabine and oxaliplatin (CAPOX) treatment in colorectal cancer (CRC) patients of South India. *J Clin Pharm Ther*. 2020;45(4):617-627. doi:10.1111/jcpt.13166
55. Awada A, Gil T, Whenham N, et al. Safety and pharmacokinetics of sorafenib combined with capecitabine in patients with advanced solid tumors: results of a phase 1 trial. *J Clin Pharmacol*. 2011;51(12):1674-1684. doi:10.1177/0091270010386226
56. Infante JR, Jones SF, Bendell JC, et al. A drug interaction study evaluating the pharmacokinetics and toxicity of sorafenib in combination with capecitabine. *Cancer Chemother Pharmacol*. 2012;69(1):137-144. doi:10.1007/s00280-011-1674-0
57. Janssen JM, Jacobs BAW, Roosendaal J, et al. Population pharmacokinetics of intracellular 5-fluorouridine 5'-triphosphate and its relationship with hand-and-foot syndrome in patients treated with capecitabine. *AAPS J*. 2021;23(1):23. doi:10.1208/s12248-020-00533-1

SUPPORTING INFORMATION

Additional supporting information can be found online in the Supporting Information section at the end of this article.

How to cite this article: Schmulenson E, Bovet C, Theurillat R, et al. Population pharmacokinetic analyses of regorafenib and capecitabine in patients with locally advanced rectal cancer (SAKK 41/16 RECAP). *Br J Clin Pharmacol*. 2022;1-12. doi:10.1111/bcp.15461

Validation results of the LC-MS/MS assay for capecitabine, DFCR and DFUR

Tab. S1-1: Intra- and inter-day (n=6) bias and coefficients of variation for capecitabine, DFCR, and DFUR

Analyte	Concentration (ng/mL)	Intraday		Interday	
		Bias (%)	CV (%)	Bias (%)	CV (%)
Capecitabine	1485	4.4	7.9	6.0	4.8
	4950	-0.8	5.5	0.7	5.1
	8910	2.8	1.8	1.9	2.9
DFCR	1485	-1.5	8.2	-1.0	4.5
	4950	-1.8	7.3	-2.6	6.1
	8910	1.2	0.1	2.0	4.3
DFUR	1485	-4.0	5.5	5.6	3.8
	4950	1.1	5.9	2.5	4.8
	8910	4.1	2.7	2.9	3.6

Tab. S1-2: Recoveries of capecitabine, DFCR and DFUR in six different plasma samples

Name	Concentration (ng/mL)	Recovery (%)	CV (%)
Capecitabine	1485	105	7.3
	4950	98	5.1
	8910	98	7.2
DFCR	1485	103	10.7
	4950	97	6.5
	8910	98	7.1
DFUR	1485	106	7.2
	4950	99	5.6
	8910	98	7.3

Tab. S1-3: Matrix effect of capecitabine, DFCR, and DFUR in six different plasma samples

Name	Concentration (ng/mL)	Matrix effect (%)
Capecitabine	1485	91 - 109%
	4950	95 - 103%
	8910	95 - 103%
DFCR	1485	83 - 104%
	4950	83 - 101%
	8910	84 - 99%
DFUR	1485	83 - 98%
	4950	85 - 103%
	8910	87 - 103%

Tab. S1-4: Carryover values for capecitabine, DFCR, and DFUR in calibrator 1 (500ng/mL, Cal 1) after alternating Cal1 and calibrator 6 (10000 ng/mL, Cal6) measurements

Name	Carryover	
	Cal 1 (%)	Cal 1 IS (%)
Capecitabine	2.6	1.7
DFCR	8.6	3.0
DFUR	-10.0	4.1

Observed plasma concentration-time profiles

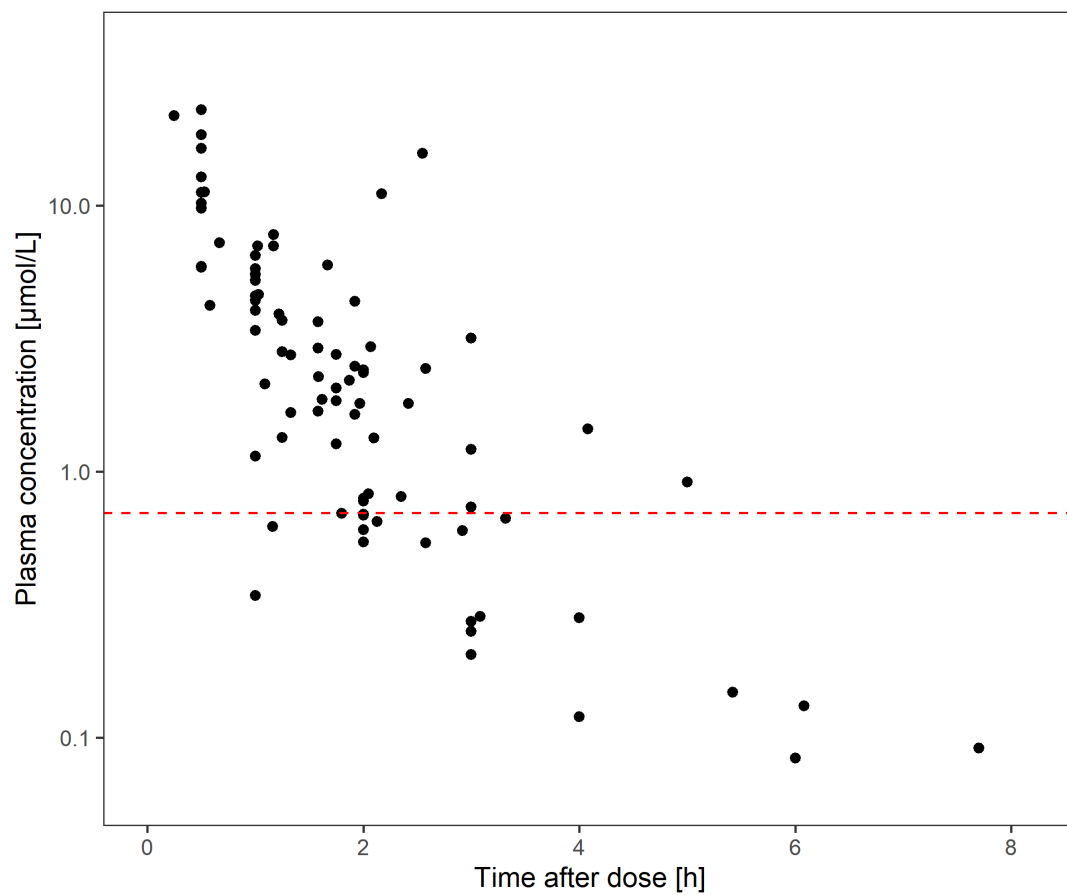


Fig. S2-1 Log scale plasma concentration-time profile of capecitabine. The red dashed line indicates the lower limit of quantification of 0.25 µg/mL.

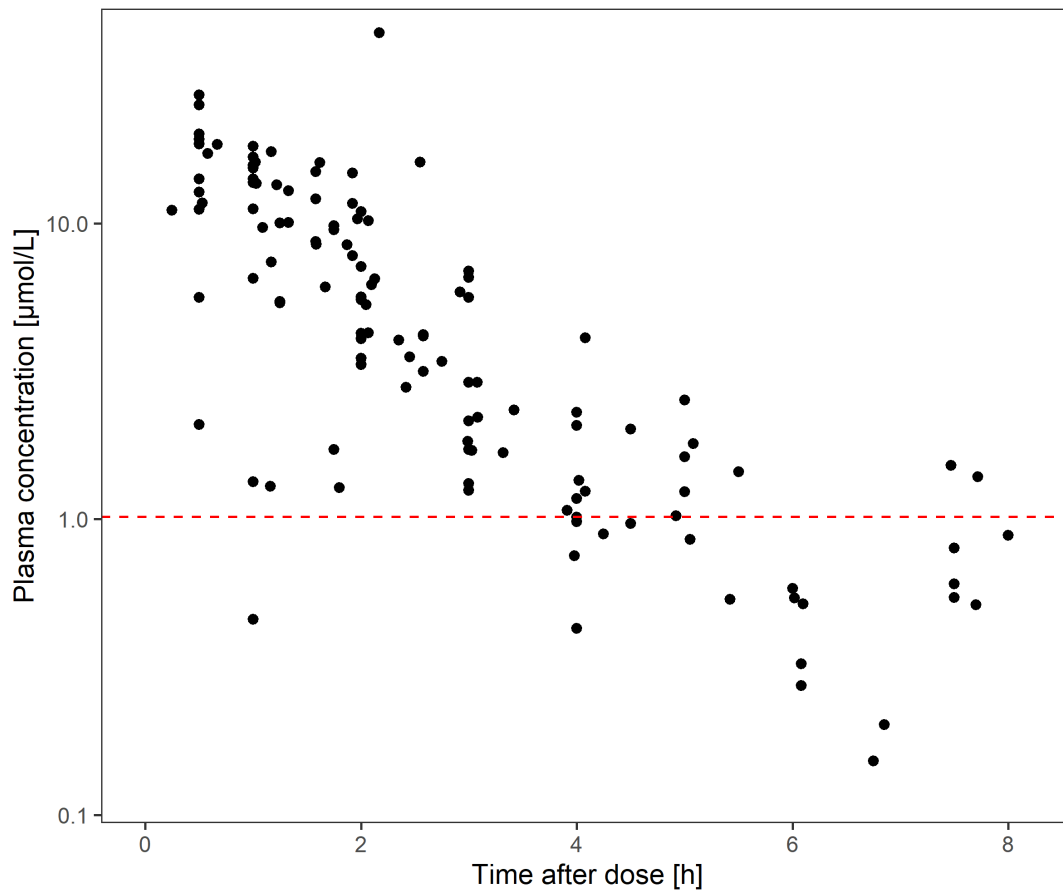


Fig. S2-2 Log scale plasma concentration-time profile of DFCR. The red dashed line indicates the lower limit of quantification of 0.25 µg/mL.

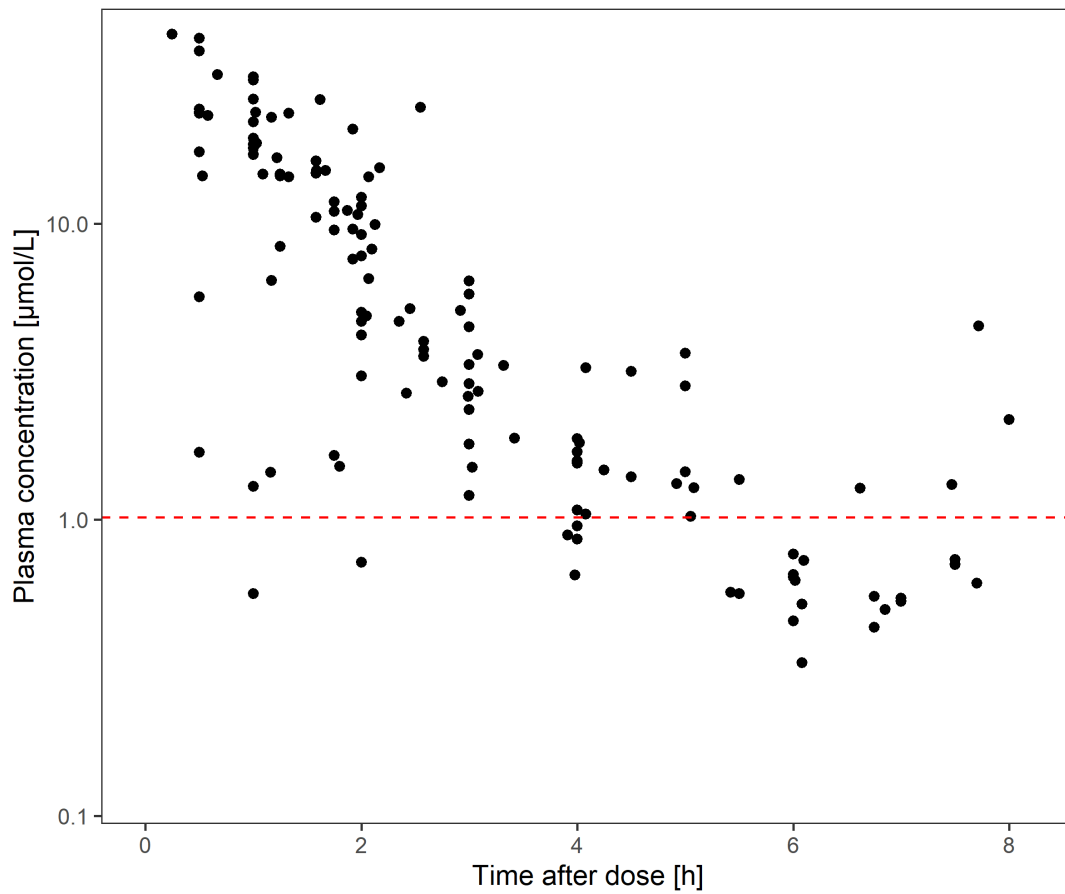


Fig. S2-3 Log scale plasma concentration-time profile of DFUR. The red dashed line indicates the lower limit of quantification of 0.25 µg/mL.

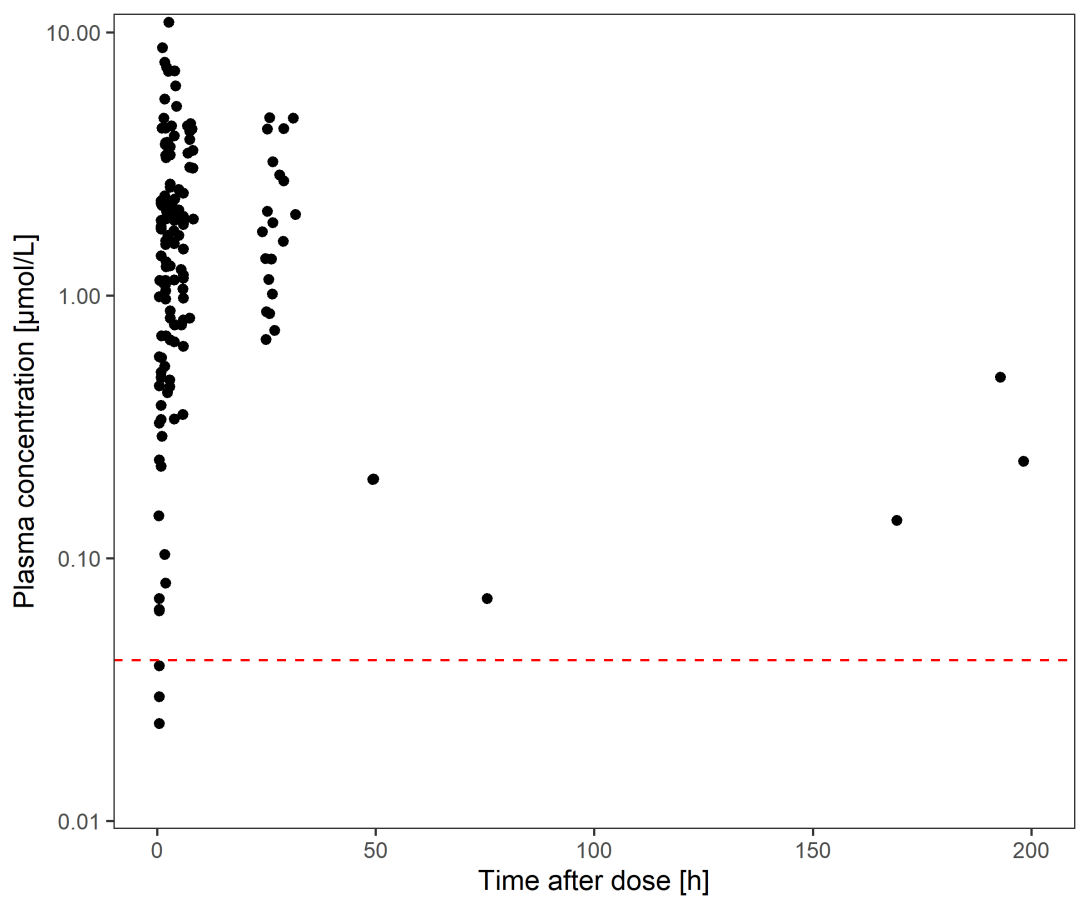


Fig. S2-4 Log scale plasma concentration-time profile of regorafenib. The red dashed line indicates the lower limit of quantification of 0.02 µg/mL.

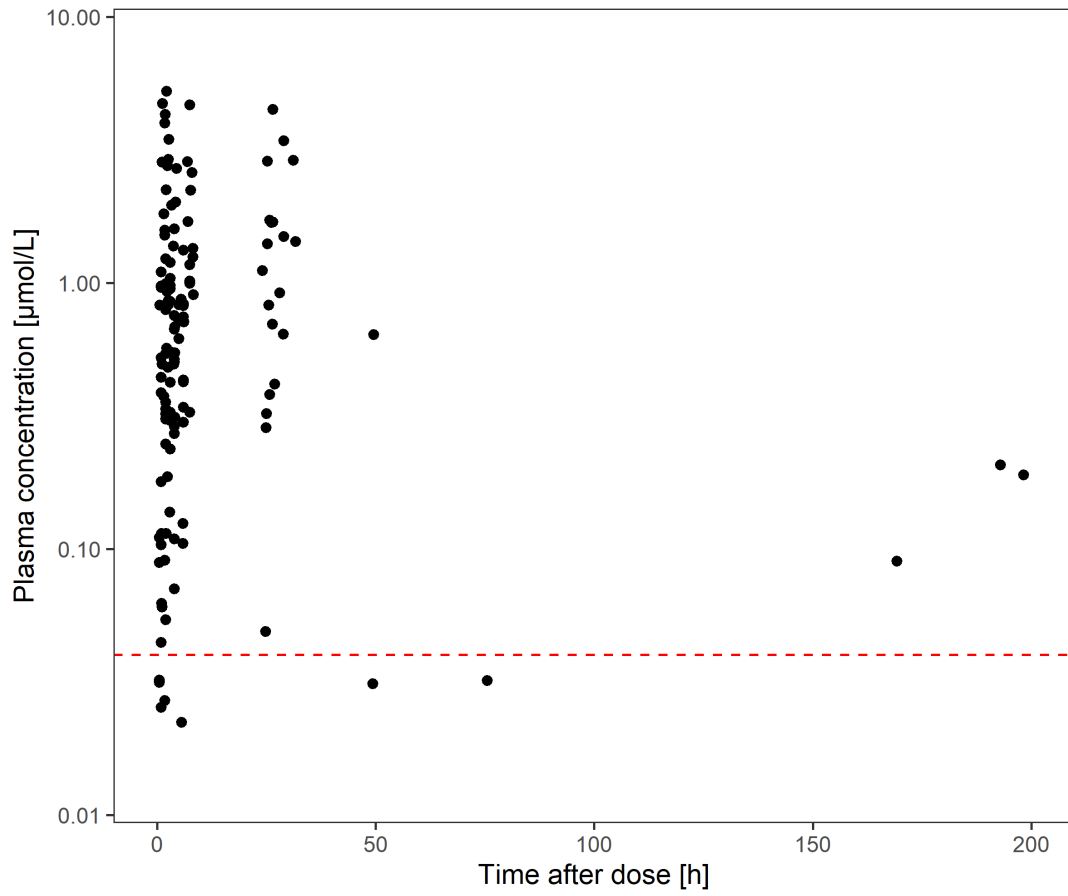


Fig. S2-5 Log scale plasma concentration-time profile of M-2. The red dashed line indicates the lower limit of quantification of 0.02 µg/mL.

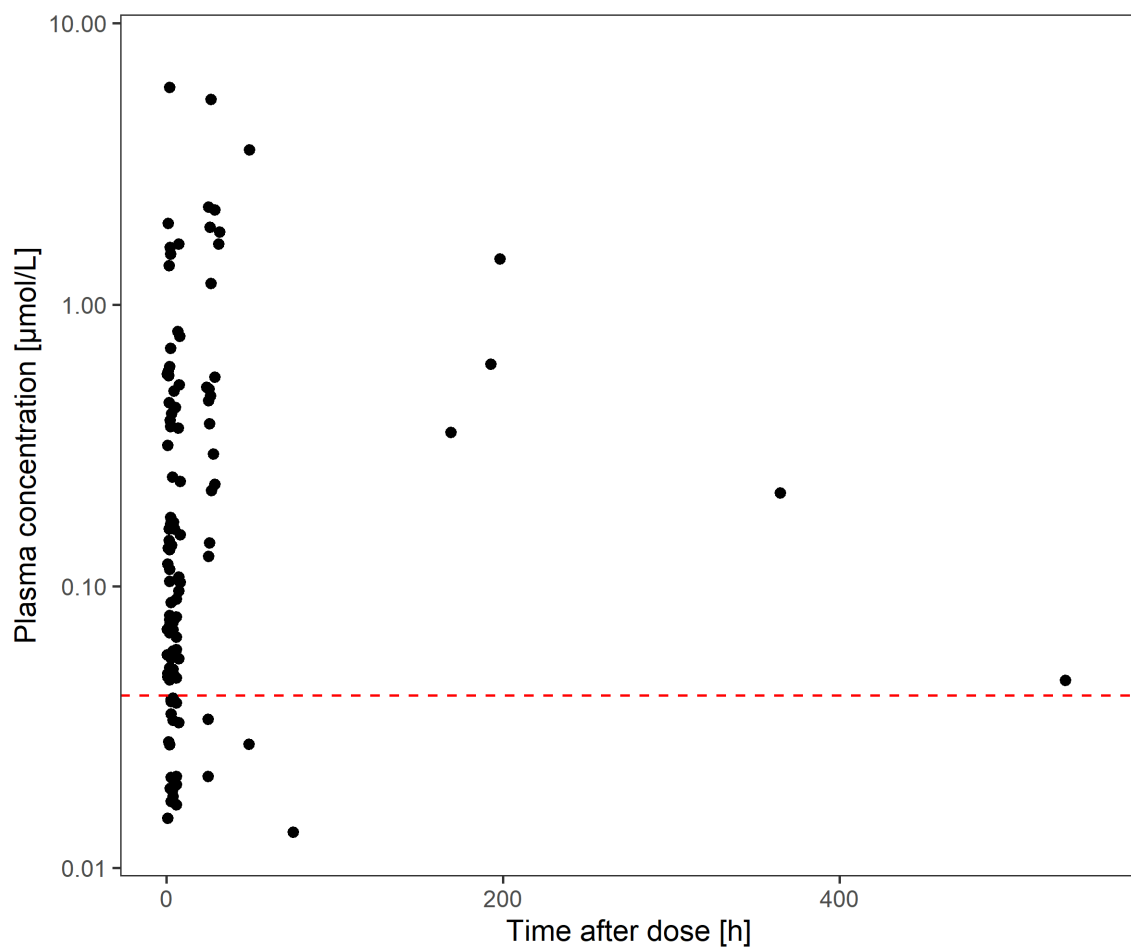


Fig. S2-6 Log scale plasma concentration-time profile of M-5. The red dashed line indicates the lower limit of quantification of 0.02 µg/mL.

Model development

Capecitabine-metabolite base model development

Tab. S3-1 Important model building steps for the capecitabine-metabolite base model

Model	Model description	OFV	AIC	Comments
Capecitabine absorption models				
1	First-order absorption	222.422	234.422	
2	Zero-order absorption	216.073	226.073	
3	First-order absorption with lag time	214.867	226.864	Failure of the covariance step
4	Parallel first- and zero-order absorption*	183.454	197.454	
5	Transit compartment model with Erlang distribution (n compartments = 2)	216.631	226.631	
6	Transit compartment model with Erlang distribution (n compartments = 3)	216.508	226.508	
7	Two parallel first-order absorption processes	184.326	198.326	RSE of one of the k_a : 79%
8	Absorption model with fixed parameters according to Jacobs et al. [S1]	-	-	Run failures
9	Absorption model with fixed parameters according to Urien et al. [S2]	250.412	260.412	
10	Absorption model with fixed parameters according to Daher Abdi et al. [S3]	294.242	304.242	
11	Absorption model with fixed parameters according to Lunar et al. [S4]	445.151	453.151	
Capecitabine-DFCR model				
12	Model with separated capecitabine elimination process (clearance + metabolism to DFCR)	551.030	577.030	Metabolism constant estimate to DFCR was close to zero (boundary issue)
13	Model with one capecitabine elimination process to the DFCR central compartment*	553.989	577.989	
Capecitabine-DFCR-DFUR model				
14	DFUR PK described by clearance and volume of distribution	917.349	953.349	DFUR volume of distribution estimate was close to zero (boundary issue)
15	DFUR PK described by elimination constant*	921.539	953.539	

AIC: Akaike information criterion, OFV: objective function value, RSE: relative standard error, PK: pharmacokinetics

*Models chosen for further model development

Covariate analysis of the capecitabine-metabolite base model

Tab. S3-2 Included covariate-parameter relationships of the capecitabine-metabolite model in chronological order

Covariate model number	Covariate effect	Difference in OFV compared to previous model (forward inclusion step)
1	Regorafenib cumulative AUC over time on capecitabine clearance	-33.918 (compared to base model)
2	Hemoglobin on capecitabine clearance	-40.816
3	M-5 cumulative AUC over time on capecitabine clearance	-9.334
4	M-2 concentration over time on $k_{e, DFUR}$	-7.967
5	Bilirubin on $k_{e, DFUR}$	-6.957
6	Body mass index on DFCR volume of distribution	-7.901
7	M-2 concentration over time on DFCR clearance	-6.398
8	Hemoglobin on capecitabine volume of distribution*	-5.268

OFV: objective function value, AUC: area under the curve, $k_{e, DFUR}$: Elimination rate constant for DFUR

* removed after backward elimination step

After the forward inclusion and backward elimination steps, seven covariate-parameter relationships were included for further analysis. However, the inclusion of all covariates did not seem to be plausible, either due to lack of physiological plausibility (hemoglobin as covariate on capecitabine clearance) or due to high correlations between the drug exposure parameters. Hence, the effects of hemoglobin, M-5 cumulative AUC over time and M-2 concentration over time were removed. A covariate model consisting of regorafenib cumulative AUC on capecitabine clearance, body mass index (BMI) on DFCR volume of distribution and bilirubin on $k_{e, DFUR}$ resulted in a physiologically implausible covariate effect of bilirubin (positive effect on $k_{e, DFUR}$). Excluding this covariate led to a model with relatively high relative standard errors (RSE) of the BMI effect on DFCR volume of distribution (41%) and the IIV term of DFCR volume of distribution (48%). In fact, only an implementation of the first identified covariate, regorafenib cumulative AUC on capecitabine clearance, led to a stable model with precisely estimated parameters along with a significant drop in OFV compared to the base model (-33.918, $p < 0.00001$).

Goodness-of-fit plots

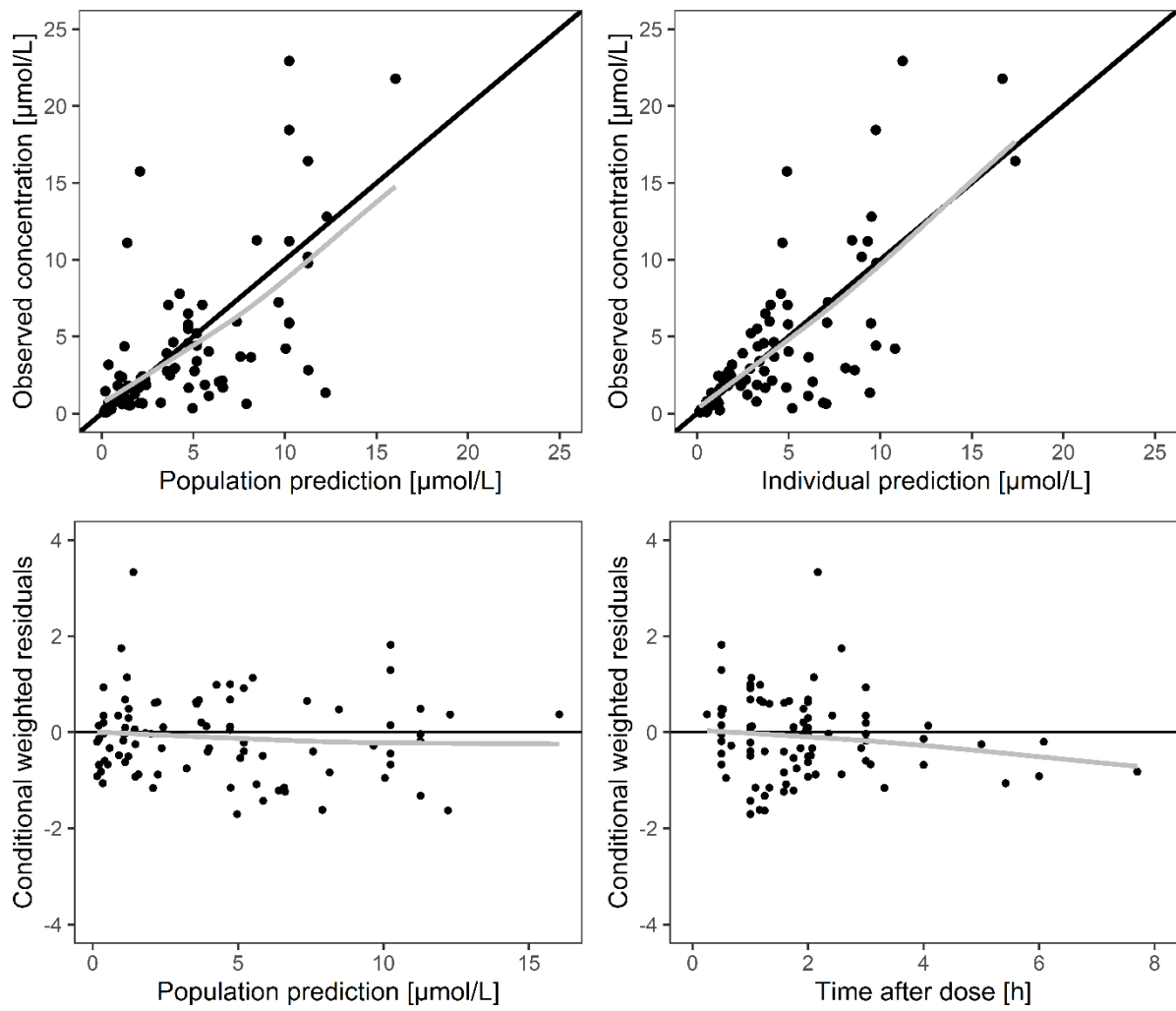


Fig. S3-1 Goodness-of-fit plots for model-predicted capecitabine concentrations. The black lines indicate the lines of identity and the grey lines are the trend in observations.

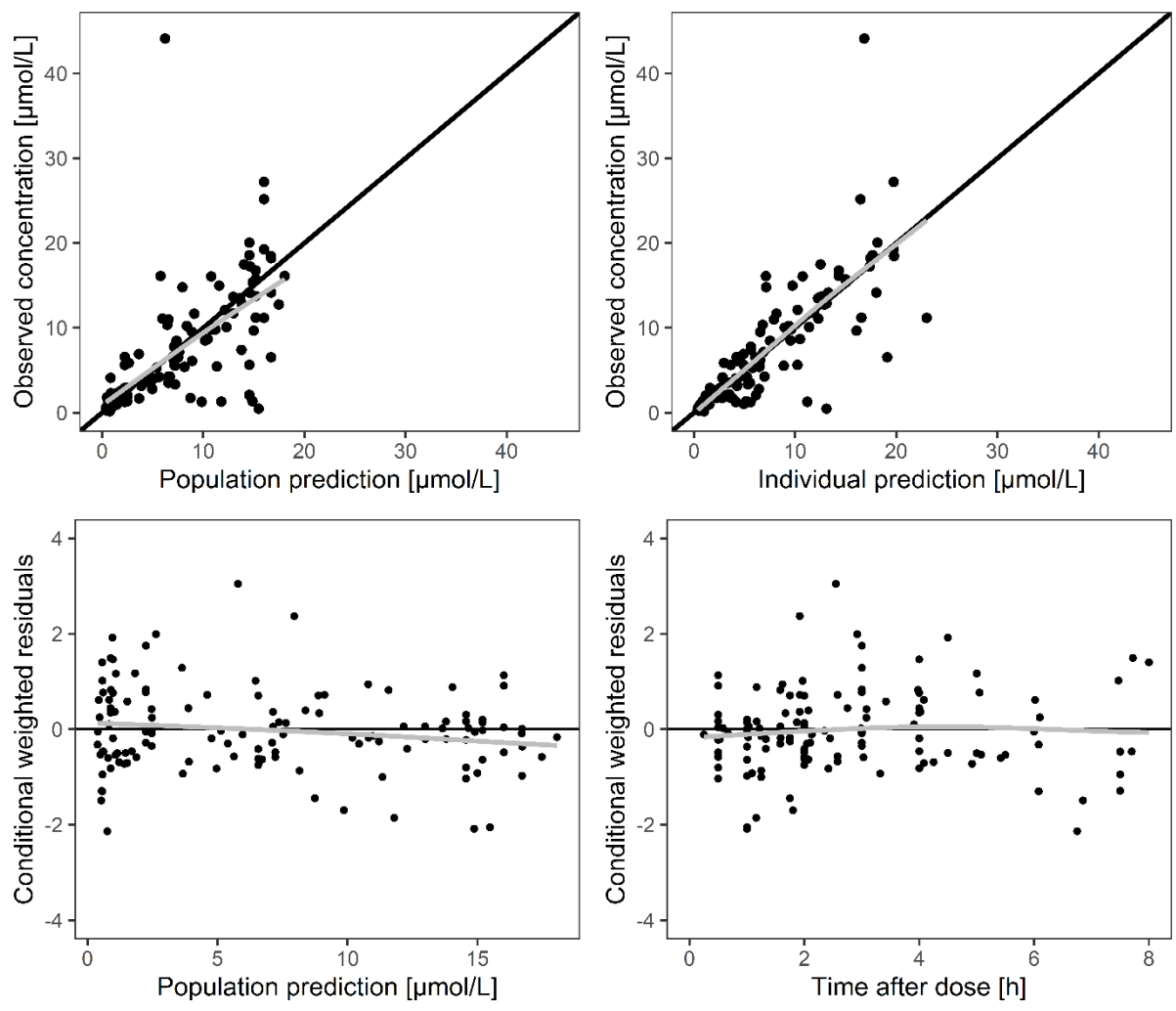


Fig. S3-2 Goodness-of-fit plots for model-predicted DFCR concentrations. The black lines indicate the lines of identity and the grey lines are the trend in observations.

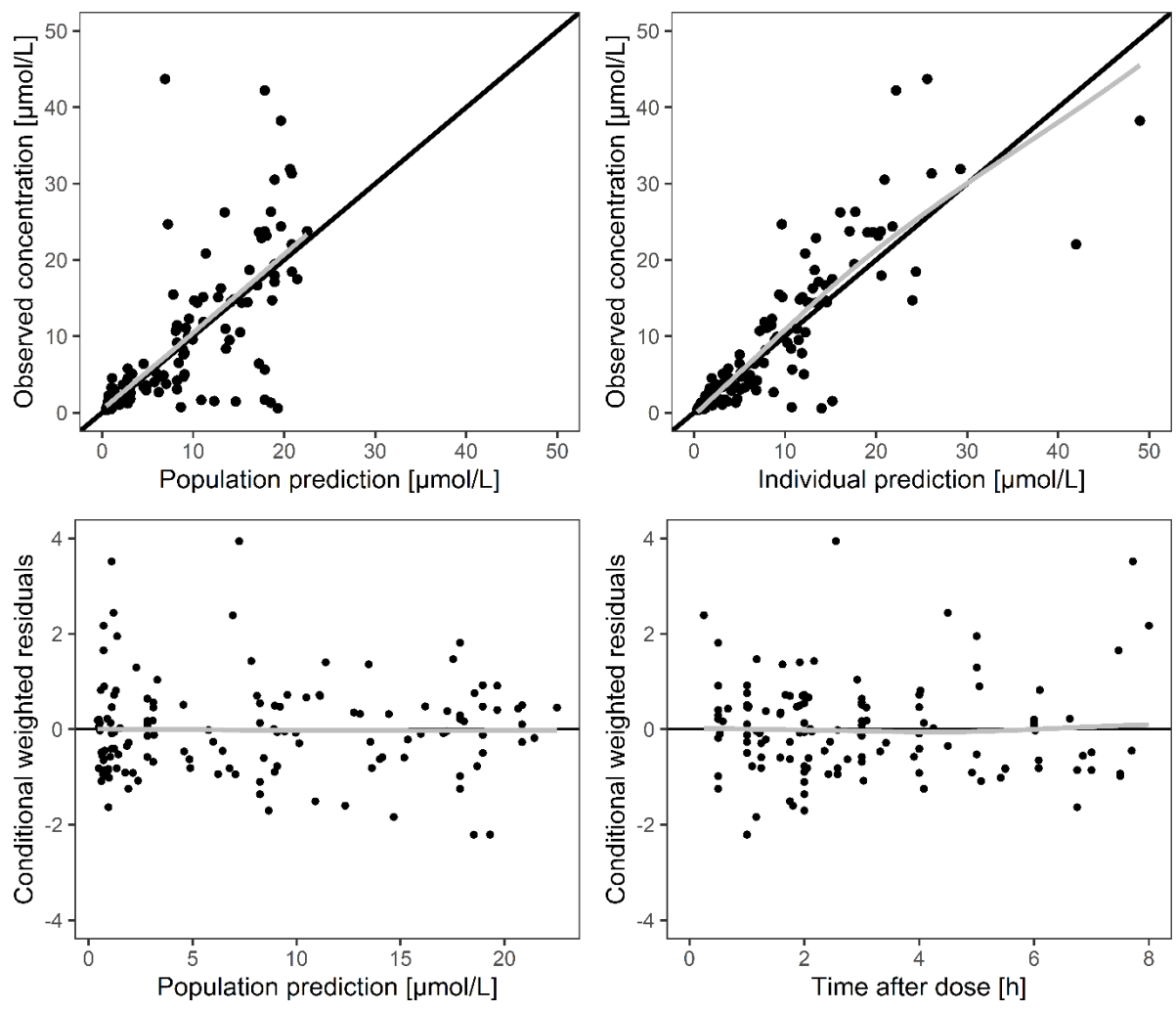


Fig. S3-3 Goodness-of-fit plots for model-predicted DFUR concentrations. The black lines indicate the lines of identity and the grey lines are the trend in observations.

Regorafenib-metabolite base model development

Tab. S3-3 Important model building steps for the regorafenib-metabolite base model

Model	Model description	OFV	AIC	Comments
Regorafenib absorption models				
1	First-order absorption	153.683	169.683	
2	Zero-order absorption	181.053	197.053	
3	First-order absorption with lag time	132.116	150.116	
4	2 transit compartments with Erlang distribution	121.694	139.694	
5	3 transit compartments with Erlang distribution*	108.463	126.463	
6	4 transit compartments with Erlang distribution	106.870	124.870	
7	1 transit compartment with first-order absorption	123.909	143.909	
8	2 transit compartments with first-order absorption	109.294	129.294	
9	3 transit compartments with first-order absorption	106.502	126.502	RSE k_a 82%
10	Parallel first- and zero-order absorption	142.827	162.827	Run failure (Minimization terminated)
11	Transit compartment model according to Savic et al. [S5]	195.819	211.819	Run failure (Minimization terminated)
12	Sequential first- and zero-order absorption	-	-	Run failure
Regorafenib-M-2 model				
13	Presystemic M-2 formation with first-order absorption	27.483	45.483	
14	M-2 formation from the central compartment of regorafenib	160.851	176.851	
15	M-2 formation from central compartment of regorafenib and presystemic formation with first order absorption	29.742	49.742	
16	Presystemic M-2 formation with 2 transit compartments (Erlang distribution)*	16.655	34.655	
17	Presystemic M-2 formation with 3 transit compartments (Erlang distribution)	16.789	34.789	
Regorafenib-M-2-M-5 model				
18	M-5 formation from the central compartment of regorafenib	-	-	Run failure
19	M-5 formation from the central compartment of M-2*	-348.393	-314.393	

*Models chosen for further model development

Covariate analysis of the regorafenib-metabolite base model

Tab. S3-4 Included covariate-parameter relationships of the regorafenib-metabolite model in chronological order

Covariate model number	Covariate effect	Difference in OFV compared to previous model (forward inclusion step)
1	DSCR concentration over time on M-2 clearance	-9.542 (compared to base model)
2	Sex on shared volume of distribution*	-6.591
3	Age on regorafenib clearance	-4.804
4	Bilirubin on regorafenib clearance	-6.876
5	Body mass index on regorafenib clearance	-5.354
6	Hemoglobin on regorafenib clearance	-6.875

OFV: objective function value

* removed after backward elimination step

Similar to the covariate analysis of the capecitabine-metabolite model, the inclusion of all identified covariates did not seem to be plausible. The identification of DSCR concentration on M-2 clearance was attributed to the influence of regorafenib on capecitabine clearance (Tab. S2). Additionally, it should be noted that M-2 cumulative AUC over time was highly correlated with the cumulative AUC from the parent drug. M-2 had a similar negative effect on capecitabine clearance as the included effect of regorafenib cumulative AUC (with an OFV difference of -32.58). Hence, the DSCR effect on M-2 was removed from the covariate model. The incorporation of the remaining four covariates only resulted in an unsuccessful model convergence due to rounding errors. Further step-wise elimination of these covariates did not result in a stable model as well, either due to failures of the covariance step or large RSE of model parameters.

Goodness-of-fit plots

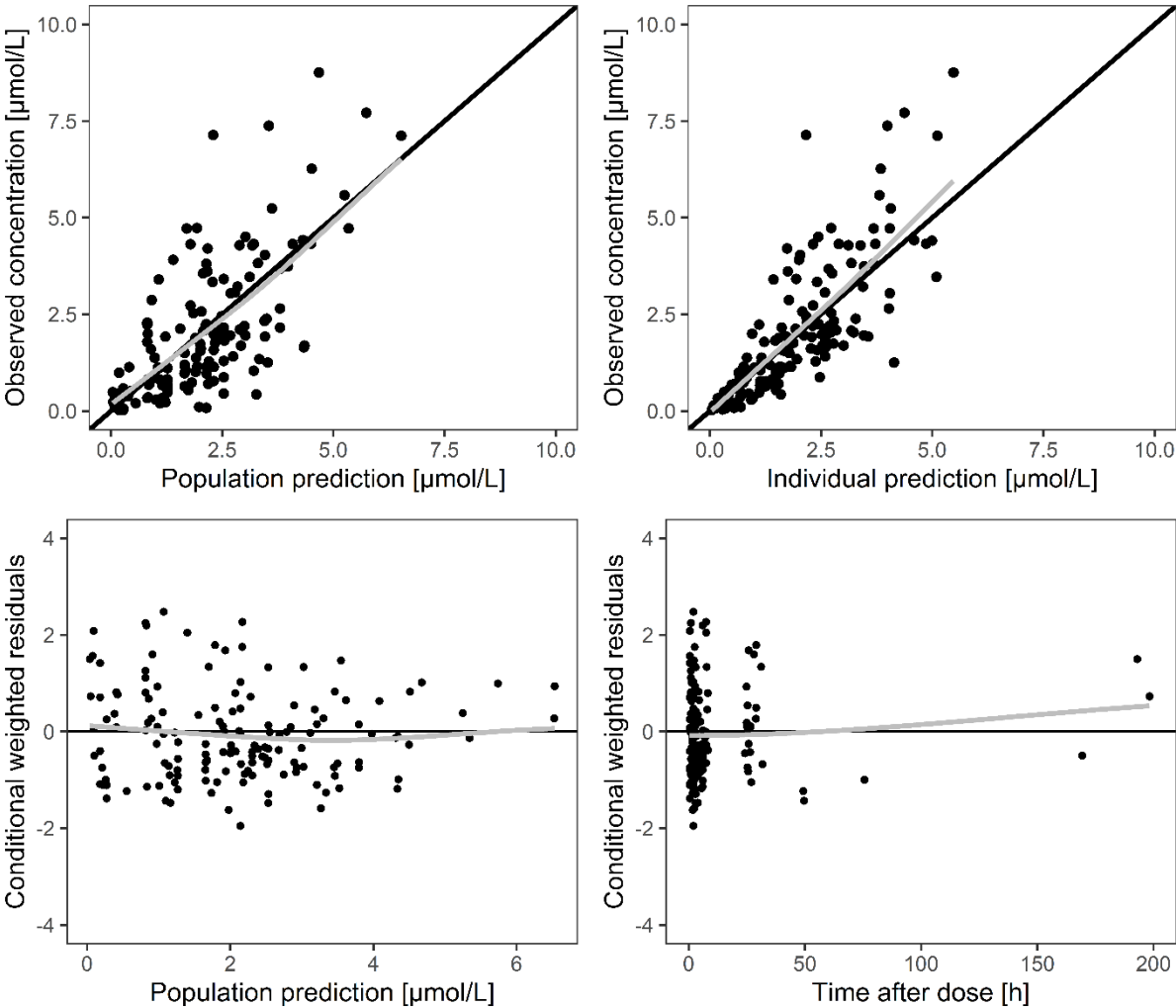


Fig. S3-4 Goodness-of-fit plots for model-predicted regorafenib concentrations. The black lines indicate the lines of identity and the grey lines are the trend in observations.

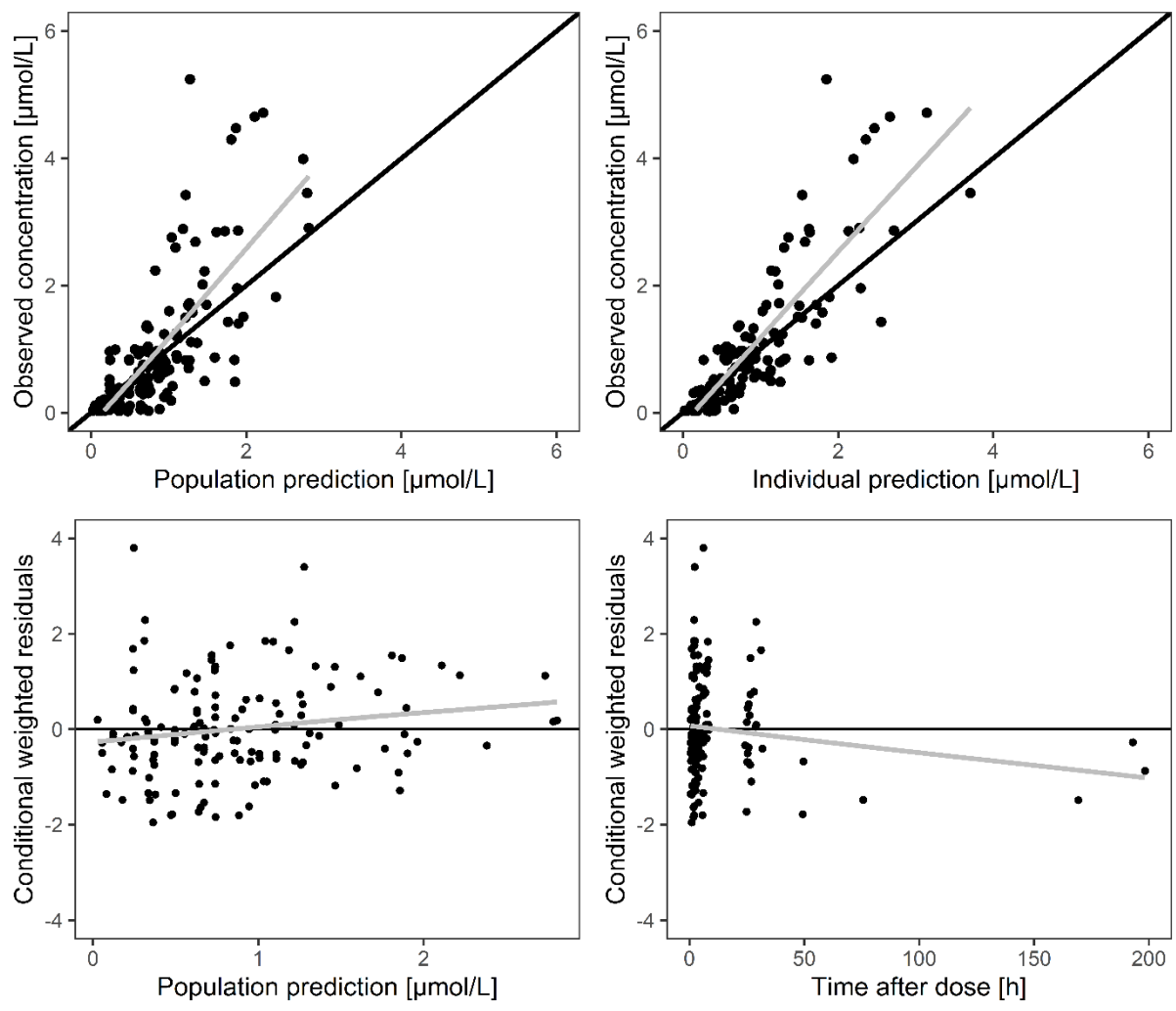


Fig. S3-5 Goodness-of-fit plots for model-predicted M-2 concentrations. The black lines indicate the lines of identity and the grey lines are the trend in observations.

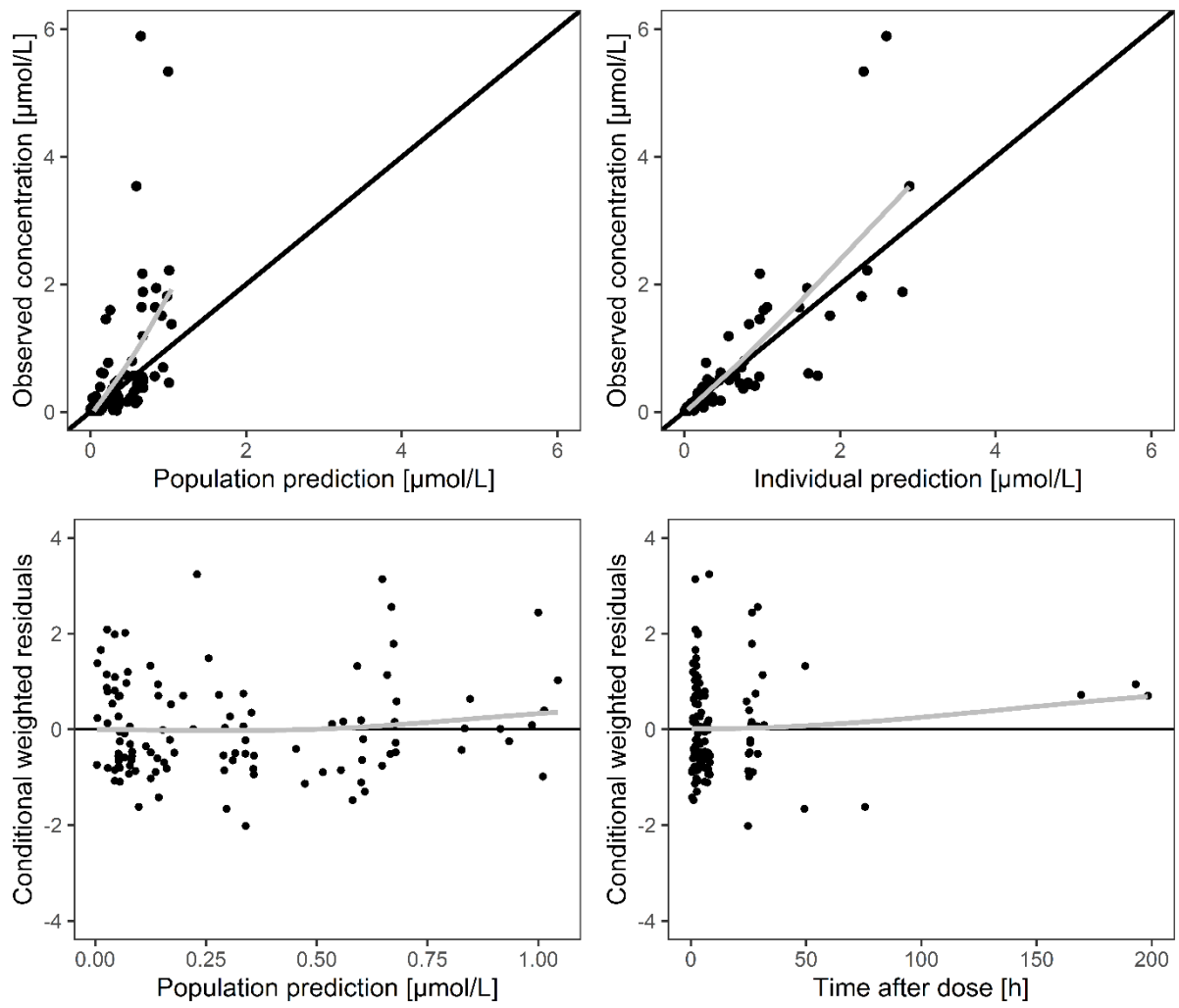


Fig. S3-6 Goodness-of-fit plots for model-predicted M-5 concentrations. The black lines indicate the lines of identity and the grey lines are the trend in observations.

Supplemental References

[S1] Jacobs BAW, Deenen MJ, Joerger M, et al. Pharmacokinetics of Capecitabine and Four Metabolites in a Heterogeneous Population of Cancer Patients: A Comprehensive Analysis. *CPT Pharmacometrics Syst Pharmacol* 2019; 8: 940-950.

[S2] Urien S, Rezaí K, Lokiec F. Pharmacokinetic modelling of 5-FU production from capecitabine--a population study in 40 adult patients with metastatic cancer. *J Pharmacokinet Pharmacodyn* 2005; 32: 817-833.

[S3] Daher Abdi Z, Lavau-Denes S, Prémaud A, et al. Pharmacokinetics and exposure-effect relationships of capecitabine in elderly patients with breast or colorectal cancer. *Cancer Chemother Pharmacol* 2014; 73: 1285-1293.

[S4] Lunar N, Etienne-Grimaldi M-C, Macaire P, et al. Population pharmacokinetic and pharmacodynamic modeling of capecitabine and its metabolites in breast cancer patients. *Cancer Chemother Pharmacol* 2021; 87: 229-239.

[S5] Savic RM, Jonker DM, Kerbusch T, et al. Implementation of a transit compartment model for describing drug absorption in pharmacokinetic studies. *J Pharmacokinet Pharmacodyn* 2007; 34: 711-726.

Simulation study

Simulated plasma concentration-time profiles of capecitabine, DFCR and DFUR depending on regorafenib dosage

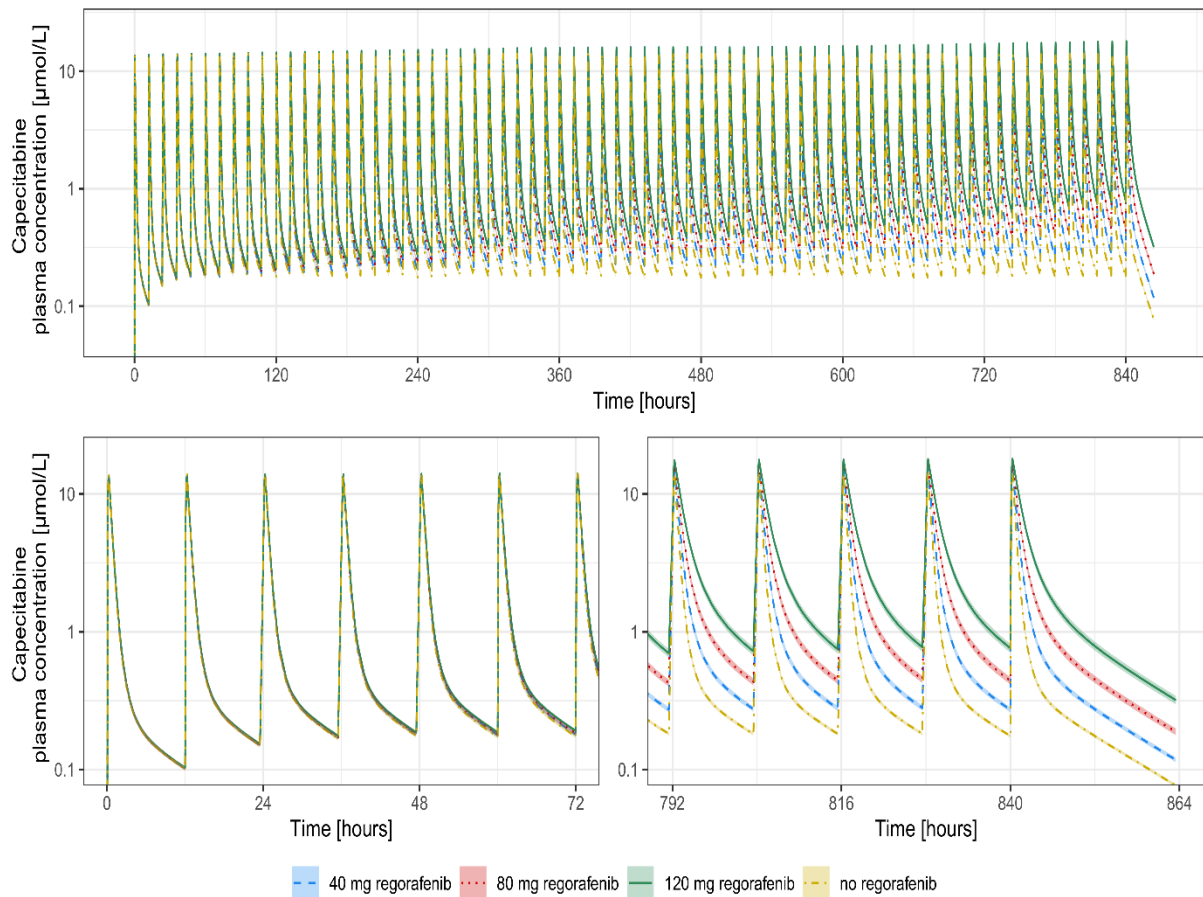


Fig. S4-1 Simulated plasma concentrations of capecitabine depending on regorafenib dosage. Upper panel: Simulated capecitabine plasma concentration-time course from 0 – 864 hours. Lower panel: Simulated capecitabine plasma concentration-time course from 0 – 72 hours and from 792 – 864 hours, respectively. Blue dashed/red dotted/green solid/yellow dash-dotted curves: Geometric mean simulated capecitabine plasma concentration under regorafenib 40 mg/80 mg/120 mg/0 mg, respectively. Blue/red/green/yellow shaded area: 95% confidence intervals of geometric mean simulated capecitabine plasma concentration under regorafenib 40 mg/80 mg/120 mg/0 mg, respectively.

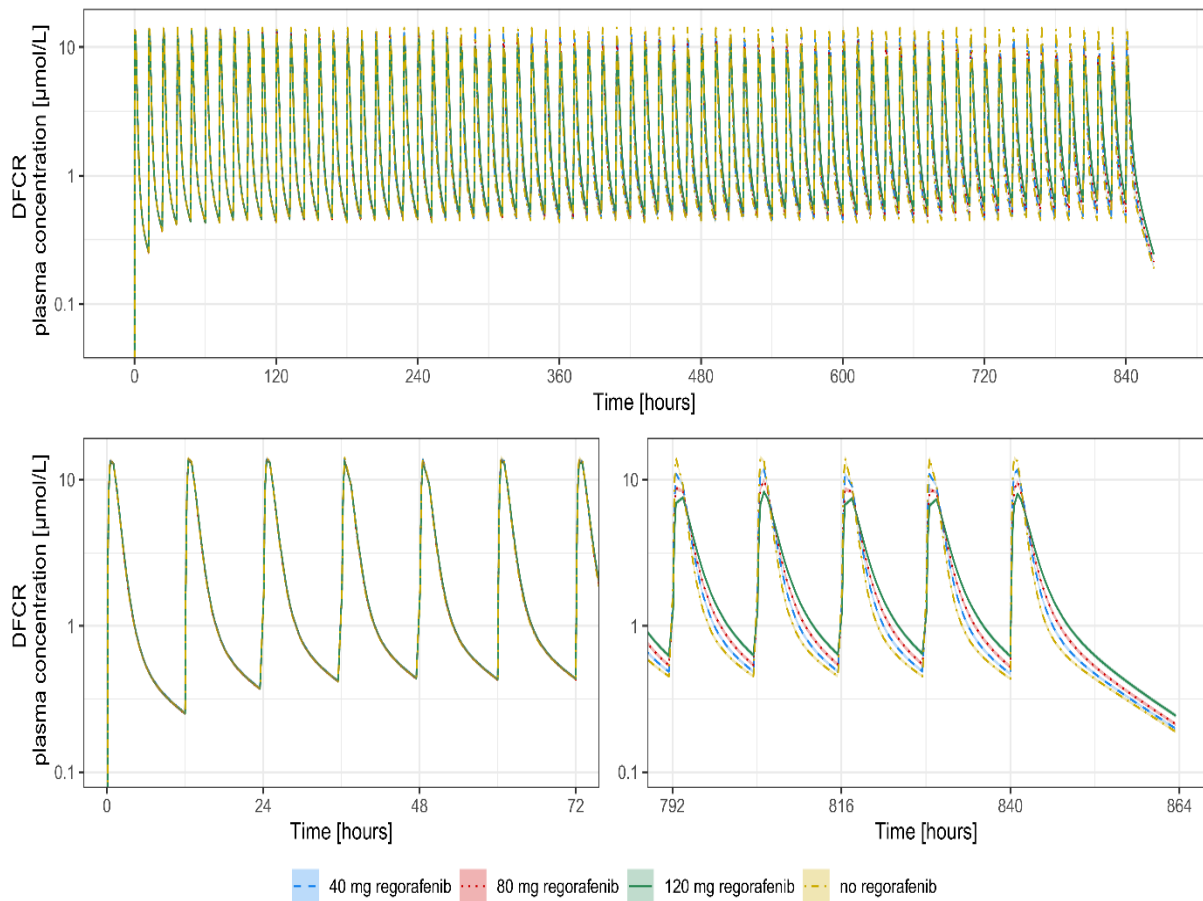


Fig. S4-2 Simulated plasma concentrations of DFCR depending on regorafenib dosage. Upper panel: Simulated DFCR plasma concentration-time course from 0 – 864 hours. Lower panel: Simulated DFCR plasma concentration-time course from 0 – 72 hours and from 792 – 864 hours, respectively. Blue dashed/red dotted/green solid/yellow dash-dotted curves: Geometric mean simulated DFCR plasma concentration under regorafenib 40 mg/80 mg/120 mg/0 mg, respectively. Blue/red/green/yellow shaded area: 95% confidence intervals of simulated geometric mean DFCR plasma concentration under regorafenib 40 mg/80 mg/120 mg/0 mg, respectively.

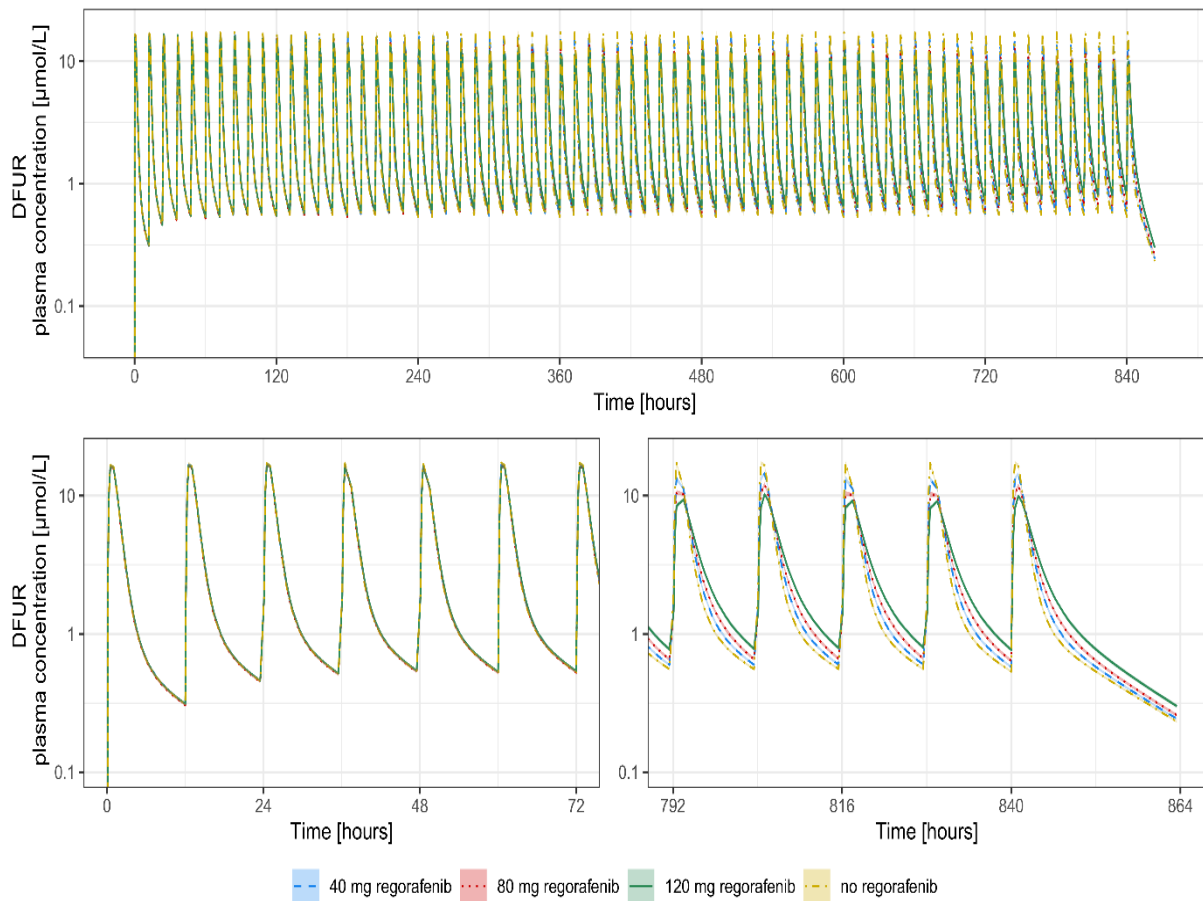


Fig. S4-3 Simulated plasma concentrations of DFUR depending on regorafenib dosage. Upper panel: Simulated DFUR plasma concentration-time course from 0 – 864 hours. Lower panel: Simulated DFUR plasma concentration-time course from 0 – 72 hours and from 792 – 864 hours, respectively. Blue dashed/red dotted/green solid/yellow dash-dotted curves: Geometric mean simulated DFUR plasma concentration under regorafenib 40 mg/80 mg/120 mg/0 mg, respectively. Blue/red/green/yellow shaded area: 95% confidence intervals of geometric mean simulated DFUR plasma concentration under regorafenib 40 mg/80 mg/120 mg/0 mg, respectively.

Tab. S4-1 Simulated capecitabine clearance on various days depending on regorafenib dose level

	Day	Regorafenib	Regorafenib	Regorafenib	Regorafenib
		0 mg	40 mg	80 mg	120 mg
Geometric mean capecitabine clearance [L/h] (95% confidence intervals)	1	285 (278 – 293)	284 (277 – 291)	283 (275 – 290)	278 (271 – 285)
	8	285 (278 – 293)	260 (254 – 267)	238 (231 – 245)	214 (208 – 221)
	15	285 (278 – 293)	236 (230 – 243)	196 (189 – 203)	160 (155 – 166)
	22	285 (278 – 293)	232 (226 – 239)	189 (183 – 196)	152 (146 – 158)
	29	285 (278 – 293)	215 (208 – 221)	161 (155 – 168)	120 (115 – 125)
	36	285 (278 – 293)	194 (187 – 200)	131 (126 – 137)	88.0 (83.8 – 92.5)

Final NONMEM codes

NONMEM code for the final capecitabine-metabolite model

\$PROBLEM Capecitabine + DFCR + DFUR PK

\$INPUT ID TIME DV MDV CMT AMT EVID RATE AUCREG

\$DATA ...

\$SUBROUTINES ADVAN6 TOL=4

\$MODEL NCOMP = 4

\$PK

TVCL = THETA(1)*EXP(THETA(12)*AUCREG) ; Regorafenib cumulative AUC effect on capecitabine CL

CL = TVCL*EXP(ETA(1))

TVV = THETA(2)

V = TVV*EXP(ETA(2))

TVKA = THETA(3)

KA = TVKA

TVD2 = THETA(5)

D2 = TVD2

F1 = THETA(6)

F2 = 1-F1

TVV2 = THETA(7)

V2 = TVV2*EXP(ETA(3))

TVCLM = THETA(8)

CLM=TVCLM*EXP(ETA(4))

TVK40 = THETA(10)

K40 = TVK40 *EXP(ETA(5))

S2 = V

S3 = V2

S4 = 1

K23 = CL/V

K34 = CLM/V2

\$DES

DADT(1) = -KA*A(1)

DADT(2) = KA*A(1) - K23*A(2)

DADT(3) = K23*A(2) - K34*A(3)

DADT(4) = K34*A(3) - K40*A(4)

\$ERROR

IPRED = F

IF(CMT.EQ.2) THEN ; Capecitabine

W = SQRT(THETA(4)*IPRED)**2

Y = IPRED+W*EPS(1)

ENDIF

IF(CMT.EQ.3) THEN ; DFCR

W = SQRT(THETA(9)*IPRED)**2

Y = IPRED+W*EPS(2)

ENDIF

IF(CMT.EQ.4) THEN ; DFUR

W = SQRT(THETA(11)*IPRED)**2

Y = IPRED+W*EPS(3)

ENDIF

DEL = 0

IF(W.EQ.0) DEL =1

IRES = DV-IPRED

IWRES = IRES/(W+DEL)

\$THETA

(0, 286) ; CL capecitabine

(0, 179) ; V capecitabine

(0, 0.0714) ; ka

(0, 0.601) ; prop. error capecitabine

(0, 0.25) ; Duration zero-order absorption

(0, 0.214) ; Fraction of first-order absorption process

(0, 71.9) ; V DFCR

(0, 123) ; CL DFCR

(0, 0.461) ; prop. error DFCR

(0, 99.2) ; keDFUR

(0, 0.452) ; prop error DFUR

(-0.00041) ; Regorafenib cumulative AUC on capecitabine CL

\$OMEGA

0.161 ; IIV CL capecitabine

0.158 ; IIV V capecitabine

0.227 ; IIV V DFCR

0.104 ; IIV CL DFCR

0.086 ; IIV keDFUR

\$SIGMA

1 FIX

1 FIX

1 FIX

; \$SIM (12345) (54321) ONLYSIM

\$EST METHOD=1 MAXEVAL=9999 NOABORT INTER PRINT=1 SIG=3

\$COV MATRIX=R PRINT=E

NONMEM code for the final regorafenib-metabolite model

```
$PROBLEM Regorafenib M2 + M5 PK
$INPUT ID      TIME  DV    MDV  CMT  AMT  EVID
$DATA ...
$SUBROUTINES ADVAN6 TOL=4
$MODEL NCOMP = 12
COMP(ABSORPTION) ;Transit compartment 1 regorafenib
COMP(CENTRAL) ; Central compartment regorafenib
COMP(PERI) ; Peripheral compartment regorafenib
COMP(DEPOT1) ;Transit compartment 2 regorafenib
COMP(DEPOT2) ;Transit compartment 3 regorafenib
COMP(M2CENT) ; Central compartment M-2
COMP(M2PERI) ; Peripheral compartment M-2
COMP(DEPOT1M) ; Transit compartment 1 M-2
COMP(DEPOT2M); Transit compartment 2 M-2
COMP(M5CENT) ; Central compartment M-5
COMP(M5PERI) ; Peripheral compartment M-5
COMP(REGAUC) ; AUC regorafenib

$PK
TVCLREG = THETA(1)
CLREG = TVCLREG*EXP(ETA(1))
TVV2 = THETA(2)
V2 = TVV2*EXP(ETA(2))

;ERLANG ABSORPTION REGORAFENIB
TVMAT = THETA(3)
```

$$\text{MAT} = \text{TVMAT} * \text{EXP}(\text{ETA}(3))$$

NN = 3 ; Number of transit compartments

$$\text{KTR} = (\text{NN}) / \text{MAT} ; \text{Calculate ktr}$$

$$\text{TVV3} = \text{THETA}(4)$$

$$\text{V3} = \text{TVV3}$$

$$\text{TVQ} = \text{THETA}(5)$$

$$\text{Q} = \text{TVQ}$$

$$\text{TVCLM2} = \text{THETA}(7)$$

$$\text{CLM2} = \text{TVCLM2} * \text{EXP}(\text{ETA}(4))$$

K18 = THETA(8) ; Presystemic metabolic rate constant

;ERLANG ABSORPTION M-2

$$\text{TVMMAT} = \text{THETA}(10)$$

$$\text{MMAT} = \text{TVMMAT}$$

MNN = 2 ; Number of transit compartments

$$\text{MKTR} = (\text{MNN}) / \text{MMAT} ; \text{Calculate ktr}$$

$$\text{K89} = \text{MKTR}$$

$$\text{K96} = \text{MKTR}$$

$$\text{TVCLM5} = \text{THETA}(11)$$

$$\text{CLM5} = \text{TVCLM5} * \text{EXP}(\text{ETA}(5))$$

$$\text{S2} = \text{V2}$$

$$S6 = V2$$

$$S10 = V2$$

$$K14 = KTR$$

$$K45 = KTR$$

$$K52 = KTR$$

$$K20 = CLREG/V2$$

$$K23 = Q/V2$$

$$K32 = Q/V3$$

$$K60 = CLM2/V2$$

$$K67 = Q/V2$$

$$K76 = Q/V3$$

$$K100 = CLM5/V2$$

$$K1011=Q/V2$$

$$K1110=Q/V3$$

\$DES

$$DADT(1) = -K14*A(1)-K18*A(1)$$

$$DADT(2) = K52*A(5) + K32*A(3) - K20*A(2) - K23*A(2)$$

$$DADT(3) = K23*A(2) - K32*A(3)$$

$$DADT(4) = K14*A(1) - K45*A(4)$$

$$DADT(5) = K45*A(4) - K52*A(5)$$

$$DADT(6) = K96*A(9) - K60*A(6) - K67*A(6) + K76*A(7)$$

$$DADT(7) = K67*A(6) - K76*A(7)$$

$$DADT(8) = K18*A(1) - K89*A(8)$$

$$DADT(9) = K89*A(8) - K96*A(9)$$

$$DADT(10) = K60*A(6) - K100*A(10) - K1011*A(10) + K1110*A(11)$$

$$DADT(11)= K1011*A(10) - K1110*A(11)$$

REGC = A(2)/V2

DADT(12) = REGC ; cumulative AUC

\$ERROR

AUCREG = A(12)

IPRED = F

IF(CMT.EQ.2) THEN ; Regorafenib

W = SQRT(THETA(6)*IPRED)**2

Y = IPRED+W*EPS(1)

ENDIF

IF(CMT.EQ.6) THEN ; M-2

W = SQRT(THETA(9)*IPRED)**2

Y = IPRED+W*EPS(2)

ENDIF

IF(CMT.EQ.10) THEN ; M-5

W = SQRT(THETA(12)*IPRED)**2

Y = IPRED+W*EPS(3)

ENDIF

DEL = 0

IF(W.EQ.0) DEL =1

IRES = DV-IPRED

IWRES = IRES/(W+DEL)

\$THETA

(0, 1.94) ; CL regorafenib

(0, 10.4) ; Central shared V

(0, 3.01) ; Mean absorption time regorafenib

(0, 63.9) ; Peripheral shared V

(0, 13.5) ; Shared intercompartmental CL

(0, 0.526) ; prop. error regorafenib

(0, 0.936) ; CL M-2

(0, 0.265) ; Presystemic metabolic rate constant

(0, 0.579) ; prop error M-2

(0, 1.9) ; Mean absorption time M-2

(0, 2.01) ; CL M-5

(0, 0.541) ; prop error M-5

\$OMEGA

0.145 ; IIV CL regorafenib

1.73 ; IIV Central shared V

0.0469 ; IIV Mean absorption time regorafenib

0.0637 ; IIV CL M-2

0.572 ; IIV CL M-5

\$SIGMA

1 FIX

1 FIX

1 FIX

; \$SIM (12345) (54321) ONLYSIM SUBPROBLEMS=1000

\$COV PRINT=E MATRIX=R

\$EST METHOD=1 INTER MAXEVAL=9999 NOABORT PRINT=1 SIG=3

RESEARCH ARTICLE

Influence of the skeletal muscle index on pharmacokinetics and toxicity of fluorouracil

Eduard Schmulenson¹  | Nigina Zimmermann¹ | Lothar Müller² |
Stefanie Kapsa¹ | Iryna Sihinevich¹ | Ulrich Jaehde¹ 

¹Department of Clinical Pharmacy,
Institute of Pharmacy, University of
Bonn, Bonn, Germany

²Onkologie UnterEms, Leer, Germany

Correspondence

Ulrich Jaehde, Institute of Pharmacy,
University of Bonn, Bonn, Germany.
Email: u.jaehde@uni-bonn.de

Abstract

Background: The body composition of patients has been associated with tolerability and effectiveness of anticancer therapy. This study aimed to assess the influence of the skeletal muscle index (SMI) on the pharmacokinetics and toxicity of fluorouracil.

Methods: Patients treated in an oncological practice with fluorouracil-based chemotherapy and undergoing therapeutic drug monitoring were retrospectively investigated. Computed tomography images were analyzed to measure abdominal skeletal muscle areas in Hounsfield units for the psoas major muscle, back and total skeletal muscle to determine the SMI. For the latter, an automated segmentation method was used additionally. SMI measures were tested as covariates on fluorouracil clearance in a population pharmacokinetic model. Furthermore, regression analyses were performed to analyze the influence of SMI measures on the probability of clinically relevant adverse events (CTCAE grades ≥ 2).

Results: Fluorouracil plasma concentrations of 111 patients were available. Covariate analyses showed significant improvements of the model fit by all SMI measures. However, interindividual variability of fluorouracil clearance was only slightly reduced, whereas the SMI of the back muscle showed the largest reduction (-1.1 percentage points). Lower SMI values of the back muscle increased the probability for polyneuropathy and lower SMI of the psoas increased the probability for fatigue.

Conclusions: Our results suggest that pharmacokinetics and toxicity of fluorouracil may be associated with specific SMI measures which deserve further investigation.

KEYWORDS

body composition, fluorouracil, pharmacokinetics, skeletal muscle index

Eduard Schmulenson and Nigina Zimmermann contributed equally to this work (listed in alphabetical order).

This is an open access article under the terms of the [Creative Commons Attribution](https://creativecommons.org/licenses/by/4.0/) License, which permits use, distribution and reproduction in any medium, provided the original work is properly cited.

© 2022 The Authors. *Cancer Medicine* published by John Wiley & Sons Ltd.

1 | INTRODUCTION

Fluorouracil (5FU) is still one of the cornerstones for the treatment of various solid tumors, particularly colorectal and head and neck cancer.¹⁻³ Typically, 5FU is dosed according to the patient's body surface area (BSA), resulting in a wide range of variability in 5FU plasma concentrations.⁴ This pharmacokinetic variability may result individually in an insufficient response to 5FU therapy or intolerable toxicity, leading to treatment discontinuations. In fact, approximately 60% of patients treated with 5FU are reported being underdosed, whereas about 15% being overdosed when BSA-based dosing is applied.⁵

Due to its hydrophilic nature, the volume of distribution of 5FU is highly correlated with lean body mass (LBM) which includes muscle mass.⁶ Since BSA does not account for changes in body composition, this additional knowledge could be of high interest when sarcopenic cancer patients are treated with anticancer drugs.⁷ Several studies found that sarcopenia in cancer patients is a predictor for low overall survival in various tumors.⁸⁻¹² An association between muscle status and toxicity under therapy with various anticancer drugs was shown as well.¹² In particular, patients with a dose-limiting toxicity under 5FU chemotherapy had a higher 5FU dose per kg of LBM compared to patients with a lower grade toxicity.^{13,14} Other metrics of body composition (total body water, fat-free mass) could be linked to 5FU pharmacokinetics,¹⁵ whereas a LBM-normalized 5FU dose was not correlated with 5FU exposure, defined as area under the concentration-time curve (AUC).¹⁶

Sarcopenia is usually defined by a reduction in skeletal muscle index (SMI) which is calculated by the total muscle cross-sectional area at the third lumbar vertebra (L3) normalized to the squared patient's height (cm²/m²).¹⁷ So far, the relationship of SMI with 5FU pharmacokinetics has not been evaluated. The aim of this study was therefore to investigate the influence of the SMI on 5FU pharmacokinetics as well as 5FU-associated toxicity.

2 | METHODS

2.1 | Patients and data

In this study, patients under a 5FU-based, infusional chemotherapy from the oncological outpatient clinic UnterEms in Leer, Germany, were retrospectively analyzed. Patients with documented therapeutic drug monitoring of 5FU, that is, quantification of 5FU plasma concentrations, and at least one computed tomography (CT) scan of the L3 area were included for analysis. 5FU plasma concentrations were obtained at steady state during continuous infusion and quantified using the My5-FUTM immunoassay

(Saladax Biomedical Inc., Bethlehem, PA, USA) with a lower limit of quantification of 86 ng/ml.¹⁸ Dose adjustments were performed at the discretion of the treating oncologist. Adverse events (AE) were graded at each patient visit according to the Common Terminology Criteria for Adverse Events (CTCAE), version 5.0.¹⁹ In order to ensure that the muscle status corresponded to measured 5FU plasma concentrations and AE, a maximum time frame between CT scan and blood sampling/AE documentation had to be defined. Chung et al. found a median change in SMI values of 8.7% in patients with stage III or high-risk stage II colon cancer treated with the FOLFOX scheme (5FU, folinate, oxaliplatin) within 210 days between pre-operative and post-chemotherapy CT.²⁰ In addition, the mean measurement error of SMI quantification via CT scans was reported to be 8.5%.²¹ Based on this information, a maximum time frame of ± 205 days between CT scan and blood sampling was defined excluding patients with a larger temporal distance between SMI and plasma concentration measurements/AE documentations from the analysis. The study was approved by the ethics committee at the Faculty of Medicine of the University of Bonn (protocol code 014/18).

2.2 | Image analysis

The SMI was assessed using routinely collected CT images from different radiological practices. As recommended by the European Working Group on Sarcopenia in Older People, measurements were performed at the L3 level since the individual skeletal muscle areas correlated the most with overall skeletal muscle.²² Muscle areas were measured based on Hounsfield units (HU) as well as an automated segmentation method provided by the software sliceOmatic[®] version 5.0 (TomoVision, Magog, Canada).²³ The HU range was set to the density of skeletal muscle (35–50 HU) to exclude any areas of different tissues.²⁴ Using this "Hounsfield method," the psoas major, back muscle, and total skeletal muscle at the L3 level were examined. For the latter, the automated segmentation method was additionally used. An overview of the different SMI measures and the respective muscle areas is provided in the Supporting Information (SI) 1, Table S1-1. All SMI measures were obtained by dividing the respective measurements by the squared patient's height.

2.3 | Population pharmacokinetic analysis

The influence of the different SMI measures on 5FU pharmacokinetics (PK) was analyzed in a population PK

model of 5FU. This model was initially developed at the Department of Clinical Pharmacy at the University of Bonn using data from the study of Wilhelm et al.²⁵ Modeling was performed with the non-linear mixed effect modeling software NONMEM® version 7.2²⁶ combined with implemented scripts in PsN (version 3.6.2).^{27,28} NONMEM® uses the maximum likelihood method to simultaneously estimate population values of fixed-effect parameters (e.g., drug clearance) and values of random-effect variables (e.g., interindividual and residual variability) in order to obtain individual parameters. Model parameters were estimated by the first-order conditional estimation method with interaction.²⁶ The likelihood-ratio test was used to discriminate between nested models. A nested model was considered superior to another when the objective function value (OFV), provided by NONMEM®, was reduced by 3.84 points (chi-square value, $p < 0.05$, one degree of freedom). Covariates which are able to explain interindividual variability (IIV) in 5FU clearance and volume of distribution were investigated as well, including age, sex, infusion time (24 or 46 h, coded as a binary covariate), laboratory parameters (creatinine, bilirubin, ALT, AST, GGT, LDH), tumor markers (CA 19-9, CEA), and BSA. These were implemented into the model in a stepwise forward inclusion and backward elimination approach using the *scm* script provided by PsN with an included fixed set of parameter-covariate parametrizations (linear, piece-wise linear, exponential, power relations).^{27,28} In the forward inclusion step, covariates which led to a significant decrease of the OFV ($p < 0.05$) were kept for further evaluation. This model was then re-evaluated by backward elimination of each included covariate with a significance level of $p < 0.01$. If a covariate was still significant in this step, it was eventually kept in the model. Model robustness and precision and bias of parameter estimates were evaluated by a non-parametric bootstrap analysis without stratification. Median and 95% confidence intervals of parameter estimates were derived from 1000 replicate datasets obtained from sampling individuals from the original dataset with replacement.

The population pharmacokinetic model was then applied to the dataset of this study and revised, where necessary. In this population PK analysis, NONMEM® version 7.5²⁹ and PsN (version 5.0.0)^{27,28} were used for model development and R (version 4.1.0)³⁰ was used for visualization of results. Piraña (version 2.9.7) served as front interface.³¹ Based on this revised model, a covariate analysis was performed in order to explore if the different SMI measures had an influence on 5FU clearance and volume of distribution. Each SMI measure was individually tested as a covariate on 5FU PK parameters and included if a statistically significant reduction ($p < 0.05$) of the OFV was found. Exponential functions were tested to describe the

relationship between the different SMI measures and 5FU PK parameters. The model fit was assessed by goodness-of-fit plots³² and prediction-corrected visual predictive checks³³ based on 1000 dataset simulations. Additionally, a non-parametric bootstrap analysis without stratification, as described above, was performed.

2.4 | Logistic regression

The influence of the SMI on 5FU toxicity was evaluated in a logistic regression analysis by correlating SMI measures with AE severity. For this analysis, every AE with a CTCAE grade of 2 or higher was defined as severe and hence clinically relevant. The AE were coded binary with “0” for CTCAE grades 0 and 1 and “1” for grades 2 to 4, respectively. Documented AE included polyneuropathy, stomatitis, hand-foot syndrome, fatigue, diarrhea, nausea, and emesis. The probability (P) for every AE was calculated as follows:

$$P(AE \geq CTCAE \text{ grade } 2) = \frac{1}{1 + e^{-z}} \quad (1)$$

The logit of z determines the linear regression model of the independent variable and consists of the observed SMI measures (x_k), the regression coefficients (β_k), and an error term (ϵ):

$$z = \beta_0 + \beta_1 \times x_1 + \beta_2 \times x_2 + \beta_3 \times x_3 + \dots \beta_k \times x_k + \epsilon \quad (2)$$

For every performed logistic regression, odds were calculated relating the probability of a severe AE to the probability of non-occurrence:

$$\text{Odds} = \frac{P(CTCAE \text{ grade} \geq 2)}{P(CTCAE \text{ grade} < 2)} = \frac{P(CTCAE \text{ grade} \geq 2)}{1 - P(CTCAE \text{ grade} \geq 2)} \quad (3)$$

Based on the odds obtained, the relative probability to develop a severe AE when the SMI increases by one unit was assessed as Odds Ratio (OR):

$$\text{OR} = \frac{\text{Odds after } 1\text{cm}^2 / \text{m}^2 \text{ increase in SMI}}{\text{Odds before } 1\text{cm}^2 / \text{m}^2 \text{ increase in SMI}} \quad (4)$$

3 | RESULTS

3.1 | Patient characteristics

The dataset consisted of routinely collected data from 175 patients between September 2014 and July 2020. Twenty of them had to be excluded due to missing CT images.

Further 44 patients were excluded because the time frame between their CT scan and blood sampling was longer than 205 days (see “Methods” section). The remaining 111 patients were included for further analyses (Table 1). For the development of the population PK model, 395 5FU plasma concentration measurements were included. All included patients received 24-h infusions of 5FU.

3.2 | Influence of the skeletal muscle index on 5FU pharmacokinetics

First, an initial population PK model based on data from the study of Wilhelm et al.²⁵ was developed. A one-compartment model with linear elimination turned out to be the best model to describe 5FU disposition. IIV terms were implemented on 5FU clearance, volume of distribution, and residual variability. The latter consisted of an additive as well as a proportional term.³⁴ However, due to model instabilities, estimates of the volume of distribution and its IIV had to be fixed to previously estimated values. Based on analyses of rich PK data from our group and data from the Cantonal Hospital St. Gallen, Switzerland, volume of distribution and its IIV were fixed to 46.1 L and 51.1%, respectively.^{35–37} Therefore, covariates could only be tested on 5FU clearance. After the forward inclusion step of the covariate analysis, BSA, infusion time, and LDH concentration were found to be significant linear covariates on 5FU clearance. LDH concentration was excluded after performing the backward elimination step. Ultimately, BSA and infusion time remained in the model. However, the bootstrap analysis revealed the estimate of the infusion time effect to be unreliable since its 95% confidence intervals included zero. Hence, this parameter was excluded from the final model. In Table 2, the development steps of the population PK model are shown. Table 3 depicts the final population PK parameter estimates as well as the median values of the bootstrap analysis.

The developed population PK model was applied to the dataset of this study. Running this initial model revealed that the estimate of the additive term of the residual variability ran into a boundary close to zero. In addition, the IIV term on residual variability was estimated with a relative standard error (RSE) of 86% and shrinkage³⁸ of 76%. Both parameters were assumed to be negligible and thus removed from the model leading to a non-significant increase in OFV (Table 4).

This revised model was then used for covariate analysis in which the different SMI measures were individually tested on 5FU clearance. Its results are presented in Table 4. All four SMI parameters showed a statistically significant reduction of OFV when included in the model. Inclusion of the SMI of the back muscle led to the largest OFV drop along with the highest reduction in IIV of

TABLE 1 Patient characteristics

Characteristic	Median (range) or n
Demographics	
Sex	
Male	75
Female	36
Age (years)	64 (35–84)
Body surface area (m ²)	1.97 (1.47–2.85)
Skeletal muscle indices (SMI)	
SMI psoas major (cm ² /m ²)	1.48 (0.46–3.78)
SMI back muscle (cm ² /m ²)	3.78 (0.94–8.41)
SMI total muscle (Hounsfield method) (cm ² /m ²)	9.58 (4.12–18.82)
SMI total muscle (Segmentation method) (cm ² /m ²)	50.26 (25.47–92.67)
Therapy-related details	
5FU dose (mg/m ²)	2283 (1441–3641)
5FU AUC ^a (mg × h/L)	19.7 (2.1–45.0)
Number of observed cycles per patient	2 (1–5)
Therapy regimen	
AIO ^b	26
FUFOX ^c (including monoclonal antibodies)	22
Paclitaxel/cisplatin/5FU/folate	30
Other	32
Tumor entity	
Colorectal cancer	56
Gastroesophageal cancer	33
Pancreatic cancer	12
Other	10

^aCalculated by multiplying the infusion time with the measured steady-state concentration.

^bWeekly 5FU infusion (2600 mg/m²) over 24 h in combination with folinate (500 mg/m²).

^cWeekly 5FU infusion (2000 mg/m²) over 24 h in combination with folinate (500 mg/m²) and oxaliplatin (50 mg/m²).

5FU clearance (−1.1 percentage points). Therefore, this covariate was chosen for the final model. 5FU clearance was parametrized as follows (Equation 5):

$$CL_{5FU} = CL_{5FU, pop} \times \left(1 + \theta_{BSA} \times (BSA - 1.97 \text{ m}^2) \right) \times e^{\left(\theta_{SMI, back} \times \left(SMI_{back} - 3.78 \frac{\text{cm}^2}{\text{m}^2} \right) \right)} \times e^{\eta_{i, CL_{5FU, pop}}} \quad (5)$$

Here, CL_{5FU} denotes for the individual 5FU clearance estimate, CL_{5FU, pop} for the population estimate of 5FU clearance, θ_{BSA} is the covariate effect estimate of the body surface area, BSA is the observed body surface area, θ_{SMI, back} denotes for the covariate effect estimate of the SMI of the back

TABLE 2 Development steps and covariate analysis of the initial 5FU population pharmacokinetic model based on data from Wilhelm et al.²⁵

Model number	Description	OFV	ΔOFV	p value
1	Base model <ul style="list-style-type: none"> One compartment with linear elimination Fixed values for volume of distribution and its IIV Combined additive and proportional residual error model 	-611.310	0	—
2	Covariate model after forward inclusion step <ul style="list-style-type: none"> Inclusion of BSA, infusion time, and LDH concentration on 5FU clearance 	-653.107	-41.797	<0.0001 ^a
3	Covariate model after backward elimination step <ul style="list-style-type: none"> Exclusion of LDH concentration as covariate 	-647.132	+5.975	0.0145
4	Final model <ul style="list-style-type: none"> Exclusion of infusion time as covariate after bootstrap analysis 	-637.090	+10.042	0.0064

Abbreviations: ΔOFV, Difference in objective function value; BSA, Body surface area; IIV, Interindividual variability; OFV, Objective function value.

^aThree degrees of freedom.

TABLE 3 Parameter estimates of the initial 5FU population pharmacokinetic model based on data from Wilhelm et al.²⁵

Parameter	Estimate	Bootstrap median (95% confidence intervals)
CL _{5FU} [L/h]	209	209 (198–220)
V _{5FU} [L]	46.1 (fixed)	46.1 (fixed)
BSA effect on CL _{5FU}	0.681	0.688 (0.455–0.933)
<i>Interindividual variability</i>		
CL _{5FU} [%CV]	16.3	15.5 (10.3–19.2)
V _{5FU} [%CV]	51.1 (fixed)	51.1 (fixed)
Residual variability [%CV]	37.5	36.1 (18.7–52.2)
<i>Residual variability</i>		
Additional error term [ng/ml]	77.4	87.2 (54.7–139)
Proportional error term [%]	19.8	18.8 (14.7–23.6)

Abbreviations: BSA, body surface area; CL, clearance; CV, coefficient of variation; V, volume of distribution.

muscle, SMI_{back} for the observed SMI of the back muscle, and $\eta_{i,CL_{5FU,POP}}$ represents the IIV term for the 5FU population clearance of the *i*th individual with a mean of 0 and a variance of ω^2 . Both covariate effects were centered around the respective observed median values of the study population.

The prediction-corrected visual predictive check (Figure 1) as well as goodness-of-fit plots (see SI 2, Figure S2-1) of the final model showed a reasonable model fit. Final parameter estimates along with bootstrap results are presented in Table 5. The NONMEM® code of the final model is outlined in SI 3.

3.3 | Influence of skeletal muscle indices on toxicity under 5FU therapy

For every AE, the number of patients suffering from AE grade 2 or higher is presented in SI 4, Table S4-1. The

logistic regression analysis showed statistically significant correlations for two AE. The SMI of the psoas major was significantly correlated to the fatigue syndrome as well as the SMI of the back muscle to the occurrence of clinically relevant polyneuropathy. An increase of the respective SMI by 1 cm²/m² decreased the probability of developing the identified AE ≥ grade 2 by 85% and 48%, respectively. The final logistic regression analyses are depicted in Figure 2. Presentations of the odds ratios for all investigated AE are outlined in SI 4, Table S4-2.

4 | DISCUSSION

This is the first study evaluating the influence of different SMI measures on 5FU PK and toxicity. The results suggest that selected SMI measures may be associated with 5FU PK. Interpreting the individual SMI measures, it should

TABLE 4 Model development steps and covariate analysis of the revised model

Model number	Description	OFV	Δ OFV	p value	IIV Clearance [%CV]
1	Initial model without BSA as covariate (Table 3)	-754.341	0	—	26.6
2	Initial model with BSA as covariate (Table 3)	-792.218	-37.877	<0.00001	22.0
3	Initial model with BSA as covariate (Table 3), without additive term and IIV term of residual variability (Revised model)	-791.624	+0.594	(0.74 ^a , referring to model 2)	22.0
3a	Revised model+SMI total muscle (Hounsfield method)	-798.302	-6.678	0.0098	21.5
3b	Revised model+SMI total muscle (segmentation method)	-798.408	-6.784	0.0092	21.1
3c	Revised model+SMI psoas major	-799.070	-7.446	0.0064	21.1
3d	Revised model+SMI back muscle	-803.910	-12.286	0.00046	20.9

Abbreviations: Δ OFV, Difference in objective function value; BSA, Body surface area; CV, Coefficient of variation; IIV, Interindividual variability; OFV, Objective function value; SMI, Skeletal muscle index.

^aTwo degrees of freedom.

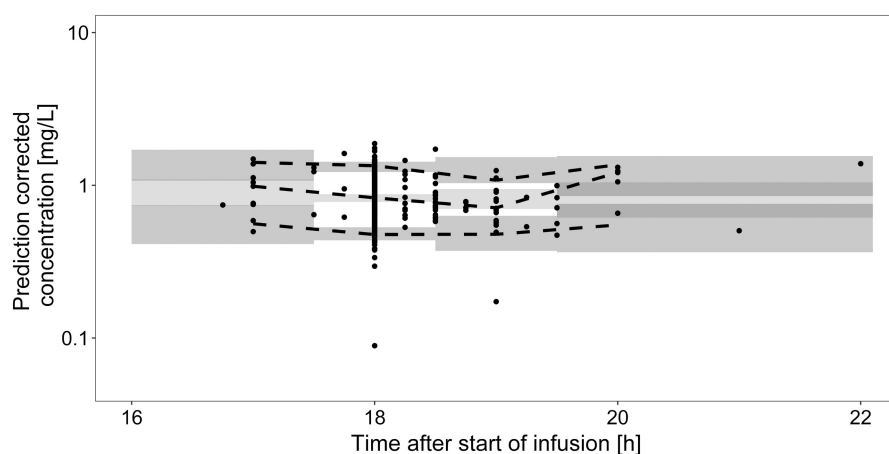


FIGURE 1 Prediction-corrected visual predictive check of the final population pharmacokinetic model of 5FU. Black dots: Prediction-corrected observations, dashed lines: 90% interval and median of the prediction-corrected observations, dark gray shaded area: 95% confidence intervals of the 5th and 95th prediction interval, light gray shaded area: 95% confidence interval of the predicted median.

be kept in mind that SMI parameter values which were obtained by the Hounsfield method were quantified using a range of 35–50 HU. This range differed from HU ranges of other studies^{13,14,39} and resulted in lower absolute values when, for example, comparing the SMI of the total muscle obtained by the Hounsfield method to the same SMI quantified by the segmentation method. However, the observed trends and associations were the same for all SMI measures analyzed in this study. Provided that these findings are confirmed in future prospective studies, the question remains how these findings may be transposed in real-world patients. In clinical routine, CT imaging of cancer patients is frequently performed, for example, for tumor staging. Therefore, even though muscle status assessment by CT imaging is not routinely conducted, there would already be raw data available to quantify different SMI measures.⁴⁰

Our population PK model was able to adequately describe the observed routine data. However, the sole availability of steady-state concentrations impeded model development. The estimate of 5FU volume of distribution had to be therefore fixed and could not be used for covariate analysis. Gusella et al. found a significant relationship between total body water and 5FU volume of distribution as well as fat-free mass and 5FU volume of distribution.¹⁵ The initially developed 5FU population PK model, which was based on data from Wilhelm et al.,²⁵ included BSA as the only significant covariate on 5FU clearance. In general, the identified covariates on 5FU PK vary considerably. A similar influence of BSA was identified in two other published population PK models as well,^{41,42} whereas other models revealed significant effects of sex,^{36,43} age,⁴⁴ or body weight.⁴⁵ When applying the initial model on the new

TABLE 5 Parameter and bootstrap estimates of the final model

Parameter	Estimate (relative standard error, %)	Shrinkage [%]	Bootstrap median (95% confidence intervals)
CL _{5FU} [L/h]	223 (2.4)		223 (212–234)
V _{5FU} [L]	46.1 (fixed estimate)		46.1 (fixed estimate)
BSA effect on CL _{5FU}	0.794 (14.5)		0.796 (0.543–1.02)
SMI _{Back} effect on CL _{5FU}	0.0570 (29.8)		0.0575 (0.0283–0.0885)
<i>Interindividual variability</i>			
CL _{5FU} [%CV]	20.9 (7.4)	15.1	20.4 (15.8–24.5)
V _{5FU} [%CV]	51.1 (fixed estimate)	100	51.1 (fixed estimate)
<i>Residual variability</i>			
Proportional error [%]	21.4 (3.3)	10.6	21.4 (19.0–23.8)

Abbreviations: BSA, body surface area; CL, clearance; CV, coefficient of variation; SMI_{back}, skeletal back muscle index; V, volume of distribution.

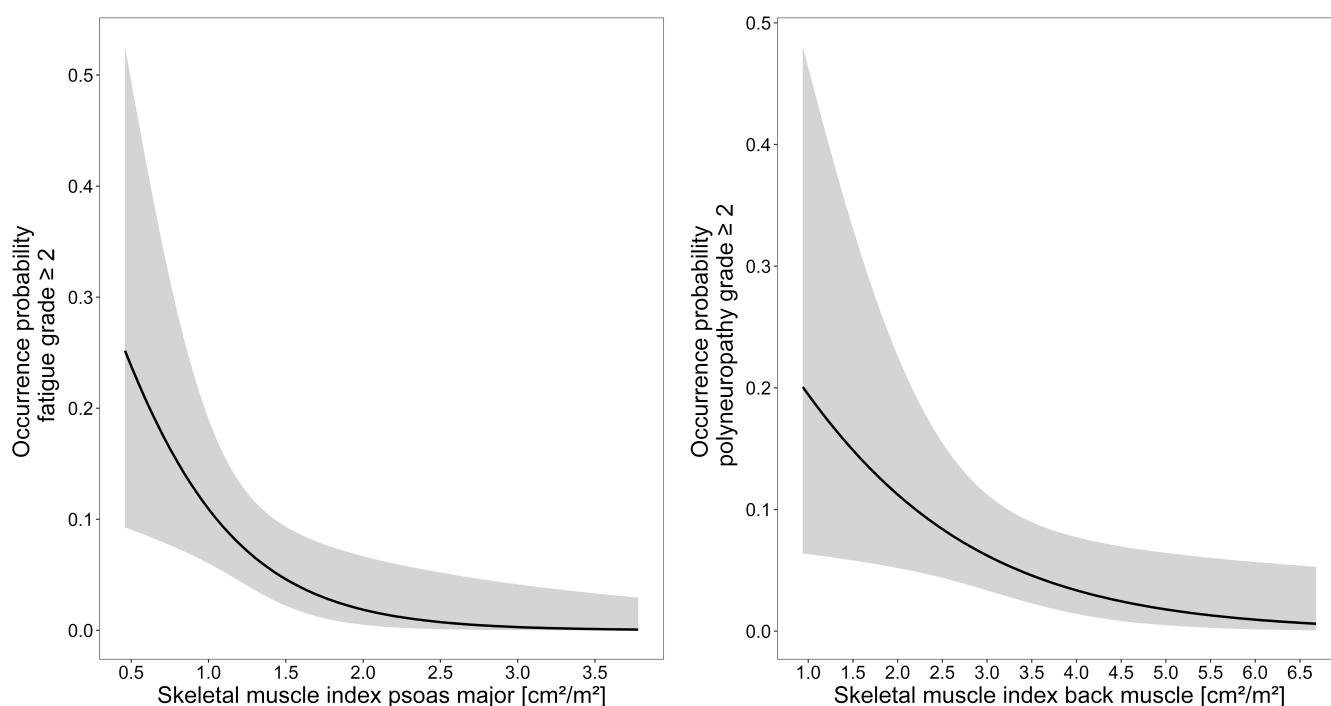


FIGURE 2 Probability of fatigue and polyneuropathy grade ≥ 2 versus different skeletal muscle indices. Black solid lines are the mean probabilities and the gray shaded areas are the respective 95% confidence intervals.

dataset, all SMI measures were positively associated with 5FU clearance when adding them as covariates and significantly improved the model fit. The inclusion of the SMI of the back muscle led to the largest improvement which deserves further investigation on physiological plausibility. While this finding gives additional hints that body composition may influence the PK of 5FU and other anticancer drugs,^{15,46–48} the minor reduction of IIV of 5FU clearance revealed that the usage of SMI for dose adjustment purposes may be of limited value. In fact, the inclusion of BSA had a higher impact on 5FU clearance (Table 4). The

wide range of SMI measures (Table 1) may further explain the limited reduction of variability in clearance. Interestingly, Molenaar-Kuijsten et al. could not identify any relationships between the SMI-derived skeletal muscle mass and the 5FU elimination rate constant in 151 patients treated with its oral prodrug capecitabine.³⁹ Williams et al. investigated the influence of LBM which was derived from the SMI on 5FU AUC but could not find any significant differences between sarcopenic and non-sarcopenic patients.¹⁶ However, they investigated a smaller patient cohort (25 patients) and only used first cycle plasma concentrations of 5FU,

whereas in our study, plasma concentrations from different cycles were available.

As a limitation of our study, it should be noted that the genotypes and the activity of the main metabolizing enzyme, dihydropyrimidine dehydrogenase (DPD), which are important predictors for 5FU exposure^{49,50} were not available for our patient cohort. However, IIV of 5FU clearance was already lower than the average IIV of 40% as reported in an extensive review on 5FU therapeutic drug monitoring by Beumer et al.⁵ This could be explained by the comparatively low prevalence of DPD risk variants which are associated with alleles producing DPD with minimal/no activity (DPYD*2A or DPYD*13) or with alleles producing DPD with decreased metabolic function (c.2846A > T or c.1129-5923C > G). Up to 1% of the European population are carriers of the non-active variants, whereas the two latter variants are present in about 5% of Europeans.⁵¹ Keeping in mind the number of patients used for model development ($n = 75$ in the study of Wilhelm et al.,²⁵ $n = 111$ in the present study), only few patients presumably were carriers of these DPD risk variants that are associated with a substantial influence on the variability in 5FU clearance.

The findings of the logistic regression analysis showed several significant associations between specific SMI measures and adverse events under 5FU therapy which was generally in accordance with previous studies.^{13,14,16} Williams et al. found a significant positive association of LBM and oxaliplatin clearance and LBM and volume of distribution as well as a significant association of low LBM and high-grade toxicity in older patients with colorectal cancer. Similar results were identified for cisplatin even though dose-limiting toxicity was not significantly correlated with body composition.⁵³ Our finding of a higher probability of the occurrence of clinically relevant polyneuropathy with decreasing SMI of the back muscle deserves further investigation. Since the psoas muscle is necessary for everyday movement, the reduction of its SMI may be an explanation for the identified increase in the probability of clinically relevant fatigue. It should be noted, however, that our analysis was focused on evaluating the general susceptibility of experiencing clinically relevant AE depending on body composition in patients treated with a 5FU-based chemotherapy. Regarding concomitant chemotherapy, only qualitative information of its administration was available for our study. In a future study, it would be of high interest to investigate the influence of individual drug PK on AE development in order to distinguish between the respective individual contributions of these drugs. In addition, the patient's performance status should be included in such an analysis as it was reported to be significantly

associated with SMI⁵⁴ and a significant predictor for drug toxicity under 5FU-based chemotherapy.⁵⁵

In conclusion, this retrospective study gives first hints that the SMI as a measure of body composition may be associated with the pharmacokinetic disposition and the development of toxicity of 5FU. A prospective study in which SMI measures and 5FU pharmacokinetics are investigated should provide additional insights into these relevant relationships between body composition and clinical outcome of 5FU-based chemotherapy.

AUTHOR CONTRIBUTION

Designed research: ES, NZ, LM, UJ. Performed research: ES, NZ, LM. Analyzed data: ES, NZ, SK, IS, UJ. Wrote or contributed to the writing of the manuscript: ES, NZ, LM, SK, IS, UJ.

FUNDING INFORMATION

This study was not funded.

ACKNOWLEDGEMENT

Open Access funding enabled and organized by Projekt DEAL. WOA Institution: RHEINISCHE FRIEDRICH-WILHELMS-UNIVERSITÄT BONN Consortia Name : Projekt DEAL

CONFLICT OF INTEREST

All authors declare that they have no conflicts of interest that are relevant to the content of this manuscript.

DATA AVAILABILITY STATEMENT

Data are available from the corresponding author upon reasonable request.

ETHICS STATEMENT

This retrospective study was approved by the local medical ethics committee.

CLINICAL TRIAL REGISTRATION

Due to the retrospective nature of this study, trial registration was not conducted.

ORCID

Eduard Schmulenson  <https://orcid.org/0000-0002-8026-609X>

Ulrich Jaehde  <https://orcid.org/0000-0002-2493-7370>

REFERENCES

1. van Cutsem E, Cervantes A, Nordlinger B, Arnold D, ESMO Guidelines Working Group. Metastatic colorectal cancer: ESMO clinical practice guidelines for diagnosis, treatment and follow-up. *Ann Oncol*. 2014;25(Suppl 3):iii1-iii9.

2. Argilés G, Taberero J, Labianca R, et al. Localised colon cancer: ESMO clinical practice guidelines for diagnosis, treatment and follow-up. *Ann Oncol*. 2020;31:1291-1305.
3. Pfister DG, Spencer S, Adelstein D, et al. Head and neck cancers, version 2.2020, NCCN clinical practice guidelines in oncology. *J Natl Compr Canc Netw*. 2020;18:873-898.
4. Schmulenson E, Zimmermann N, Mikus G, Joerger M, Jaehde U. Current status and future outlooks on therapeutic drug monitoring of fluorouracil. *Expert Opin Drug Metab Toxicol*. 2021;17:1407-1422.
5. Beumer JH, Chu E, Allegra C, et al. Therapeutic drug monitoring in oncology: International Association of Therapeutic Drug Monitoring and Clinical Toxicology Recommendations for 5-fluorouracil therapy. *Clin Pharmacol Ther*. 2019;105:598-613.
6. Morgan DJ, Bray KM. Lean body mass as a predictor of drug dosage. *Clin Pharmacokinet*. 1994;26:292-307.
7. Prado CMM, Maia YLM, Ormsbee M, Sawyer M, Baracos V. Assessment of nutritional status in cancer—the relationship between body composition and pharmacokinetics. *Anticancer Agents Med Chem*. 2013;13:1197-1203.
8. Martin L, Birdsell L, Macdonald N, et al. Cancer cachexia in the age of obesity: skeletal muscle depletion is a powerful prognostic factor, independent of body mass index. *J Clin Oncol*. 2013;31:1539-1547.
9. Caan BJ, Cespedes Feliciano EM, Prado CM, et al. Association of muscle and adiposity measured by computed tomography with survival in patients with nonmetastatic breast cancer. *JAMA Oncol*. 2018;4:798-804.
10. Prado CMM, Lieffers JR, McCargar LJ, et al. Prevalence and clinical implications of sarcopenic obesity in patients with solid tumours of the respiratory and gastrointestinal tracts: a population-based study. *Lancet Oncol*. 2008;9:629-635.
11. Shachar SS, Williams GR, Muss HB, Nishijima TF. Prognostic value of sarcopenia in adults with solid tumours: a meta-analysis and systematic review. *Eur J Cancer*. 2016;57:58-67.
12. Ryan AM, Prado CM, Sullivan ES, Power DG, Daly LE. Effects of weight loss and sarcopenia on response to chemotherapy, quality of life, and survival. *Nutrition*. 2019;67-68:110539.
13. Prado CMM, Baracos VE, McCargar LJ, et al. Body composition as an independent determinant of 5-fluorouracil-based chemotherapy toxicity. *Clin Cancer Res*. 2007;13:3264-3268.
14. Ali R, Baracos VE, Sawyer MB, et al. Lean body mass as an independent determinant of dose-limiting toxicity and neuropathy in patients with colon cancer treated with FOLFOX regimens. *Cancer Med*. 2016;5:607-616.
15. Gusella M, Toso S, Ferrazzi E, Ferrari M, Padrini R. Relationships between body composition parameters and fluorouracil pharmacokinetics. *Br J Clin Pharmacol*. 2002;54:131-139.
16. Williams GR, Deal AM, Shachar SS, et al. The impact of skeletal muscle on the pharmacokinetics and toxicity of 5-fluorouracil in colorectal cancer. *Cancer Chemother Pharmacol*. 2018;81:413-417.
17. Baracos VE, Arribas L. Sarcopenic obesity: hidden muscle wasting and its impact for survival and complications of cancer therapy. *Ann Oncol*. 2018;29:ii1-ii9.
18. Beumer JH, Boisdron-Celle M, Clarke W, et al. Multicenter evaluation of a novel nanoparticle immunoassay for 5-fluorouracil on the Olympus AU400 analyzer. *Ther Drug Monit*. 2009;31:688-694.
19. National Cancer Institute. Common Terminology Criteria for Adverse Events v5.0 (CTCAE); 2018. Available at: <http://ctep.cancer.gov/>. Accessed 6 Mar 2022.
20. Chung E, Lee HS, Cho E-S, et al. Changes in body composition during adjuvant FOLFOX chemotherapy and overall survival in non-metastatic colon cancer. *Cancers (Basel)*. 2019;12:60.
21. Mitsiopoulos N, Baumgartner RN, Heymsfield SB, Lyons W, Gallagher D, Ross R. Cadaver validation of skeletal muscle measurement by magnetic resonance imaging and computerized tomography. *J Appl Physiol*. 1985;1998(85):115-122.
22. Cruz-Jentoft AJ, Bahat G, Bauer J, et al. Sarcopenia: revised European consensus on definition and diagnosis. *Age Ageing*. 2019;48:16-31.
23. Popuri K, Cobzas D, Esfandiari N, Baracos V, Jagersand M. Body composition assessment in axial CT images using FEM-based automatic segmentation of skeletal muscle. *IEEE Trans Med Imaging*. 2016;35:512-520.
24. Mei K, Schwaiger BJ, Kopp FK, et al. Bone mineral density measurements in vertebral specimens and phantoms using dual-layer spectral computed tomography. *Sci Rep*. 2017;7:17519.
25. Wilhelm M, Mueller L, Miller MC, et al. Prospective, multicenter study of 5-fluorouracil therapeutic drug monitoring in metastatic colorectal cancer treated in routine clinical practice. *Clin Colorectal Cancer*. 2016;15:381-388.
26. Beal S, Sheiner LB, Boeckmann A, Bauer RJ. *NONMEM User's Guides (1989–2018)*. Icon Development Solutions; 2018.
27. Lindbom L, Ribbing J, Jonsson EN. Perl-speaks-NONMEM (PsN)—a Perl module for NONMEM related programming. *Comput Methods Programs Biomed*. 2004;75:85-94.
28. Lindbom L, Pihlgren P, Jonsson EN, et al. PsN-toolkit—a collection of computer intensive statistical methods for non-linear mixed effect modeling using NONMEM. *Comput Methods Programs Biomed*. 2005;79:241-257.
29. Bauer RJ. *NONMEM Users Guide*. Icon Development Solutions; 2021.
30. R Core Team. (2022). *R: a language and environment for statistical computing*. R Foundation for Statistical Computing. Available at: <http://www.R-project.org/>. Accessed 6 Mar 2022.
31. Keizer RJ, Karlsson MO, Hooker A. Modeling and simulation workbench for NONMEM: tutorial on Pirana, PsN, and Xpose. *CPT Pharmacometrics Syst Pharmacol*. 2013;2:e50.
32. Nguyen THT, Mouksassi M-S, Holford N, et al. Model evaluation of continuous data Pharmacometric models: metrics and graphics. *CPT Pharmacometrics Syst Pharmacol*. 2017;6:87-109.
33. Bergstrand M, Hooker AC, Wallin JE, Karlsson MO. Prediction-corrected visual predictive checks for diagnosing nonlinear mixed-effects models. *AAPS J*. 2011;13:143-151.
34. Mould DR, Upton RN. Basic concepts in population modeling, simulation, and model-based drug development-part 2: introduction to pharmacokinetic modeling methods. *CPT Pharmacometrics Syst Pharmacol*. 2013;2:e38.
35. Streit M, Jaehde U, Stremetzne S, et al. Five-day continuous infusion of 5-fluorouracil and pulsed folinic acid in patients with metastatic colorectal carcinoma: an effective second-line regimen. *Ann Oncol*. 1997;8:163-165.
36. Mueller F, Büchel B, Köberle D, et al. Gender-specific elimination of continuous-infusional 5-fluorouracil in patients with gastrointestinal malignancies: results from a prospective population pharmacokinetic study. *Cancer Chemother Pharmacol*. 2013;71:361-370.

37. Hendrayana T, Kurth V, Krolop L, et al. Variability in fluorouracil exposure during continuous intravenous infusion. *Int J Clin Pharmacol Ther.* 2012;50:82-84.
38. Savic RM, Karlsson MO. Importance of shrinkage in empirical Bayes estimates for diagnostics: problems and solutions. *AAPS J.* 2009;11:558-569.
39. Molenaar-Kuijsten L, Jacobs BAW, Kurk SA, et al. Worse capecitabine treatment outcome in patients with a low skeletal muscle mass is not explained by altered pharmacokinetics. *Cancer Med.* 2021;10:4781-4789.
40. Rinninella E, Cintoni M, Raoul P, et al. Muscle mass, assessed at diagnosis by L3-CT scan as a prognostic marker of clinical outcomes in patients with gastric cancer: a systematic review and meta-analysis. *Clin Nutr.* 2020;39:2045-2054.
41. Arshad U, Ploylearmsaeng S-A, Karlsson MO, et al. Prediction of exposure-driven myelotoxicity of continuous infusion 5-fluorouracil by a semi-physiological pharmacokinetic-pharmacodynamic model in gastrointestinal cancer patients. *Cancer Chemother Pharmacol.* 2020;85:711-722.
42. Terret C, Erdociain E, Guimbaud R, et al. Dose and time dependencies of 5-fluorouracil pharmacokinetics. *Clin Pharmacol Ther.* 2000;68:270-279.
43. Bressolle F, Joulia JM, Pinguet F, et al. Circadian rhythm of 5-fluorouracil population pharmacokinetics in patients with metastatic colorectal cancer. *Cancer Chemother Pharmacol.* 1999;44:295-302.
44. Etienne M-C, Chatelut E, Pivot X, et al. Co-variables influencing 5-fluorouracil clearance during continuous venous infusion. A NONMEM analysis. *Eur J Cancer.* 1998;34:92-97.
45. Climente-Martí M, Merino-Sanjuán M, Almenar-Cubells D, Jiménez-Torres NV. A Bayesian method for predicting 5-fluorouracil pharmacokinetic parameters following short-term infusion in patients with colorectal cancer. *J Pharm Sci.* 2003;92:1155-1165.
46. Mir O, Coriat R, Blanchet B, et al. Sarcopenia predicts early dose-limiting toxicities and pharmacokinetics of sorafenib in patients with hepatocellular carcinoma. *PLoS ONE.* 2012;7:e37563.
47. Prado CMM, Lima ISF, Baracos VE, et al. An exploratory study of body composition as a determinant of epirubicin pharmacokinetics and toxicity. *Cancer Chemother Pharmacol.* 2011;67:93-101.
48. Massicotte M-H, Borget I, Broutin S, et al. Body composition variation and impact of low skeletal muscle mass in patients with advanced medullary thyroid carcinoma treated with vandetanib: results from a placebo-controlled study. *J Clin Endocrinol Metab.* 2013;98:2401-2408.
49. Lee JJ, Beumer JH, Chu E. Therapeutic drug monitoring of 5-fluorouracil. *Cancer Chemother Pharmacol.* 2016;78:447-464.
50. Diasio RB, Johnson MR. Dihydropyrimidine dehydrogenase: its role in 5-fluorouracil clinical toxicity and tumor resistance. *Clin Cancer Res.* 1999;5:2672-2673.
51. Hamzic S, Aebi S, Joerger M, et al. Fluoropyrimidine chemotherapy: recommendations for DPYD genotyping and therapeutic drug monitoring of the swiss Group of Pharmacogenomics and Personalised Therapy. *Swiss Med Wkly.* 2020;150:w20375.
52. Williams GR, Al-Obaidi M, Rower J, et al. Does oxaliplatin pharmacokinetics (PKs) explain associations between body composition and chemotherapy toxicity risk in older adults with gastrointestinal (GI) cancers? *J Clin Oncol.* 2021;39:3095.
53. Chargi N, Molenaar-Kuijsten L, Huiskamp LFJ, Devriese LA, de Bree R, Huitema ADR. The association of cisplatin pharmacokinetics and skeletal muscle mass in patients with head and neck cancer: the prospective PLATISMA study. *Eur J Cancer.* 2022;160:92-99.
54. Dolan RD, Daly LE, Simmons CP, et al. The relationship between ECOG-PS, mGPS, BMI/WL grade and body composition and physical function in patients with advanced cancer. *Cancers (Basel).* 2020;12:1187.
55. Sargent DJ, Köhne CH, Sanoff HK, et al. Pooled safety and efficacy analysis examining the effect of performance status on outcomes in nine first-line treatment trials using individual data from patients with metastatic colorectal cancer. *J Clin Oncol.* 2009;27:1948-1955.

SUPPORTING INFORMATION

Additional supporting information can be found online in the Supporting Information section at the end of this article.

How to cite this article: Schmulenson E, Zimmermann N, Müller L, Kapsa S, Sihinevich I, Jaehde U. Influence of the skeletal muscle index on pharmacokinetics and toxicity of fluorouracil. *Cancer Med.* 2022;00:1-10. doi: [10.1002/cam4.5118](https://doi.org/10.1002/cam4.5118)

Image analysis

Tab. S1-1 Measured skeletal muscle areas and methods used

Skeletal muscle index (SMI)	Measured skeletal muscle areas	Method
SMI Psoas	Psoas major	Hounsfield
SMI back muscle	Erector spinae	Hounsfield
	Quadratus lumborum	
SMI total skeletal muscle	Psoas major	Hounsfield/Segmentation
	Erector spinae	
	Quadratus lumborum	
	Transversus abdominalis	
	Internal/external Musculus obliquus abdominis	
	Rectus abdominis	

Population pharmacokinetic analysis

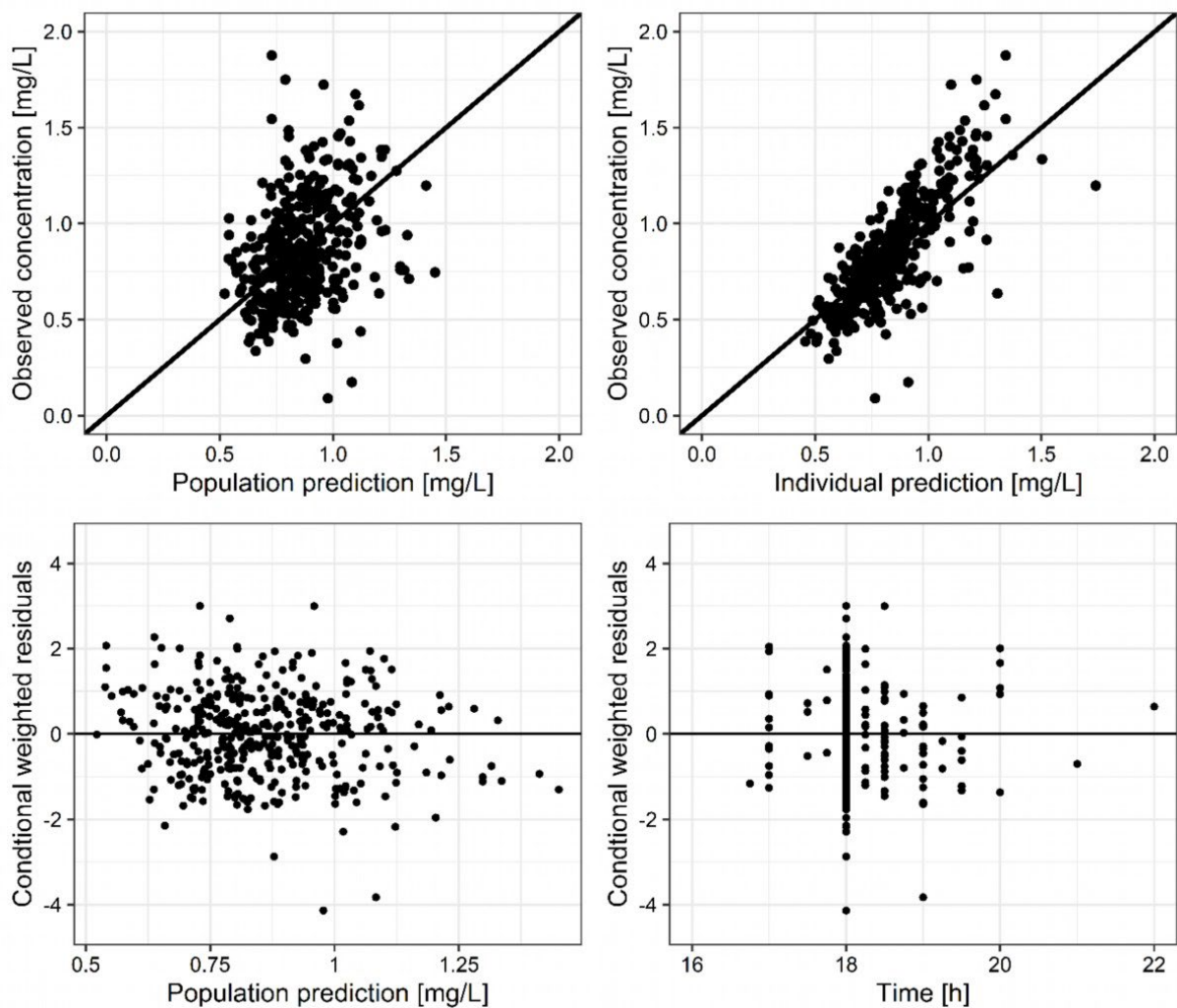


Fig. S2 Goodness-of-fit plots for model-predicted fluorouracil concentrations. The black lines indicate the lines of identity.

NONMEM code of the final model

\$PROBLEM 5FU PK model

\$INPUT

ID

SMIB ; SMI of the back muscle

EVID

BSA

TIME

RATE

DV

AMT

MDV

\$DATA ...

\$SUBROUTINES ADVAN1 TRANS2

\$PK

CLCOV = (1 + THETA(4) * (BSA - 1.97)) * EXP(THETA(5) * (SMIB - 3.78)) ; Covariate relations

TVCL = THETA(1) * CLCOV

CL = TVCL * EXP(ETA(1))

TVV = THETA(2)

V = TVV * EXP(ETA(2))

S1 = V

\$ERROR

IPRED = F

DEL = 0

W = SQRT((THETA(3) * IPRED)**2)

Y = IPRED + W * EPS(1)

IF(W.EQ.0) DEL = 0.0001

IRES = DV - IPRED

IWRES = IRES/(W+DEL)

\$THETA

(0, 223) ; CL

46.1 FIX ; V

(0, 0.214) ; prop. error

0.794 ; BSA on CL

0.057 ; SMIB

\$OMEGA

0.0437 ; IIV CL

0.261 FIX ; IIV V

\$SIGMA 1 FIX

\$EST METHOD=1 INTER MAXEVAL=9999 NOABORT SIG=3 PRINT=1 POSTHOC

\$COV UNCONDITIONAL SLOW MATRIX=S

Toxicity analysis

Tab. S4-1 Frequency of clinically relevant adverse event severity

Adverse event	Number of patients with CTCAE grade ≥ 2 (% of total patients)
Diarrhea	38 (34.2)
Stomatitis	2 (1.8)
Polyneuropathy	9 (8.1)
Hand-foot syndrome	4 (3.6)
Fatigue	8 (7.3)
Nausea	13 (11.7)
Emesis	15 (13.5)

CTCAE: Common Terminology Criteria for Adverse Events

Tab. S4-2 Results of the logistic regression analysis

Skeletal muscle index	Adverse event	Odds ratio	95% confidence intervals
Psoas major	Diarrhea	0.793	0.461 – 1.46
	Stomatitis	0.125	0.002 – 2.43
	Polyneuropathy	0.513	0.127 – 1.75
	Hand-foot syndrome	1.78	0.288 – 7.96
	Fatigue	0.155	0.033 – 0.595*
	Nausea	0.657	0.227 – 1.71
	Emesis	0.428	0.137 – 1.19
Back muscle	Diarrhea	0.922	0.706 – 1.20
	Stomatitis	0.522	0.128 – 1.65
	Polyneuropathy	0.524	0.287 – 0.900*
	Hand-foot syndrome	1.80	0.806 – 4.40
	Fatigue	0.853	0.523 – 1.37
	Nausea	0.940	0.617 – 1.42
	Emesis	0.760	0.491 – 1.15
Total muscle (Hounsfield method)	Diarrhea	0.977	0.87 – 1.09
	Stomatitis	0.800	0.386 – 1.31
	Polyneuropathy	0.882	0.674 – 1.11
	Hand-foot syndrome	1.07	0.751– 1.43
	Fatigue	0.869	0.678 – 1.07
	Nausea	0.901	0.733 – 1.08
	Emesis	0.859	0.691 – 1.04
Total muscle (Segmentation method)	Diarrhea	0.982	0.948 – 1.02
	Stomatitis	0.876	0.708 – 1.03
	Polyneuropathy	1.00	0.937 – 1.07
	Hand-foot syndrome	1.04	0.941 – 1.13
	Fatigue	0.947	0.882 – 1.01
	Nausea	0.949	0.892 – 1.00
	Emesis	0.975	0.920 – 1.03

*significant at $p < 0.05$



Evaluation of patient-reported severity of hand–foot syndrome under capecitabine using a Markov modeling approach

Eduard Schmulenson¹ · Linda Krolop¹ · Sven Simons¹ · Susanne Ringsdorf¹ · Yon-Dschun Ko² · Ulrich Jaehde¹

Received: 28 March 2020 / Accepted: 11 August 2020 / Published online: 27 August 2020
© The Author(s) 2020

Abstract

Purpose The inclusion of the patient’s perspective has become increasingly important when reporting adverse events and may assist in management of toxicity. The relationship between drug exposure and toxicity can be quantified by combining Markov elements with pharmacometric models. A minimal continuous-time Markov model (mCTMM) was applied to patient-reported outcomes using hand–foot syndrome (HFS) induced by capecitabine anti-cancer therapy as an example.

Methods Patient-reported HFS grades over time of 150 patients from two observational studies treated with oral capecitabine were analyzed using a mCTMM approach. Grading of HFS severity was based on the Common Terminology Criteria for Adverse Events. The model was evaluated by visual predictive checks (VPC). Furthermore, a simulation study of the probability of HFS severity over time was performed in which the standard dosing regimen and dose adjustments according to HFS severity were investigated.

Results The VPC of the developed dose–toxicity model indicated an accurate description of HFS severity over time. Individual absolute daily dose was found to be a predictor for HFS. The simulation study demonstrated a reduction of severe HFS using the recommended dose adjustment strategy.

Conclusion A minimal continuous-time Markov model was developed based on patient-reported severity of hand–foot syndrome under capecitabine. Thus, a modeling framework for patient-reported outcomes was created which may assist in the optimization of dosage regimens and adjustment strategies aiming at minimizing symptom burden during anti-cancer drug therapy.

Keywords Markov model · Capecitabine · Hand–foot syndrome · Patient-reported outcomes

Introduction

Anticancer treatment is frequently associated with adverse events. Thus, the management of toxic effects is a major aspect of a successful therapy. To account for the severity of adverse events, the Common Terminology Criteria for Adverse Events (CTCAE) are widely used for evaluation

of toxicity [1]. The grading of adverse events is conducted by the study personnel. However, since reports suggest that this method is associated with underestimations of adverse event severity [2, 3], the patient’s perspective has become increasingly important. Therefore, a version of Patient-Reported Outcomes (PRO-CTCAE) has been developed and is increasingly used [4].

Pharmacokinetic–pharmacodynamic (PKPD) modeling approaches have proved to be useful to quantify the relationship between drug exposure and toxicity. Whereas some adverse events can be classified by metric data, such as myelosuppression [5], others, such as the severity of hand–foot syndrome or fatigue, lack objectively quantifiable parameters. Particularly, patient-reported data are often categorical as they are generated by subjective grading. One possibility to link categorical longitudinal toxicity data with drug exposure are Markov models. By applying these models, the probability of developing an adverse event of a certain grade

Electronic supplementary material The online version of this article (<https://doi.org/10.1007/s00280-020-04128-7>) contains supplementary material, which is available to authorized users.

✉ Ulrich Jaehde
u.jaehde@uni-bonn.de

¹ Department of Clinical Pharmacy, Institute of Pharmacy, University of Bonn, An der Immenburg 4, 53121 Bonn, Germany

² Department of Internal Medicine, Evangelische Kliniken Bonn gGmbH, Johanniter Hospital, Bonn, Germany

can be estimated. Karlsson et al. introduced Markov models into the field of PKPD by analyzing sleep stages in insomnia patients [6]. Since then, Markov models were applied to a wide field of scenarios, such as diarrhea and rash, in cancer patients [7, 8], proteinuria [9] or improvement scores in rheumatoid arthritis [10].

Capecitabine is an orally administered prodrug of the cytotoxic agent fluorouracil (5-FU) used for the treatment of various tumor entities, such as colorectal and breast cancer. The metabolic activation of capecitabine to 5-FU occurs primarily in tumor cells minimizing the systemic toxic effects of 5-FU [11]. However, it causes a higher incidence of hand–foot syndrome (HFS) than intravenously administered 5-FU [12, 13]. Because the occurrence and severity of HFS were assumed to be dose-dependent the management of HFS toxicity includes dose reductions [14, 15]. Hénin et al. already linked capecitabine exposure to HFS toxicity using a Markov modeling approach [16] but could only consider CTCAE grades which were described by clinicians. Therefore, a model-based extension towards a patient perspective would allow to improve the management of adverse events.

The aim of this project was to develop a modeling and simulation framework to describe and predict patient-reported HFS severity in patients treated with capecitabine. Based on this example, the suitability of Markov models to simulate the time course of patient-reported toxic symptoms should be assessed.

Methods

Patients and data

For this work, raw data from a total of 150 capecitabine-naïve patients were pooled from two open, prospective multi-centered observational cohort studies. Both studies aimed at evaluating the effect of pharmaceutical care on adherence of capecitabine-treated patients and were approved by the ethics committee at the Faculty of Medicine of the University of Bonn [17, 18]. A summary of the observed data can be found in Table 1. Capecitabine was administered orally twice daily as an intermittent regimen in 3-week cycles (14 days of treatment and seven-day break). Dose modifications, treatment interruptions and discontinuations were conducted at the sole discretion of the treating oncologists.

Occurrence and severity of HFS were assessed by the patients using a questionnaire developed at the Department of Clinical Pharmacy at the University of Bonn. The description of HFS severity grades (0 to 3) was based on the descriptions provided by the CTCAE grades, version 3.0 [1]. Grade 0 was described as the absence of symptoms, patients with grade 1 had minimal skin alterations (e.g. redness) without any pain.

Grade 2 was described as skin reactions (e.g. fissures, blisters, swelling) and/or pain without impairment of activities of daily living and patients with HFS grade 3 had severe skin reactions (e.g. peeling, blisters, bleeding) and/or severe pain, including impaired activities of daily living. Patients were asked to complete the questionnaire after each conducted cycle. Therefore, up to six HFS grade assessments per patient were collected. Before starting capecitabine treatment, patients were considered asymptomatic.

Data analysis

This population pharmacodynamic analysis was performed using non-linear mixed effect modeling. Model parameters were estimated by the Laplacian method implemented in the software NONMEM 7.4.3 [19]. The likelihood-ratio test was used to discriminate between nested models. The inclusion of an extra parameter or covariate required a statistically significant reduction ($p \leq 0.01$) of the objective function value (OFV) provided by NONMEM. Furthermore, visual predictive checks (VPC) assisted in model selection.

Implemented scripts in PsN (version 4.8.1) [20, 21] were also used for model development and R (version 3.5.1) [22] was used for visualization of results as well as generating random numbers for simulation analyses. Piraña (version 2.9.7) [23] served as a front interface.

Model building

Since HFS can only be graded on a categorical scale, the probability of each grade was modeled with a proportional odds model which was extended with Markov elements. In this work, a minimal continuous-time Markov model (mCTMM) was applied to analyze the severity of HFS. The mCTMM was developed by Schindler and Karlsson and is a simplification of standard continuous-time Markov models [24]. A compartmental structure with four compartments was used, with each compartment representing one HFS severity grade (0, 1, 2, and 3) [7]. The probability of each grade was modeled as an amount in the respective compartment and described by differential equations in which solely transitions between adjacent states were considered (Eq. 1):

$$\begin{aligned} \frac{dP(0)}{dt} &= K_{10} \cdot P(1) - K_{01} \cdot P(0) \\ \frac{dP(1)}{dt} &= K_{01} \cdot P(0) + K_{21} \cdot P(2) - K_{10} \cdot P(1) - K_{12} \cdot P(1) \\ \frac{dP(2)}{dt} &= K_{12} \cdot P(1) + K_{32} \cdot P(3) - K_{21} \cdot P(2) - K_{23} \cdot P(2) \\ \frac{dP(3)}{dt} &= K_{23} \cdot P(2) - K_{32} \cdot P(3) \end{aligned} \quad (1)$$

Table 1 Summary of observed data [17, 18]

Patients analyzed (male/female)	150 (39/101)
Age (years), median (range)	62 (28–93)
Tumor entity	
Colorectal cancer	71
Breast cancer	67
Other	12
Therapy-related details	
Capecitabine monotherapy	71
Capecitabine combination therapy	79
Absolute daily dose (mg), median (range)	3000 (1000 – 5000)
Number of observed cycles per patient, mean (range)	5.2 (1 – 6)
Number of patients with treatment interruptions	33
Duration of treatment interruptions (days), median (range)	8 (1 – 118)
Number of treatment discontinuations	56
Number of observed transitions between adverse event grades	
0 → 0	254
0 → 1	93
0 → 2	41
0 → 3	7
1 → 0	26
1 → 1	125
1 → 2	44
1 → 3	9
2 → 0	8
2 → 1	34
2 → 2	69
2 → 3	12
3 → 0	2
3 → 1	6
3 → 2	9
3 → 3	22

$dP(\text{grade})/dt$ represents the rate of change over time of the probability of experiencing grades 0, 1, 2 or 3, $P(\text{grade})$ is the probability of experiencing one of the HFS grades, $K_{\text{grade, grade}+1}$ and $K_{\text{grade, grade}-1}$ are transition rate constants for worsening to higher grades and for recovering to lower grades, respectively.

When an observation event occurred, the amount in the compartment corresponding to the respective severity grade was set to 1 whereas the other compartments were set to 0 before the next observation. This introduced the Markov property. Between two observations, rate constants defined the transitions of probabilities between different grades. In an mCTMM, it is assumed that the transition rate between two consecutive grades is independent of the grade resulting in fewer model parameters than in other Markov models. Only the mean equilibration time (MET) was introduced as a constant parameter characterizing the transition rates across different grades. The transition rate constants govern the rate at which the probability of the

adverse event severity distributes between two observations. They were defined as functions of the MET and the probabilities of the respective severity grades [24].

The calculation of the probabilities experiencing one of the HFS grades was similar to a proportional odds model [25]. Since four different HFS grades were considered, three probabilities had to be estimated. The fourth probability was defined as 1 minus the sum of the three others. Logit transformation was conducted to express the respective probability as a value within the interval between 0 and 1 (Eq. 2):

$$\text{logit}(P(\text{Gr}_{ij} \geq n)) = \log\left(\frac{P(\text{Gr}_{ij} \geq n)}{1 - P(\text{Gr}_{ij} \geq n)}\right) = \alpha_n + g(x_i) + \eta_i \quad (2)$$

Gr_{ij} is the HFS grade for the i th individual at the j th occasion. $P(\text{Gr}_{ij} \geq n)$ represents the probability that the HFS grade is greater than or equal to grade n . This can be

also defined as the cumulative probability of grade n . α_n is the intercept on the logit scale and $g(x_i)$ represents a linear function on the logit scale which contains explanatory factors, such as drug exposure or covariates, such as age or sex. These factors are related to the probability experiencing HFS. η_i represents the interindividual random effect for the i th individual assuming a normal distribution with a mean of 0 and a variance of ω^2 . To ensure that the cumulative probability of the respective next higher grade is lower, the following parametrization of the logit intercept was used (Eq. 3):

$$\alpha_{n+1} = \alpha_n + b_{n+1} \quad (3)$$

The parameter b_{n+1} is negatively constrained and has to be estimated in the model.

Using the inverse logit function (also called expit function), $P(\text{Gr}_{ij} \geq n)$ can be directly calculated as follows (Eq. 4):

$$P(\text{Gr}_{ij} \geq n) = \frac{1}{1 + e^{-(\alpha_n + g(x_i) + \eta_i)}} \quad (4)$$

Additionally, an interindividual variability (IIV) as an exponential function of the MET was included.

After building the base model, the effects of dose and time on the MET and the logit intercepts were tested. Here, dose was tested as a time-varying covariate between therapy cycles. Moreover, a covariate analysis was performed. Continuous (patient's age) as well as categorical covariates (sex, tumor entity and concomitant chemotherapy) were included based on their statistical significance of reducing the OFV, i.e. improving the model fit. For one additional parameter in the model the OFV had to decrease by at least 6.64 which corresponds to a p value ≤ 0.01 in the case of one degree of freedom. Additionally, adherence was tested as a covariate. It was measured using an electronic medication event monitoring system (MEMS™) [17, 18] and assessed as pooled overall adherence per patient over the course of therapy. Patients were allocated to one of three groups (Overall adherence $> 100\%$, $90\text{--}100\%$ or $< 90\%$).

Model evaluation

To assess the model fit, visual predictive checks for categorical data were used. 95% confidence intervals (CI) were generated from 1000 dataset simulations based on the observed dataset and superimposed by the observed proportions of patients experiencing the individual HFS grades over time.

In addition, model robustness as well as precision and bias of parameter estimates were evaluated by a non-parametric bootstrap analysis without stratification. Median and 95% CI of parameter estimates were derived from 1000

replicate datasets obtained from sampling individuals from the original dataset with replacement.

Simulation study

The developed model was used to perform a simulation study based on 1000 virtual patients to assess the appropriateness of the standard dosing regimen for capecitabine monotherapy of 1250 mg/m^2 twice daily and the proposed dose adjustments based on HFS severity according to the summary of product characteristics (SmPC) [15]. Since no information of body surface areas (BSA) of the patients from the observational studies [17, 18] was provided, random BSA values were generated using the `rnorm` function in R. BSA means and standard deviations were obtained from published data [26]. Two simulation approaches were performed: (1) A simulation was performed in 1000 virtual patients with the above-mentioned starting dose of 1250 mg/m^2 for six cycles without dose adjustments. (2) A step-wise simulation was performed in the same 1000 patients with the same dose and total simulation duration as in (1). When meeting the criteria for dose adjustment according to the SmPC [15], the capecitabine dose was adjusted after each conducted cycle. To have an equal number of patients in both simulation scenarios, patients for whom a treatment discontinuation would be recommended were kept in the analysis. After adjusting the dose, the simulation of the subsequent cycle was performed. The HFS grade corresponding to the highest simulated probability was used to assess toxicity.

Predictive performance

The ability of the model to predict individual HFS severity was assessed by a simulation of patients with the same characteristics as in the original dataset. Therefore, the included random effect parameters were estimated by a Bayesian approach up to a certain cycle. Then, the HFS severity of the subsequent cycle was simulated based on the Bayesian estimates and covariate effects. This approach was conducted for predictions of cycle 2 up to cycle 6. Since Markov models can only predict the probability for each toxicity grade but not the grade itself, the grade corresponding to the highest probability was compared to the respective observed HFS grade. All grades were allocated to one of the following two groups: The first group consisted of HFS grades ≥ 2 which were classified as clinically relevant since dose reductions or treatment interruptions are conducted at grade 2 or higher [15], the second group consisted of HFS grades 0 and 1. For the first group, a positive predictive value (PPV) was calculated. It indicated the ability of predicting clinically relevant HFS:

$$PPV = \frac{N \text{ true predicted events with grade } \geq 2}{N \text{ total predicted events with grade } \geq 2} \quad (5)$$

The ability of predicting the absence of toxicity \geq grade 2 was assessed by calculation of a negative predictive value (NPV) within the second group:

$$NPV = \frac{N \text{ true predicted events with grade } \leq 1}{N \text{ total predicted events with grade } \leq 1} \quad (6)$$

Since patients were considered asymptomatic before starting therapy, predicted HFS grades at baseline were not included for calculation of both NPV and PPV.

Results

Model building

In total, 911 observations from 150 patients were used for model building (Table 1). Three exemplary time profiles of individual HFS severity are depicted in Fig. 1. It should be noted that 25 patients sent back HFS questionnaires after they discontinued therapy. These patients were also included in this analysis and their capecitabine dose was set to zero after discontinuation. A base minimal continuous-time Markov model (mCTMM) for hand–foot syndrome (HFS) was developed including interindividual variability (IIV) for both mean equilibration time (MET) and logit intercept α_n , respectively. The results of the analysis of various covariates are presented in Table 2.

The final mCTMM included a linear effect of absolute daily capecitabine dose on the logit intercept α_n indicating larger probabilities of experiencing HFS with an increasing dose (Δ OFV = − 23.45, $p < 0.00001$). None of the other examined covariates or time effects resulted in a statistically significant reduction of the OFV after inclusion. Additionally, after the dose effect was included into the base model, a further analysis of the mentioned covariates or time effects did not result in a significant improvement of the model fit. The final equation described the cumulative probabilities as follows (Eq. 7):

$$P(\text{Gr}_{ij} \geq n) = \frac{1}{1 + e^{-(\alpha_n + \theta_{\text{Dose}} \times (\text{Dose (mg)} - 3000 \text{ mg}) + \eta_i)}} \quad (7)$$

θ_{Dose} represents the slope of the linear dose effect on the logit scale. The dose effect was centered on the population median daily dose of 3000 mg. The final model code used in NONMEM is provided in the electronic supplementary material.

A summary of the parameter estimates including the bootstrap results is depicted in Table 3. Parameters were well

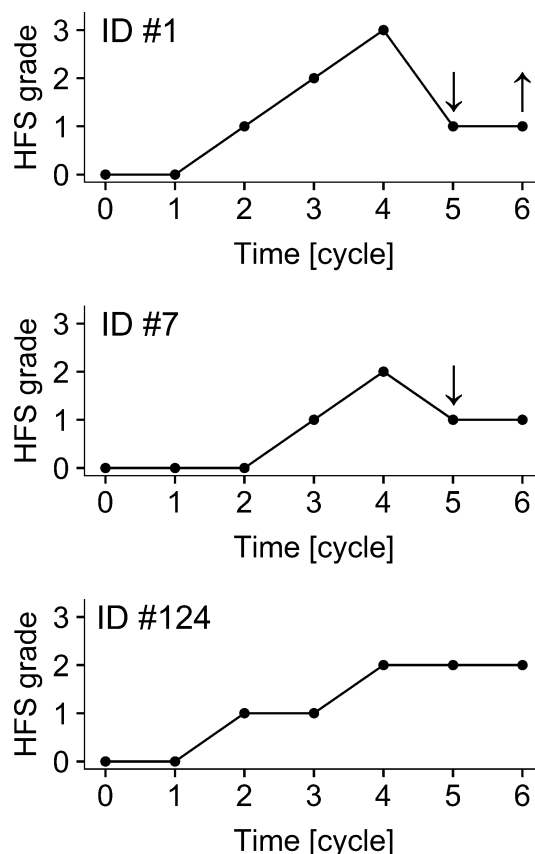


Fig. 1 Observed hand–foot syndrome (HFS) grades over time of three representative individuals. ID #1 was a patient with a median daily starting dose of capecitabine including a dose reduction and dose increase, indicated by downwards and upwards pointing arrows, respectively. ID #7 was a patient of median age who had a dose reduction (cycle 5). ID #124 was a patient who took the median daily capecitabine dose over the whole observed period of six cycles

estimated with relative standard errors below 25%, except for the IIV parameter associated with α_1 .

Model evaluation

The categorical visual predictive check revealed an accurate description of the provided data. The simulated proportions of patients experiencing one of the HFS grades described the respective observed proportions of patients over time well (Fig. 2).

Simulation study

Based on the developed dose–toxicity model and on the results of the simulation study (Fig. 3), it was evident that dose adjustments decreased the probability of severe HFS during therapy while increasing the probabilities of the absence of clinically relevant toxicity (grades 0 and 1).

Table 2 Development of the final model including various covariates

Model	Δ OFV	<i>p</i> value
Base model	0	–
Sex effect on logit intercept α_n	– 3.454	0.063
Sex effect on MET	– 1.348	0.246
Absolute daily dose on logit intercept α_n	– 23.45	<0.00001
Absolute daily dose on MET	– 0.445	0.505
Capecitabine monotherapy (yes/no) on logit intercept α_n	– 1.358	0.244
Capecitabine monotherapy (yes/no) on MET	+ 1.006	–
Breast cancer (yes/no) on logit intercept α_n	– 1.274	0.259
Breast cancer (yes/no) on MET	– 0.139	0.709
Colorectal cancer (yes/no) on logit intercept α_n	– 1.978	0.160
Colorectal cancer (yes/no) on MET	– 0.467	0.494
Other tumor entities (yes/no) on logit intercept α_n	– 0.391	0.532
Other tumor entities (yes/no) on MET	+ 0.488	–
Age effect on logit intercept α_n	– 0.077	0.930
Age effect on MET	– 0.132	0.716
Overall adherence (> 100%/90–100%/< 90%) on logit intercept α_n	– 0.130	0.937 ^a
Overall adherence (> 100%/90–100%/< 90% adherence) on MET	– 1.316	0.518 ^a
Time effect on logit intercept α_n	– 4.179	0.041
Time effect on MET	– 1.4	0.237

Δ OFV difference in the objective function value between the covariate model and the base model, MET mean equilibration time

^aTwo degrees of freedom

Table 3 Parameter estimates

Parameter	Estimate (relative standard error, %)	Bootstrap median	Bootstrap 95% confidence intervals
α_1	1.81 (14)	1.88	1.38 to 2.51
b_2	– 1.80 (11)	– 1.79	– 2.23 to (– 1.45)
b_3	– 2.08 (13)	– 2.05	– 2.73 to (– 1.57)
MET (cycle)	1.09 (10)	1.11	0.896 to 1.430
θ_{Dose}	8.33×10^{-4} (24)	8.28×10^{-4}	4.05×10^{-4} to 1.48×10^{-3}
$\omega_{\alpha 1}$	1.12 (37)	0.981	0.0112 to 1.65
ω_{MET}	0.542 (22)	0.560	0.310 to 0.842

$\alpha 1$ intercept parameter on the logit scale for HFS grade 1, b_n parameter for grade n such that $an = an-1 + bn$, MET mean equilibration time, θ_{Dose} slope of the linear daily dose effect on the logit scale, ωP standard deviation of the interindividual variability of parameter P

In particular, grade 3 toxicity was more probable when no dose adjustments were performed whereas the probabilities of grade 2 did not differ between the two simulation approaches. The simulation study also clearly showed that patients without dose adjustments tended to remain in grade 3 for a longer period of time which is characterized by a higher transition count from grade 3 to 3 compared to the approach which included dose adjustments (transition count of 442 and 234, respectively). However, the transition counts from grade 2 to 2 were comparable in both simulation groups (769 without and 774 with dose adjustments).

Predictive performance

The predictive ability of the model for individual patients was assessed by calculating the positive and negative predictive value (PPV, NPV) for each cycle (from cycle 2) based on Bayesian estimates of both random effect parameters from the previous cycle as well as the dose effect. PPV ranged from 21.9 to 34.2% whereas NPV ranged from 61.9 to 73.3%. Both values indicated a rather poor predictive performance on an individual patient level.

Fig. 2 Categorical visual predictive check showing the proportions of patients experiencing patient-reported CTCAE-based HFS grades from 0 to 3 over time. Solid black lines indicate the observed proportion of patients and the grey shaded areas are the 95% confidence intervals of simulated proportions based on 1000 simulated datasets using the final model

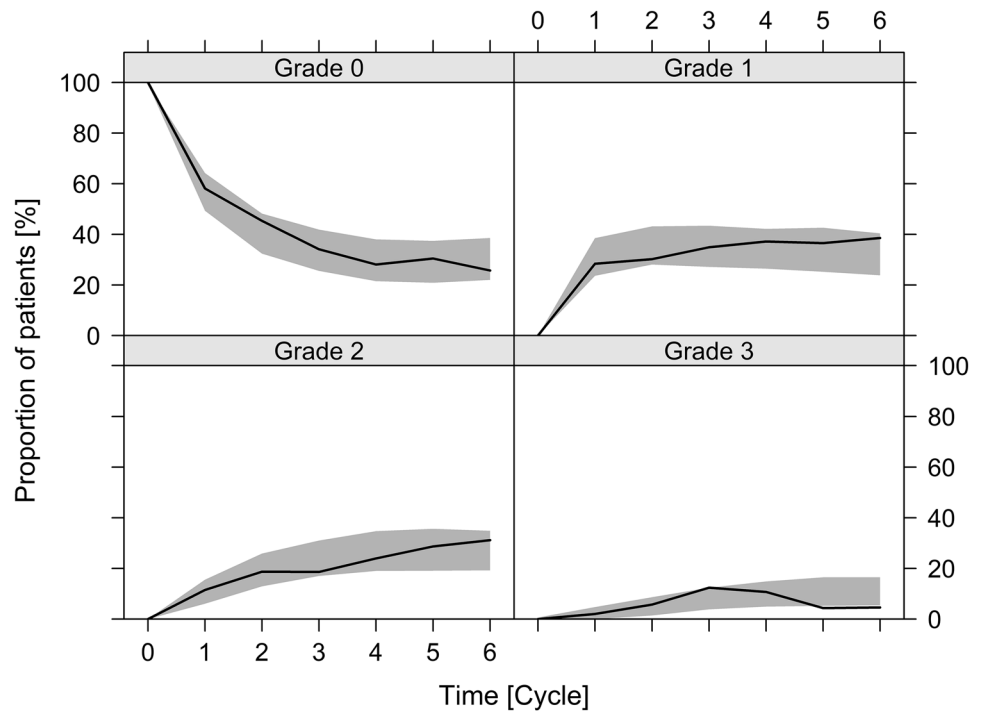
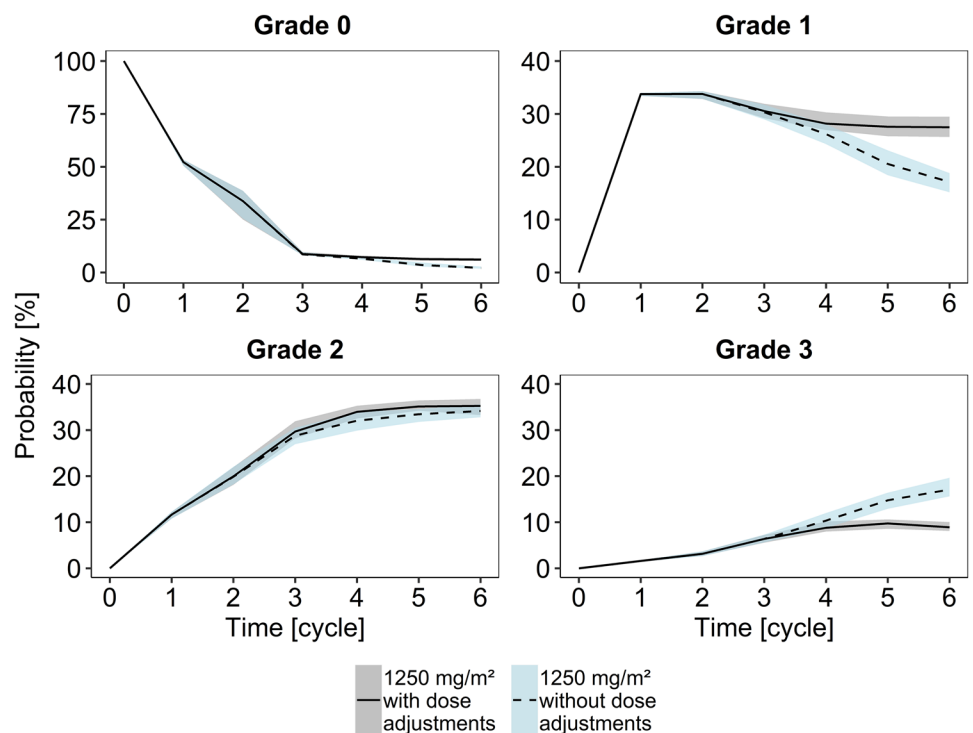


Fig. 3 Simulated probabilities versus time for HFS grades 0–3 of 1000 virtual patients. Solid lines indicate the median probability when dose adjustments were performed according to the capecitabine SmPC [15]. Grey shaded areas are the respective 95% confidence intervals of the median. Dashed lines indicate the median probability when no dose adjustments were performed. Blue shaded areas are the respective 95% confidence intervals of the median



Discussion

This is the first study evaluating the time course of patient-reported adverse event severity in clinical routine during anti-cancer therapy with a Markov modeling approach. A heterogeneous patient group with different tumor entities was analyzed regarding the occurrence and severity of

HFS during treatment with capecitabine. A parsimonious version of a continuous-time Markov model, the mCTMM, was applied requiring fewer model parameters to be estimated compared to other Markov modeling approaches [24]. Thus, the mCTMM can also be applied to sparse-data situations to obtain precisely estimated parameters. Additionally, only transitions between adjacent grades

were allowed since only a small proportion of transitions between non-neighboring grades were observed (Table 1). Therefore and because of the generally small number of observations per patient, a mCTMM was chosen instead of a continuous-time Markov model. The absolute daily dose of capecitabine was found to be a predictor of development of HFS which was in accordance with the observed dose-dependency [14, 27]. Since data on height and weight were not gathered in the studies used for this model, effects of normalized doses could not be investigated. Other covariates did not lead to a significant model improvement including overall adherence. A previous study found a possible influence of over-adherence on high-grade toxicity [28]. In addition, the study of Hénin et al. in which clinician-reported HFS severity in patients with colorectal cancer was analyzed with a discrete-time Markov model, found that creatinine clearance was a significant covariate for HFS severity [16]. However, renal function was not estimated in both studies used for our model. Therefore, a wider selection of covariates would potentially be able to improve the model fit.

Model parameters could be well estimated except for a comparatively higher standard error of the IIV of α_1 . This phenomenon was also observed by Schindler and Karlsson [24]. They suggested that the absence of HFS before starting therapy (at therapy cycle zero) caused these large uncertainties of IIV [24]. However, the logit intercept parameter itself could be precisely estimated in this study. Another reason for larger uncertainties of the IIV parameter estimate may be due to the overall low number of transitions between HFS grades per patient. Only a maximum of seven time points could be analyzed (one per therapy cycle plus baseline grade) in which the patients reported the maximum HFS grade per therapy cycle. Therefore, distinguishing between HFS severities within the respective cycle was not possible which resulted in a low transition number. For the same reason, time delays due to treatment interruptions could not be considered for this model. The time variation of covariates within one cycle (such as dose) could not be implemented either. A more frequent grading would be required to improve the ability of Markov models of predicting the probabilities of the respective grades for individual patients as shown in the study of Lu et al. [29]. For example, an already validated one-week recall period as in the PRO-CTCAE item library [30, 31] would be more suitable for model development. However, our questionnaire was developed before a German version of the PRO-CTCAE questionnaire was available [32]. Using a validated, entity-specific PRO-CTCAE questionnaire would enhance the development and application of Markov models for evaluation of categorical adverse event severity.

Despite the subjectivity of the patient-reported HFS severity, the limited number of both observed grades and potential covariates as well as the real-world setting, the model was able to accurately describe the observed data on the population level. It also showed that the recommended dosage regimen of 1250 mg/m² for capecitabine monotherapy is appropriate to minimize the probability of HFS grade 3 and increase the probability of the absence of clinically relevant toxicity. Thus, population-based recommendations of dose adjustments can be supported using this model. However, the predictive performance for individual patients was not satisfactory which is probably due to the limited number of observations. As mentioned above, a more frequent grading, particularly within a therapy cycle, might enhance the individual predictive performance. Another reason could be the assumption that the patient-reported HFS grade equaled the “true” grade. Therefore, a misclassification of the actual grade could not be excluded. A possibility to account for the error between a categorical observation and the actual grade would be a model extension towards a hidden Markov model [33]. In such a model the unobserved “true” grade could be described as well. Therefore, our model has to be further improved before it can be applied to make individual predictions.

In conclusion, minimal continuous-time Markov models can be set up using patient-reported outcomes. Our modeling framework may assist in the optimization of dosage regimens and adjustment strategies on the population level aiming at minimizing symptom burden during anti-cancer drug therapy. Predictive performance on the individual patient level may be improved by more frequent PRO measurements and more sophisticated modeling approaches.

Acknowledgements This study was supported by a Ph.D. scholarship (to ES) from the Federal Ministry of Education and Research (BMBF) in cooperation with the Bonn International Graduate School of Drug Sciences (BIGS DrugS).

Funding This study was funded by the Health Research Framework Programme of the Federal Ministry of Education and Research (BMBF). Open Access funding was provided by Projekt DEAL.

Availability of data and material Data are available from the corresponding author upon reasonable request.

Compliance with ethical standards

Conflict of interest All authors declare that they have no conflicts of interest that are relevant to the content of this manuscript.

Ethical approval Data were pooled from two previously published observational cohort studies which were in accordance with the 1964 Helsinki declaration and its later amendments.

Consent to participate Informed consent was obtained from all individual participants included in the study.

Consent for publication Not applicable.

Code availability The modeling code is provided in the Electronic Supplementary Material.

Open Access This article is licensed under a Creative Commons Attribution 4.0 International License, which permits use, sharing, adaptation, distribution and reproduction in any medium or format, as long as you give appropriate credit to the original author(s) and the source, provide a link to the Creative Commons licence, and indicate if changes were made. The images or other third party material in this article are included in the article's Creative Commons licence, unless indicated otherwise in a credit line to the material. If material is not included in the article's Creative Commons licence and your intended use is not permitted by statutory regulation or exceeds the permitted use, you will need to obtain permission directly from the copyright holder. To view a copy of this licence, visit <http://creativecommons.org/licenses/by/4.0/>.

References

- National Cancer Institute (2018) Common terminology criteria for adverse events v5.0 (CTCAE). <https://ctep.cancer.gov>. Accessed 20 Aug 2020
- Basch E (2009) Patient-reported outcomes in drug safety evaluation. *Ann Oncol* 20:1905–1906. <https://doi.org/10.1093/annonc/mdp542>
- Galizia D, Milani A, Geuna E, Martinello R, Cagnazzo C, Foresto M et al (2018) Self-evaluation of duration of adjuvant chemotherapy side effects in breast cancer patients: a prospective study. *Cancer Med* 7:4339–4344. <https://doi.org/10.1002/cam4.1687>
- Basch E, Reeve BB, Mitchell SA, Clauser SB, Minasian LM, Dueck AC et al (2014) Development of the National Cancer Institute's patient-reported outcomes version of the common terminology criteria for adverse events (PRO-CTCAE). *J Natl Cancer Inst* 106:dju244. <https://doi.org/10.1093/jnci/dju244>
- Friberg LE, Henningsson A, Maas H, Nguyen L, Karlsson MO (2002) Model of chemotherapy-induced myelosuppression with parameter consistency across drugs. *J Clin Oncol* 20:4713–4721. <https://doi.org/10.1200/JCO.2002.02.140>
- Karlsson MO, Schoemaker RC, Kemp B, Cohen AF, van Gerwen JM, Tuk B et al (2000) A pharmacodynamic Markov mixed-effects model for the effect of temazepam on sleep. *Clin Pharmacol Ther* 68:175–188. <https://doi.org/10.1067/mcp.2000.108669>
- Suleiman AA, Frechen S, Scheffler M, Zander T, Nogova L, Kocher M et al (2015) A modeling and simulation framework for adverse events in erlotinib-treated non-small-cell lung cancer patients. *AAPS J* 17:1483–1491. <https://doi.org/10.1208/s12248-015-9815-8>
- Niebecker R, Maas H, Staab A, Freiwald M, Karlsson MO (2019) Modeling exposure-driven adverse event time courses in oncology exemplified by afatinib. *CPT Pharmacomet Syst Pharmacol* 8:230–239. <https://doi.org/10.1002/psp4.12384>
- Keizer RJ, Gupta A, Mac Gillavry MR, Jansen M, Wanders J, Beijnen JH et al (2010) A model of hypertension and proteinuria in cancer patients treated with the anti-angiogenic drug E7080. *J Pharmacokinet Pharmacodyn* 37:347–363. <https://doi.org/10.1007/s10928-010-9164-2>
- Lacroix BD, Karlsson MO, Friberg LE (2014) Simultaneous exposure-response modeling of ACR20, ACR50, and ACR70 improvement scores in rheumatoid arthritis patients treated with certolizumab pegol. *CPT Pharmacomet Syst Pharmacol* 3:e143. <https://doi.org/10.1038/psp.2014.41>
- Reigner B, Blesch K, Weidekamm E (2001) Clinical pharmacokinetics of capecitabine. *Clin Pharmacokinet* 40:85–104. <https://doi.org/10.2165/00003088-200140020-00002>
- Cassidy J, Twelves C, van Cutsem E, Hoff P, Bajetta E, Boyer M et al (2002) First-line oral capecitabine therapy in metastatic colorectal cancer: a favorable safety profile compared with intravenous 5-fluorouracil/leucovorin. *Ann Oncol* 13:566–575. <https://doi.org/10.1093/annonc/mdf089>
- Twelves C, Scheithauer W, McKendrick J, Seitz JF, van Hazel G, Wong A et al (2012) Capecitabine versus 5-fluorouracil/folinic acid as adjuvant therapy for stage III colon cancer: Final results from the X-ACT trial with analysis by age and preliminary evidence of a pharmacodynamic marker of efficacy. *Ann Oncol* 23:1190–1197. <https://doi.org/10.1093/annonc/mdr366>
- Scheithauer W, Blum J (2004) Coming to grips with hand-foot syndrome. *Insights from clinical trials evaluating capecitabine. Oncology (Williston Park, NY)* 18:1161–1168
- Electronic Medicines Compendium (2018) Capecitabine 500 mg film-coated tablets: summary of product characteristics. <https://www.medicines.org.uk/emc/product/9939>. Accessed 20 Aug 2020
- Hénin E, You B, VanCutsem E, Hoff PM, Cassidy J, Twelves C et al (2009) A dynamic model of hand-and-foot syndrome in patients receiving capecitabine. *Clin Pharmacol Ther* 85:418–425. <https://doi.org/10.1038/clpt.2008.220>
- Simons S, Ringsdorf S, Braun M, Mey UJ, Schwindt PF, Ko YD et al (2011) Enhancing adherence to capecitabine chemotherapy by means of multidisciplinary pharmaceutical care. *Support Care Cancer* 19:1009–1018. <https://doi.org/10.1007/s00520-010-0927-5>
- Krolop L, Ko YD, Schwindt PF, Schumacher C, Fimmers R, Jaehde U (2013) Adherence management for patients with cancer taking capecitabine: a prospective two-arm cohort study. *BMJ Open* 3:e003139. <https://doi.org/10.1136/bmjopen-2013-003139>
- Beal S, Sheiner LB, Boeckmann A, Bauer RJ (2018) NONMEM user's guides (1989–2018). Icon Development Solutions, Gaithersburg
- Lindbom L, Pihlgren P, Jonsson EN, Jonsson N (2005) PsN-Toolkit—a collection of computer intensive statistical methods for non-linear mixed effect modeling using NONMEM. *Comput Methods Programs Biomed* 79:241–257. <https://doi.org/10.1016/j.cmpb.2005.04.005>
- Lindbom L, Ribbing J, Jonsson EN (2004) Perl-speaks-NONMEM (PsN)—a Perl module for NONMEM related programming. *Comput Methods Programs Biomed* 75:85–94. <https://doi.org/10.1016/j.cmpb.2003.11.003>
- R Core Team (2018) R: a language and environment for statistical computing. R Foundation for Statistical Computing, Vienna, Austria. <https://www.R-project.org/>. Accessed 11 Mar 2020
- Keizer RJ, Karlsson MO, Hooker A (2013) Modeling and simulation workbench for NONMEM: tutorial on Pirana, PsN, and Xpose. *CPT Pharmacomet Syst Pharmacol* 2:e50. <https://doi.org/10.1038/psp.2013.24>
- Schindler E, Karlsson MO (2017) A minimal continuous-time Markov pharmacometric model. *AAPS J* 19:1424–1435. <https://doi.org/10.1208/s12248-017-0109-1>
- Sheiner LB (1994) A new approach to the analysis of analgesic drug trials, illustrated with bromfenac data. *Clin Pharmacol Ther* 56:309–322. <https://doi.org/10.1038/clpt.1994.142>
- de Man FM, Veerman GDM, Oomen-de Hoop E, Deenen MJ, Meulendijks D, Mandigers CMPW et al (2019) Comparison of toxicity and effectiveness between fixed-dose and body surface area-based dose capecitabine. *Ther Adv Med Oncol* 11:1–14. <https://doi.org/10.1177/1758835919838964>
- Kara IO, Sahin B, Erkisi M (2006) Palmar-plantar erythrodysesthesia due to docetaxel-capecitabine therapy is treated with

- vitamin E without dose reduction. *Breast* 15:414–424. <https://doi.org/10.1016/j.breast.2005.07.007>
28. Le Saux O, Bourmaud A, Rioufo C, Colombari O, Guitton J, Schwartz V et al (2018) Over-adherence to capecitabine: a potential safety issue in breast and colorectal cancer patients. *Cancer Chemother Pharmacol* 82:319–327. <https://doi.org/10.1007/s00280-018-3612-x>
 29. Lu T, Yang Y, Jin JY, Kågedal M (2020) Analysis of Longitudinal ordered categorical data for muscle spasm adverse event of vismodegib: comparison between different pharmacometric models. *CPT Pharmacomet Syst Pharmacol* 9:96–105. <https://doi.org/10.1002/psp4.12487>
 30. Mendoza TR, Dueck AC, Bennett AV, Mitchell SA, Reeve BB, Atkinson TM et al (2017) Evaluation of different recall periods for the US National Cancer Institute's PRO-CTCAE. *Clin Trials* 14:255–263. <https://doi.org/10.1177/1740774517698645>
 31. Dueck AC, Mendoza TR, Mitchell SA, Reeve BB, Castro KM, Rogak LJ et al (2015) Validity and reliability of the US National Cancer Institute's Patient-reported outcomes version of the common terminology criteria for adverse events (PRO-CTCAE). *JAMA Oncol* 1:1051–1059. <https://doi.org/10.1001/jamaoncol.2015.2639>
 32. Hagelstein V, Ortlund I, Wilmer A, Mitchell SA, Jaehde U (2016) Validation of the German patient-reported outcomes version of the common terminology criteria for adverse events (PRO-CTCAE™). *Ann Oncol* 27:2294–2299. <https://doi.org/10.1093/annonc/mdw422>
 33. Brekkan A, Jönsson S, Karlsson MO, Plan EL (2019) Handling underlying discrete variables with bivariate mixed hidden markov models in NONMEM. *J Pharmacokinet Pharmacodyn* 46:591–604. <https://doi.org/10.1007/s10928-019-09658-z>

Publisher's Note Springer Nature remains neutral with regard to jurisdictional claims in published maps and institutional affiliations.

Supplementary Document

Evaluation of patient-reported severity of hand-foot syndrome under
capecitabine using a Markov modeling approach

Eduard Schmulenson¹, Linda Krolop¹, Sven Simons¹, Susanne Ringsdorf¹, Yon-Dschun Ko², Ulrich
Jaehde^{1*}

¹Institute of Pharmacy, Department of Clinical Pharmacy, University of Bonn, Bonn, Germany

²Department of Internal Medicine, Evangelische Kliniken Bonn gGmbH, Johanniter Hospital, Bonn,
Germany

***Corresponding author**

Prof. Dr. Ulrich Jaehde

Institute of Pharmacy

University of Bonn

An der Immenburg 4

53121 Bonn

Germany

Phone: +49 228 73 5252

Fax: +49 228 73 9757

Email: u.jaehde@uni-bonn.de

NONMEM code of the final model

\$PROBLEM Capecitabin HFS mCTMM

\$INPUT

ID ; No. of the patient

TIME ; Therapy cycle no. as time unit

DV ; No AE -> DV = 1, otherwise DV = 2-4 (grades 1-3)

AMT ; Probability for AE compartments

CMT ; 1-4 = AE compartments

DOSEDAY ; Absolute dose per day

EVID

MDV

AGE

SEX

MAMMA ; tumor entity: mamma carcinoma

COLON ; tumor entity: colorectal cancer

OTHER ; other tumor entity

MONO ; Capecitabin monotherapy yes/no

\$DATA HFS_total.csv

\$SUBROUTINES ADVAN6 TOL = 4

\$MODEL

NCOMP = 4

COMP = (G0) ; No AE

COMP = (G1) ; Mild AE

COMP = (G2) ; Moderate AE

COMP = (G3) ; Severe AE

\$ABB COMRES = 1

\$PK

IF(NEWIND.NE.2) THEN

PSDV = 0

COM(1) = 0

ENDIF

PRSP = PSDV ; Previous DV

IF(TIME.EQ.0) F1 = 1

IF(PRSP.EQ.1) COM(1) = 0

IF(PRSP.EQ.2) COM(1) = 1

IF(PRSP.EQ.3) COM(1) = 2

IF(PRSP.EQ.4) COM(1) = 3

F1=0

F2=0

F3=0

F4=0

IF(COM(1).EQ.0) F1 = 1

IF(COM(1).EQ.1) F2 = 1

IF(COM(1).EQ.2) F3 = 1

IF(COM(1).EQ.3) F4 = 1

;--- mCTMM model parameters

MET = THETA(4)*EXP(ETA(2)) ; Mean equilibration time

ET1 = ETA(1)

\$DES

A1 = THETA(1)+ET1 + THETA(5)*(DOSEDAY-3000) ; alpha_1 with linear dose effect

B2 = THETA(2) ; beta_2

B3 = THETA(3) ; beta_3

; Logit of the cumulative probabilities

LGE1 = A1 ; >=Grade 1

LGE2 = LGE1 + B2 ; >=Grade 2

LGE3 = B3 + LGE2 ; Grade 3

; Cumulative probabilities

PGE1 = EXP(LGE1)/(1+EXP(LGE1)) ; >=Grade 1

PGE2 = EXP(LGE2)/(1+EXP(LGE2)) ; >=Grade 2

PGE3 = EXP(LGE3)/(1+EXP(LGE3)) ; Grade 3

; Probabilities

P0 = (1-PGE1) ; Probability of grade 0

P1 = (PGE1-PGE2) ; Probability of grade 1

P2 = (PGE2-PGE3) ; Probability of grade 2

P3 = PGE3 ; Probability of grade 3

; Transfer rate constants

L01 = 1/(MET*(1+P0/P1))

L10 = L01 *P0/P1

L12 = 1/(MET*(1+P1/P2))

L21 = L12 *P1/P2

L23 = 1/(MET*(1+P2/P3))

L32 = L23 *P2/P3

; Differential equations for the probability of each grade

$$DADT(1) = L10*A(2) - L01 *A(1) ; \text{Grade 0}$$

$$DADT(2) = L01*A(1)+L21*A(3)-(L10+L12)*A(2) ; \text{Grade 1}$$

$$DADT(3) = L12*A(2)+L32*A(4)-(L21+L23)*A(3) ; \text{Grade 2}$$

$$DADT(4) = L23*A(3) - L32 *A(4) ; \text{Grade 3}$$

\$ERROR

;--- Redefine variables from \$DES

$$A1X = THETA(1) + ET1+ THETA(5)*(DOSEDAY-3000)$$

$$B2X = THETA(2)$$

$$B3X = THETA(3)$$

$$LGE1X = A1X$$

$$LGE2X = LGE1X + B2X$$

$$LGE3X = B3X + LGE2X$$

$$PGE1X = \text{EXP}(LGE1X)/(1+\text{EXP}(LGE1X))$$

$$PGE2X = \text{EXP}(LGE2X)/(1+\text{EXP}(LGE2X))$$

$$PGE3X = \text{EXP}(LGE3X)/(1+\text{EXP}(LGE3X))$$

$$POX = (1-PGE1X)$$

$$P1X = (PGE1X-PGE2X)$$

$$P2X = (PGE2X-PGE3X)$$

$$P3X = PGE3X$$

; --- Define Y

$$POX = A(1) ; \text{Probability of observing grade 0}$$

$$P1X = A(2) ; \text{Probability of observing grade 1}$$

P2X = A(3) ; Probability of observing grade 2

P3X = A(4) ; Probability of observing grade 3

IF(DV.EQ.1.AND.CMT.EQ.0) Y=P0X

IF(DV.EQ.2.AND.CMT.EQ.0) Y=P1X

IF(DV.EQ.3.AND.CMT.EQ.0) Y=P2X

IF(DV.EQ.4.AND.CMT.EQ.0) Y=P3X

; Cumulative probabilities

CUP0 = P0X

CUP1 = CUP0 + P1X

CUP2 = CUP1 + P2X

CUP3 = CUP2 + P3X

; Start of simulation

IF(ICALL.EQ.4) THEN

IF(CMT.EQ.0) THEN

CALL RANDOM (2,R)

IF(R.LE.CUP0) DV = 1

IF(R.GT.CUP0.AND.R.LE.CUP1) DV = 2

IF(R.GT.CUP1.AND.R.LE.CUP2) DV = 3

IF(R.GT.CUP2) DV = 4

ENDIF

ENDIF

; End of simulation

; Store DV

PSDV = DV

\$THETA

(1.81) ; 1 alpha_1

(-1000000, -1.8,0) ; 2 beta_2

(-1000000, -2.08,0) ; 3 beta_3

(0, 1.09) ; 4 MET

(0.00083) ; Dose effect

\$OMEGA

1.25 ; IIV alpha_1

0.294 ; IIV MET

\$COV PRINT=E MATRIX=R

\$ESTIMATION MAXEVAL=9999 METHOD=1 LAPLACE LIKE PRINT=1 NOABORT SIG=2

;\$SIM (7776) (8877 UNIFORM) ONLYSIM NOPREDICTION